

Fano resonances in nanoscale structures

Andrey E. Miroshnichenko,^{1,*} Sergej Flach,² and Yuri S. Kivshar¹

¹*Nonlinear Physics Center and Center for Ultra-high bandwidth Devices for Optical Systems (CUDOS),
Research School of Physics and Engineering, Australian National University, Canberra ACT 0200, Australia*

²*Max-Planck-Institut für Physik komplexer Systeme, D-01187 Dresden, Germany*

Nowadays nanotechnology allows to scale-down various important devices (sensors, chips, fibres, etc), and, thus, opens up new horizon for their applications. Nevertheless, the efficiency most of them is still based on the fundamental physical phenomena, such as resonances. Thus, the understanding of the resonance phenomena will be beneficial. One of the well-known examples is the resonant enhancement of the transmission known as Breit-Wigner resonances, which can be described by a Lorentzian function. But, in many physical systems the scattering of waves involves propagation along different paths, and, as a consequence, results in interference phenomena, where constructive interference corresponds to resonant enhancement and destructive interference to resonant suppression of the transmission. Recently, a variety of experimental and theoretical work has revealed such patterns in different branches of physics. The purpose of this Review is to demonstrate that this kind of resonant scattering is related to the Fano resonances, known from atomic physics. One of the main features of the Fano resonances is the asymmetric profile. The asymmetry comes from the close coexistence of resonant transmission and resonant reflection. Fano successfully explained such a phenomenon in his seminal paper in 1961 in terms of interaction of a discrete (localized) state with a continuum of propagation modes. It allows to describe both resonant enhancement and resonant suppression in a unified manner. All of these properties can be demonstrated in the frame of a very simple model, which will be used throughout the Review to show that resonant reflections observed in different complex systems are indeed closely related to the Fano resonances.

Contents		VI. Charge transport through quantum dots	23
I. Historical remarks	1	A. General remarks	23
II. The Fano resonance	3	B. From a single electron transistor to quantum interference	24
III. Scattering by complex geometries	6	C. From Coulomb blockade to Fano resonances	25
A. General remarks	6	D. From Fano interferometers to Aharonov-Bohm interferometers	27
B. Fano-Anderson model	6	E. From strong correlations to spin filters	27
C. Nonlinear Fano resonance	7	1. Correlations	28
D. Extensions	8	2. Interferences	28
1. Resonant reflection of solitons	9	3. Spin filters	29
2. Light scattering in quadratic waveguide arrays	9	F. More	30
IV. Scattering by time-periodic potentials	10	VII. More	31
A. General remarks	10	A. Matter wave scattering in Bose-Einstein condensates	31
B. Scattering by Discrete Breathers	10	B. Detection of Efimov states via quantum interference	32
C. Possible applications	12	C. Transport through carbon nanotubes	33
1. Light scattering by optical solitons	13	D. Resonant four-wave mixing induced autoionization	34
2. Plasmon scattering in Josephson junction ladders	13	E. Raman scattering of heavily doped semiconductors	35
V. Light propagation in photonic devices	14	VIII. Conclusions	36
A. General remarks	14	References	36
B. Green's function formalism	14		
C. Waveguide-cavity systems	15	I. HISTORICAL REMARKS	
1. Defects in the waveguide	15		
2. Sharp bends as Fano resonances	15		
3. Add-drop filters	16		
D. All-optical switching and bistability	17		
E. Fano-Feshbach resonances	18		
F. Guided resonances in photonic crystal slabs	19		
G. Light scattering by spherical nanoparticles	21		
H. Plasmonic nanocavities and tunable Fano resonance	22		
I. Extraordinary transmission of light through metallic gratings	23		

*Electronic address: aem124@rsphysse.anu.edu.au

One of the important diagnostic tools in physics is the scattering. It provides us with the understanding of the radiation-matter interaction which can be used in two ways. From one side, it allows us to investigate the key properties of the matter and, from the other side, it allows to control the radiation. For example, Rydberg spectral lines (1888) of the hydrogen atom allowed Niels Bohr to deduce his model of an atom (1913), which created the basis of the quantum mechanics. Later, Beutler (1935) observed that some of the Rydberg spectral atomic lines may exhibit sharp asymmetric profiles

in the absorption. It was Ugo Fano (1935b) who suggested the first theoretical explanation of this effect and suggested the formula (also known as the Beutler-Fano formula) which predicts the shape of spectral lines based on a superposition principle of quantum mechanics. The whole complexity of the physical phenomena were encapsulated in a few key parameters, which made this formula a workhorse of many fields of physics, including nuclear, atomic, molecular, and condensed-matter physics. According to Fano: *"the Beutler spectra showed unusual intensity profiles which struck me as reflecting interference between alternative mechanisms of excitation"* (Fano, 1977). The interpretation provided by Fano of these "strange looking shapes" of spectral absorption lines is based on the interaction of a discrete excited state of an atom with a continuum sharing the same energy level, which results in interference phenomena. The first paper with the derivation of the line-shape formula (Fano, 1935b), was published in 1935, when Ugo Fano was a young postdoctoral fellow in the group of Enrico Fermi. Fano has acknowledged the influence of his teacher on the derivation of this key result. The second much elaborated paper (Fano, 1961) became one of the most important publications in the physics of the XX century, rated between the first three most relevant works published in *The Physical Review* (Redner, 2004), and it has been cited more than 5300 times by now (October 2008). *"The paper appears to owe its success to accidental circumstances, such as the timing of its publication and some successful features of its formulation. The timing coincided with a rapid expansion of atomic and condensed matter spectroscopy, both optical and collisional. The formulation drew attention to the generality of the ingredients of the phenomena under consideration. In fact, however, the paper was a rehash of work done 25 years earlier . . ."* (Fano, 1935a, 1977; Vittorini-Orgeas and Bianconi, 2008). In these pioneering papers, Ugo Fano introduced an important new view on matter-radiation interaction in atomic physics, making him a key player in XX century physics, being acknowledged by Fermi Award in 1995 for "his seemingly formal use of fundamental theory" leading to "the underpinning of a vast variety of practical results which developed naturally from this understanding".

Remarkably, that the first observation of the asymmetric line-shapes can be traced back to the discovery made by Wood in 1902, namely, the presence of unexpected narrow bright and dark bands in the spectrum of an optical reflection grating illuminated by a slowly varying light source (Wood, 1902). Wood was astounded to see that under special illumination conditions the grating efficiency in a given order dropped from maximum to minimum illumination, within a wavelength range not greater than the distance between the sodium lines. These rapid variations of intensities of the various diffracted spectral orders in certain narrow frequency bands were termed *anomalies*, since the effects could not be explained by the conventional grating theory (Wood, 1935). The first theoretical treatment of these anomalies



FIG. 1 Ugo Fano (1912-2001) - "outstanding interpreter of how radiation interacts with atoms and cells" (Clark, 2001), and much more! (see this Review).

is due to Lord Rayleigh (1907). His "dynamical theory of the grating" was based on an expansion of the scattered electromagnetic field in terms of outgoing waves only. This theory correctly predicted the wavelength (Rayleigh wavelengths) at which anomalies occurred. However, one of the limitations of Rayleigh's approach was that it indicates a singularity at the Rayleigh wavelength, and, therefore, does not yield the shape of the bands associated with the anomaly. Fano tried to overcome this difficulty in a series of papers (Fano, 1936, 1937, 1938, 1941) by assuming that a grating consisting of lossy dielectric material, and suggesting that anomalies could be associated with the excitation of a surface wave along the grating. The resonant excitation of leaky surface waves near the grating, which occurs when a suitable phase matching between the incident plane wave and the guided wave is satisfied, leads to a strong enhancement of the field near the grating surface (de Abajo, 2007; Hessel and Oliner, 1965; Sarrazin *et al.*, 2003). As it was pointed out in Ref. (Sarrazin *et al.*, 2003), the observed asymmetric profiles can be fitted by the Fano formula with a great accuracy. Thus, the interaction of excited leaky modes with an incoming radiation leads to the similar interference phenomena as in absorption by Rydberg atoms, where a leaky mode can be associated with a discrete state, and incoming radiation with a continuum. These examples reveal the universality of the Fano approach in describing the origin of asymmetric line-shapes in terms of interference phenomena, regardless of the nature of the constituting waves. The power of this approach is its possibility to predict both the position and width of the resonances.

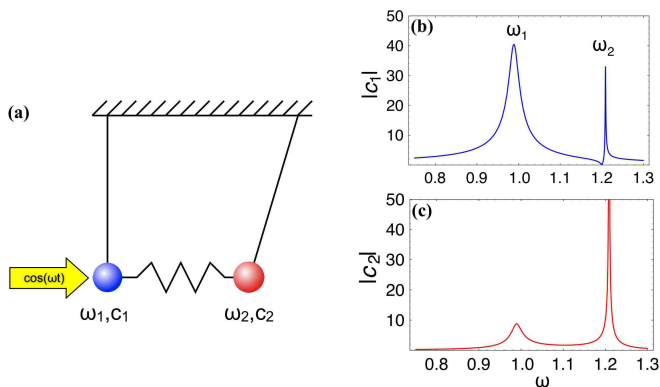


FIG. 2 (Color online) Resonances of parametrically driven coupled oscillators. (a) Schematic view of two coupled oscillators with a driving force applied to one of them. The resonant behaviour of the amplitude of the forced oscillator $|c_1|$ (b) and coupled one $|c_2|$ (c). There are two resonances in the system. The forced oscillator exhibits resonances with symmetric and asymmetric profiles near the eigenfrequencies $\omega_1 = 1$ and $\omega_2 = 1.2$ (b), respectively. The second coupled oscillator demonstrates only symmetric resonant profiles (c). Adapted from Joe *et al.* (2006).

Similar asymmetric profiles were observed in various systems. But sometimes it is very tricky to explain them, since it is not so obvious where the interference comes from. In the present survey paper, we provide a very general explanation of appearance of the Fano resonances in various physical systems based on a simple physical model, which sheds light on the origin of the interference phenomena. We believe that this approach can be further extended to many other systems in accordance with Steven Weinberg who said: "our job in physics is to see things simply, to understand many complicated phenomena in a unified way, in terms of a few simple principles." (1979 Nobel Prize Lecture).

It is worth to note, that Fano initiated the "Colloquium" series in Review of Modern Physics, in order to spread the understanding of important phenomena among various branches of physics. We are very proud of making this small contribution into his effort by trying to present the deep universality of the Fano effects and their important in many branches of modern physics.

II. THE FANO RESONANCE

One of the most important phenomena in physics is a resonance. Usually, it is thought to be an enhancement of the response of a system on an external periodic excitation at a particular frequency. It is called the resonant frequency, or natural frequency of the system. One of the simplest examples is a harmonic oscillator under periodic force. When the frequency of the driving force is close to the eigenfrequency of the oscillator, its amplitude is growing towards the maximal value. Unlikely, many physical systems exhibit an opposite phenomenon, where their re-

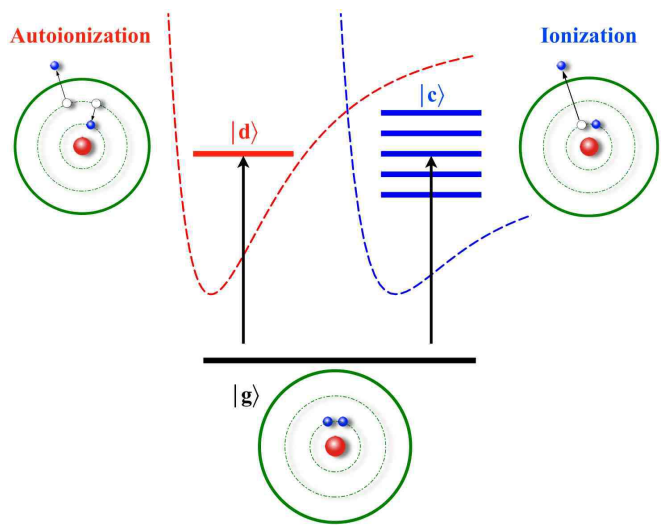


FIG. 3 (Color online) Fano resonance as a quantum interference of two processes - direct ionization of a deep inner-shell electron and autoionization of two excited electrons followed by the Auger effect. This process can be represented as a transition from the ground state of an atom $|g\rangle$ either to a discrete excite autoionizing state $|d\rangle$ or to a continuum $|c\rangle$. Dashed lines indicate double excitations and ionization potentials.

sponse is suppressed at the resonant condition. Sometimes, it's even called an anti-resonant phenomenon. This can be illustrated by using two weakly coupled harmonic oscillators, where only one of them is driven by a periodic force [see Fig. 2(a)]. In such a system, in general, there are two resonances located close to eigenfrequencies ω_1 and ω_2 of the oscillators (Joe *et al.*, 2006). One of the resonances of the forced oscillator demonstrates the standard enhancement of the amplitude near its eigenfrequency ω_1 , while another resonance exhibits unusual sharp suppression of the amplitude near the eigenfrequency of the second oscillator ω_2 [see Fig. 2(b,c)]. The first resonance is characterized by a symmetric profile, described by Lorentzian function, and known as Breit-Wigner resonance (Breit and Wigner, 1936). The second resonance is characterized by an asymmetric profile, which was described for the first time by Fano (1935b, 1961). His attention was attracted by unusual sharp peaks in absorption spectra of noble gases observed by Beutler (1935). Although, it was realized that such peculiar behaviour corresponds to the excitation of some kind of quasi-discrete states, the nature of asymmetry remained mysterious until the theory of configuration mixing established by Fano (1961). It was discovered that photoionization of an atom can happen in various ways. The first, straightforward one, is the excitation of the inner-shell electron above the ionization threshold $A + \hbar\nu \rightarrow A^+ + e$. Another possibility is excite atom into some quasi-discrete level, which can spontaneously ionize by ejecting an electron into the continuum $A + \hbar\nu \rightarrow A^* \rightarrow A^+ + e$. Such levels were named autoionizing ones after Shenstone (1938). In other words,

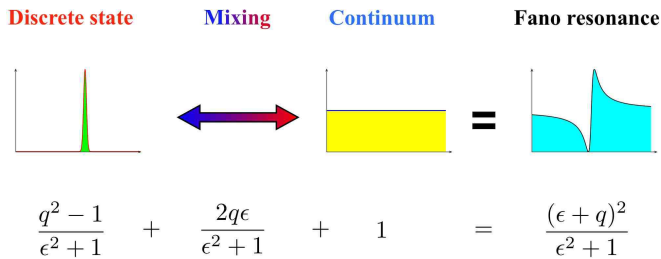


FIG. 4 (Color online) Illustration of the Fano formula (1) as a superposition of the Lorentzian lineshape of the discrete level with flat continuous background.

the autoionize state is a bound state of an atom with the energy above the first ionizing threshold. Autoionization is one of the most fundamental electron-electron correlation phenomena, and it is forbidden in the independent particle approximation (Connerade, 1998). Of the examples is the excitation of two electrons by one photon, when the excitation energies of each electron are of the same order of magnitude, and the total excitation energy exceeds the atom ionization threshold. The interaction between electrons leads to the decay of this state when one electron transfers into a lower state, and the second electron is ejected into the continuum by taking an energy excess. In spectroscopy this process is known as Auger effect (Auger, 1925a,b, 1926). Different types of other autoionizing states are described in (Smirnov, 2003). In general, autoionization can be considered as a mechanism which couples bound states of one channel and continuous states of another. Due to superposition principle of the quantum mechanics, whenever two levels are coupled by different paths, the interference may occur.

Fano used a perturbation approach to explain the appearance of asymmetric resonances. The main trick which led him to success was to consider so-called prediagonalized state by putting the coupling between a discrete bound state degenerate in energy with a continuum to zero. Such prediagonalized state does not exist as such in realistic systems, and is simply a mathematical convenience, which allows to solve the problem. As a result he obtained the formula for the shape of the resonance profile (Fano, 1935b, 1961)

$$\sigma = \frac{(\epsilon + q)^2}{\epsilon^2 + 1} \quad (1)$$

in terms of phenomenological shape parameter q and reduced energy ϵ defined by $2(E - E_F)/\Gamma$, with E_F being resonant energy, and Γ width of the auto-ionized state. The simple analysis of the formula (1) suggests that there are exactly one maximum and one minimum of the Fano profile

$$\begin{aligned} \sigma_{\min} &= 0, \quad \text{at } \epsilon = -q \\ \sigma_{\max} &= 1 + q^2, \quad \text{at } \epsilon = 1/q. \end{aligned} \quad (2)$$

In his original paper Fano (1961) has introduced the asymmetry parameter q as a ratio of transition probabilities to the 'mixed' state and to the continuum. Thus, in the limit $|q| \rightarrow \infty$, the transition to the continuum is very weak, and the lineshape is entirely determined by the transition through the discrete state only with the standard "Lorentzian" profile of a Breit-Wigner resonance. When the asymmetry parameter q is order of unity both the continuum and discrete transition are of the same strength resulting is the asymmetric profile (1), with the maximum value at $E_{\max} = E_F + \Gamma/(2q)$ and minimum value at $E_{\min} = E_F - \Gamma q/2$. The case of zero asymmetry parameter $q = 0$ is very unique to the Fano resonance and describes a symmetrical dip, sometimes called an anti-resonance (see Fig. 5). The main difference of the Fano resonance is a possibility of destructive interference, leading to asymmetric line shapes (Bandopadhyay *et al.*, 2004; Bianconi, 2003; Lee and Kim, 2000a; Nockel and Stone, 1994; Piao *et al.*, 1990; Rau, 2004). In other words, the actual resonant frequency of the discrete level E_F lies somewhere in between the maximum and minimum of the asymmetric profile, and the parameter q describes the relative deviation. In the situation $|q| \rightarrow \infty$ the resonant frequency corresponds to the maximum of the profile, while in the case $q = 0$ the resonant frequency corresponds to the minimum. For all other values of q the resonant frequency is between minimum and maximum, and it lies exactly in the middle for $q = 1$ (see Fig. 5).

Experiments on absorption cross-section of a single quantum dot, which can be considered as an artificial atom, have revealed that the asymmetry parameter q can be continuously tuned with the power of the laser (Kroner *et al.*, 2008). In this system, the transition to the discrete level saturates at high power, while the rate of the continuum transition does not. Eventually, initially weak continuum transition will match the saturated transition to the discrete level with increasing laser power. As a result, symmetric Lorentzian profile at low power will transform to asymmetric Fano profile at sufficiently large power (see Fig. 6). This particular example demonstrates of the nonlinear Fano resonance in photoabsorption at high powers.

On contrary, in biased semiconductor superlattices the Fano coupling parameter Γ between the discrete state and the continuum can be continuously tuned by varying the applied electric field (Holfeld *et al.*, 1998). For each Wannier-Stark state the electron-hole relative motion is discretized due to Coulomb interaction. Such quantized states become degenerate with the exciton continua of the lower subbands, resulting in asymmetric absorption spectra of Wannier-Stark transitions (Hino and Toshima, 2005; S. J. Xu and Zheng, 2006). The external bias determines the energy spacing of a Wannier-Stark subband, and, thus, control the effective coupling between the discrete states and continua. It allows to study the dephasing dynamics of the Fano resonance.

Due to recent advances in the generation of ultrashort

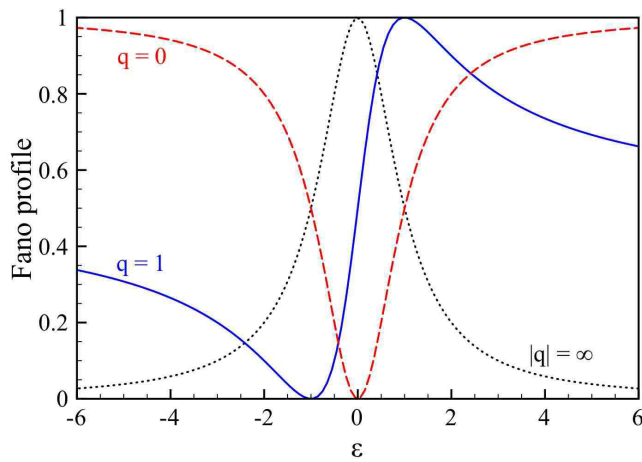


FIG. 5 (Color online) Normalized Fano profiles (1) with the prefactor $1/(1+q^2)$ (2) for various values of the asymmetry parameter q .

sub-fs pulses it becomes possible to observe the buildup of the Fano resonance in time by using attosecond streaking techniques (Wickenhauser *et al.*, 2005). Excitation by the ultrashort pump pulse opens two interfering paths from ground state to the continuum, which are then investigated by the weak probe pulse. After the characteristic time of the autoionizing level, the transient coupling to the resonant state starts to "burn a hole" in the energy distribution of the initial Gaussian. This method is very useful in determining both coherent and incoherent pathways to ionization.

In general, the asymmetry parameter q is not restricted to be only real. In systems with broken time reversal symmetry transition amplitudes to the discrete level and continuum may become complex, and so does the asymmetry parameter. The Fano resonance in such systems can be studied by analysing the dynamical response. In particular, Misochko *et al.* (2005) found that time-dependent reflection of a bismuth single crystal after the excitation by an ultrashort laser pulse exhibits Fano asymmetric profile in Fourier transform of a time-oscillating signal. They demonstrated that asymmetric parameter varies periodically with the time delay between pump and probe pulses. The breaking of time reversal symmetry is indicated by the change of the sign of the asymmetry parameter.

The Fano formula (1) was successfully applied to fit and explain various experimental data (Kleinpoppen and McDowell, 1976) (Aoki *et al.*, 1996; Armstrong *et al.*, 1978,?; Bandopadhyay *et al.*, 2004; Bandrauk and Laplante, 1976; Bar-Ad *et al.*, 1997; Becker *et al.*, 1986; Bortchagovsky and Fischer, 2003; Chergui *et al.*, 1991; Davis and Feldkamp, 1977; dell'Orto *et al.*, 1995; Dixit and Lambropoulos, 1979; Druger, 1977; Eichmann *et al.*, 2003; Fano, 1964, 1965; Fano and Cooper, 1965, 1968; Fano and Lee, 1973; Feneuille *et al.*, 1979; Fransson and Balatsky, 2007; Ganz *et al.*, 1984;

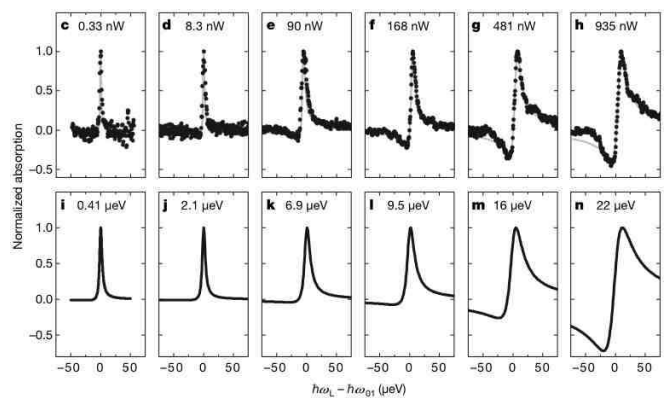


FIG. 6 Measured (upper row) and calculated (bottom row) absorption spectra of a single quantum dot for various laser powers. Absorption profile varies from symmetrical to asymmetrical one with increase of the laser power, indicating the enhancement of the continuum transition. From Kroner *et al.* (2008).

Glutsch, 2002; Harmin, 1985; Hase *et al.*, 2006a; Heinzmann *et al.*, 1970; Heller and Mukamel, 1979; Janzen *et al.*, 1985; Kessler and Lorenz, 1970; Kokoouline *et al.*, 2002; Kolorenc *et al.*, 2005; Lee, 1998; Ley *et al.*, 1984; Maeda *et al.*, 1992; Margulis and Pyataev, 2004; Marinho *et al.*, 2001; Mehlhorn, 1998; Meijerink and Blasse, 1989; Nockel and Stone, 1994; Nussenzweig *et al.*, 1990; Oliveira and Wilkins, 1985; Patthey *et al.*, 1999; Pichl *et al.*, 2000; Ramaker and Schrader, 1974; Roney, 1994a,b, 1995; S. J. Xu and Zheng, 2006; Sanchez and Martin, 1994; Siegner *et al.*, 1995; Simonian *et al.*, 1995; Simpson and Fano, 1963; Smith *et al.*, 1973; Sturm *et al.*, 1992; Syage and Wessel, 1987; Taylor and Johnson, 1993; Ueda, 1987; Waligorski *et al.*, 1997; Wickenhauser *et al.*, 2005; Winstead and Langhoff, 1991; Yafet, 1981), thus, revealing the underlying mechanism of the observed resonances in terms of quantum-mechanical interaction between discrete and continuous states. In nuclear and atomic physics, Fano interference is often described as interaction of open (continuum) and closed (discrete levels) channels, by using a theoretical framework developed in a series of papers by Feshbach (1958, 1962). Bhatia and Temkin (1984) unified Fano and Feshbach approaches by providing *ab initio* calculations and deriving a rigorous expression of the asymmetry parameter q by using "the incisiveness and beauty of the Feshbach theory" (Bhatia and Temkin, 1984).

Although, the Fano formula (1) is quite general, there are some limitations of its applicability (Connerade, 1998). First, it can be applied to describe single, isolated resonance. Second, the width of the discrete level must be much smaller than any other resonant effect in the system. In its turn, it requires that the background continuum should be flat, and its slope should be checked.

When two particles (atoms or molecules) collide with

each other a quasi-bound state can be formed, which is characterized by a complex energy $E = E_F + i\Gamma$. In scattering theory this quasi-bound state is called a resonance since it possesses a finite life-time \hbar/Γ . The quasi-bound state is formed due to excitation and sharing of common electrons, and, thus, can be understood in terms of interaction of discrete and continuous states [see Fig. 3(b)]. In a similar manner, observed asymmetric resonances in pre-dissociation (Bandrauk and Laplante, 1976; Cotting *et al.*, 1994; Lebech *et al.*, 2006; Lewis *et al.*, 2001; Palfy *et al.*, 2007) (or fragmentation) of molecules were explained by Rice (Rice, 1933) in terms of auto-ionization.

In general, the Coulomb interaction of outgoing electron e^- and charged ion core A^+ during auto-ionization leads to renormalization of energy levels of many-electron system. Such renormalization is known as the quantum defect of Rydberg series. To precisely describe the positions and width of the resonances the multichannel quantum defect theory was developed by Seaton (1966) and Fano (1970), which provides a rigorous description of the process. It allows to derive all asymptotic quantities such as phase shifts or the amplitudes of the auto-ionized levels. The Eq. (1) derived by Fano was obtained by neglecting effects due to long-range Coulomb potential, but, nevertheless, provides the physical insight into auto-ionization in terms of quantum-mechanical interference of discrete and continuum states.

At resonances the phase of the scattering wave changes sharply from zero to π . Thus, the interaction of resonant and nonresonant scattering waves will result in constructive and destructive interference phenomena located very close to each other, corresponding to maximum E_{\max} and minimum E_{\min} of the transmission (absorption), respectively. The width of the resonance is proportional to the distance between them $\Gamma \sim |E_{\max} - E_{\min}|$. In principle, they may be located very close to each other $E_{\max} \approx E_{\min}$, resulting in a very narrow resonance $\Gamma \approx 0$, corresponding to a very long-lived quasi-bound state. There are situations where a quasi-bound state may give rise a birth to a "bound state in the continuum" with infinite lifetime (Stillinger and Herrick, 1975), which can be characterized by a zero-width resonance $\Gamma = 0$. The existence of such states was claimed by von Neumann and Wigner (1929), where they suggested a method to explicitly construct one-dimensional potentials which support such kind of states. These potentials are quite artificial and cannot be realized in a realistic physical situation, but prove the concept. By applying Feshbach's theory of resonances to two overlapping Fano resonances, Friedrich and Wintgen (1985a,b) demonstrated that interference of several auto-ionizing levels of a Rydberg atom may "naturally" lead to formation of bound states in the continuum with anomalously narrow resonances.

Despite the complexity of the system where the Fano resonance was explained for the first time, it turned out to be an universal phenomenon, observed in various phys-

ical systems. Such universality of the Fano resonance comes from its underlying physics, i.e. interference phenomena. The aim of this Review is to demonstrate that the concept of the Fano resonance can be applied to control transport and scattering properties of nanoscale devices.

III. SCATTERING BY COMPLEX GEOMETRIES

A. General remarks

One of the necessary conditions for a Fano resonance to occur is the possibility for scattering waves to interfere. From geometrical point of view, this condition imposes coexistence of several paths for scattering waves to propagate. It can be achieved by local variation of degrees of freedom, which will ensure that propagating waves will interfere at the output. In this Section the basic geometries supporting the Fano resonance will be considered. They will provide an insight of the existence of the Fano resonances in more complex systems.

B. Fano-Anderson model

One of the simplest models which describes the physics and the main features of the Fano resonance is the so-called Fano-Anderson model (Mahan, 1993), which mimics the energy levels structures [see Fig. 3(a)] of the model proposed by Fano (1961).

We will use the simplified discrete model (Miroshnichenko *et al.*, 2005b), which can be described by the following Hamiltonian

$$H = \sum_n C \phi_n \phi_{n-1}^* + E_F |\psi|^2 + V_F \psi^* \phi_0 + \text{c.c.}, \quad (3)$$

where the asterisk denotes the complex conjugation. This model describes the interaction of two subsystems. One of the subsystems is a linear discrete chain with the complex field amplitude ϕ_n at site n which are coupled by nearest-neighbor coupling C . This system supports propagation of plane waves with dispersion $\omega_k = 2C \cos k$. The second subsystem consists of a single state ψ with the local energy value E_F . The interaction between these two subsystems is described by the coupling coefficient V_F from the state ψ to one site of the discrete chain ϕ_0 .

From the lattice Hamiltonian (3) the following dynamical equations can be derived

$$\begin{aligned} i\dot{\phi}_n &= C(\phi_{n-1} + \phi_{n+1}) + V_F \psi \delta_{n0}, \\ i\dot{\psi} &= E_F \psi + V_F \phi_0, \end{aligned} \quad (4)$$

where the dot stands for the derivative in time. Due to gauge invariance of Eqs. (4), the time dependence can be eliminated with the help of the ansatz

$$\phi_n(\tau) = A_n e^{-i\omega\tau}, \quad \psi(\tau) = B e^{-i\omega\tau}, \quad (5)$$

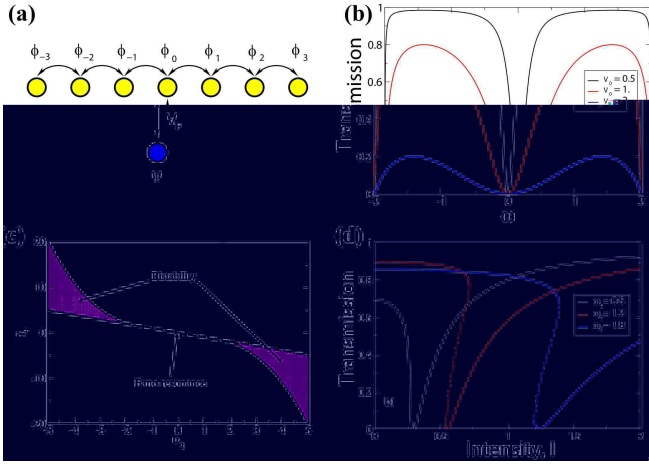


FIG. 7 (Color online) Fano-Anderson model as a discrete one-dimensional system with the single side-coupled defect. (a) The array of yellow circles corresponds to a linear chains, and the isolated blue circle is a defect. Arrows indicate the coupling between different states; (b) Transmission coefficient (10) for various values of the coupling coefficient V_F . Others parameters are $C = 1$, and $E_F = 0$; (c) Areas of bistability (solid color) of the nonlinear Fano resonance (dashed line) in the parameter space (α_k, γ_k) ; (d) Nonlinear transmission coefficient versus input intensity for various frequencies ω_q for $C = 1$, $V_F = 0.8$, $E_F = 0$ and $\lambda = 1$. Regions of bistability are indicated by dashed lines, corresponding to unstable solutions. Adapted from Miroshnichenko *et al.* (2005b).

giving the static set of equations

$$\begin{aligned}\omega A_n &= C(A_{n-1} + A_{n+1}) + V_F B \delta_{n0}, \\ \omega B &= E_F B + V_F A_0.\end{aligned}\quad (6)$$

For the scattering problem, the system (6) should be solved for frequencies from the propagation band $\omega = \omega_q$ with the following boundary conditions

$$A_n = \begin{cases} I e^{ikn} + \rho e^{-ikn}, & n < 0, \\ \tau e^{ikn}, & n > 0, \end{cases}\quad (7)$$

where I , r , and t have the meaning of the incoming, reflected and transmitted wave amplitudes, respectively.

The discrete state ψ can be easily eliminated from the system (6) as

$$B = \frac{V_F A_0}{\omega_k - E_F},\quad (8)$$

and the system of coupled equations (6) will be reduced to

$$\omega_k A_n = C(A_{n-1} + A_{n+1}) + \frac{V_F^2}{\omega_k - E_F} A_0 \delta_{n0}.\quad (9)$$

One of the interesting feature of the derived system (9) is that the strength of the scattering potential $V_F^2/(\omega_k - E_F)$ depends on the frequency of the incoming wave ω_q . If the self-energy of the discrete state lies inside the propagation

band of the linear chain $|E_F| < 2C$, the scattering potential may become infinitely large for certain frequency $\omega_k = E_F$, and nothing will be able to propagate through it. This resonant behavior of the scattering potential leads to the resonant suppression of the transmission, which is the main feature of the Fano resonance.

Transmission coefficient $T = |\tau/I|^2$ can be found by using the transfer matrix approach (Tong *et al.*, 1999), and expressed in the following form (Miroshnichenko *et al.*, 2005b)

$$T = \frac{\alpha_k^2}{\alpha_k^2 + 1},\quad (10)$$

where

$$\alpha_k = c_k(E_F - \omega_k)/V_F^2, \quad c_k = 2C \sin k.\quad (11)$$

Indeed, transmission vanishes at $\omega_k = E_F$, as was expected from the considerations above. Moreover, one may notice that the expression of the transmission coefficient (10) corresponds to the Fano formula (1), where α_k plays the role of the dimensionless energy, E_F is the resonant frequency, with zero asymmetry parameter. In other words, the discrete state may be considered as extra degree of freedom providing with an additional local path for scattering waves. It gives the possibility of waves propagating in the pure linear chain to interact with ones propagating through the discrete state. The latter undergoes resonant phase jump leading to interference phenomena.

The width of the resonance is defined as

$$\Gamma = \frac{V_F^2}{C \sin k_F},\quad (12)$$

where k_F is the wavenumber at the resonance, $E_F = \omega_{k_F}$. Since the width of the resonance is proportional to the coupling strength V_F , the weaker coupling, the narrower resonance is [see Fig. 7(b)]. It is known, that the width of a resonance is inversionally proportional to a Q-factor $\Gamma \sim 1/Q$.

C. Nonlinear Fano resonance

The discrete state becomes maximally excited

$$|B_{\max}|^2 = 4V_F^2 |I|^2 / \Gamma^2,\quad (13)$$

exactly at the resonance q_F , and the level of excitation is much higher compare to the continuum $|B_{\max}|^2 \gg |A_n|^2$. This feature can be used to study the nonlinear Fano resonances (Miroshnichenko *et al.*, 2005b; Zhang *et al.*, 2006) by introducing the Kerr-type nonlinearity to the discrete state only(6)

$$\omega B = E_F B + \lambda |B|^2 B + V_F A_0,\quad (14)$$

since at resonances the excitation of the rest of the system is relatively small, and the nonlinear effect there can be neglected.

The nonlinear transmission coefficient can be expressed in the following form (Miroshnichenko *et al.*, 2005b)

$$T = \frac{x^2}{x^2 + 1}, \quad (15)$$

where $x = -\cot \delta(k)$ is the function of the scattering phase $\delta(k)$, and satisfies the cubic equation

$$(x^2 + 1)(x - \alpha_k) - \gamma_k = 0, \quad (16)$$

with the parameter $\gamma_k = \lambda c_k^3 |I|^2 / V_F^4$. The nonlinear Fano resonances correspond to zero solutions $x = 0$ of Eq.(16), which take place when the condition $\gamma_k = -\alpha_k$ is satisfied [see Fig. 7(c)]. In the nonlinear regime, the transmission coefficient depends not only on the frequency of the incoming wave ω_k , but on its intensity $|I|^2$ as well. The presence of nonlinearity leads to the renormalization of the self-energy of the discrete state, and consequent intensity-dependent shift of the resonance. Miroshnichenko *et al.* (2005b) have analytically proved that the nonlinear Fano resonance exists for any value of the input intensity $|I|^2$ [see Fig. 7(c)]. It brings the tunability to the nonlinear Fano resonance, where it can be observed almost for any frequency by proper choosing the input intensity. Since at resonance the discrete state is highly excited, the nonlinear Fano resonance may take place for very low input powers. In general, there might exist up to three solutions of the cubic Eq.(16), which will result in bistable transmission [see Fig. 7(d)].

All of these make the nonlinear Fano resonance of a great importance for future practical applications, which will be discussed below on some particular examples.

The Fano-Anderson model (3) is the simplest one, which supports the Fano resonance, and allows to understand where it comes from. It allows to derive analytical results, and may serve as a guideline for the analysis of more complicated physical models associated with the Fano resonance. There are many variations of this model (Burioni *et al.*, 2005, 2006; Chakrabarti, 2006; Miroshnichenko and Kivshar, 2005a), which demonstrate some interesting properties of the Fano resonance, which might find their useful applications.

D. Extensions

The basic Fano-Anderson model (3) describes the resonant suppression of the transmission with symmetric lineshape, emphasizing the main property of the Fano resonance which is destructive interference (resonant reflection). But, the Fano resonance is very well known for its asymmetric lineshape, where both resonant suppression and resonant enhancement of the transmission are located close to each other. By introducing a defect $E_L \phi_L \delta_{nL}$ in the main array (4) [see Fig. 8(a)], both paths for scattering waves will lead to resonant phase

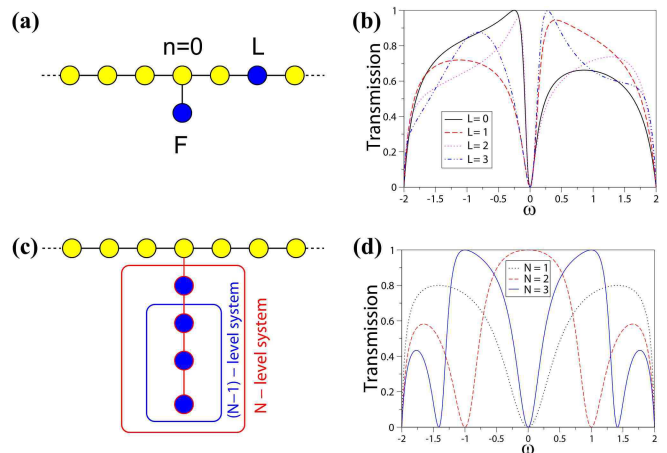


FIG. 8 (Color online) Variations of the Fano-Anderson model. (a) Schematic view of the Fano-Anderson model with additional defect in the main array. (b) Transmission coefficient of combined Fano and δ -like defect for different distances between them for parameters $C = 1$, $V_F = 0.5$, $E_F = 0$, and $E_L = 1$. (c) Schematic view of the Fano-Anderson model with locally coupled N -defect chainlet. (d) Transmission coefficient of the N -site chainlet. All site in the chainlet are identical with zero eigenfrequencies $E_m = 0$, and the couplings are $C = V_m = 1$. Adapted from Miroshnichenko and Kivshar (2005a).

accumulations. As a result, both constructive and destructive interference phenomena may coexist, generating asymmetric transmission profiles [see Fig. 8(b)]. As one might notice in Fig. 8(b) the sign of asymmetry alternates (which is known as q -reversal (Kim and Yoshihara, 1993)) with the distance between the side-coupled defect and the defect in the main array

$$\text{sign}(\omega_{T_{max}} - \omega_{T_{min}}) = (-1)^l. \quad (17)$$

Moreover, the maximum of the transmission does not reach one in some cases $\omega_{T_{max}} < 1$ as a result of incomplete constructive interference due additional phase accumulation during propagation distance between two defects. But it does not affect the destructive interference condition. This example indicates the underlying difference between constructive and destructive interference phenomena of the Fano resonances.

As the second example we consider the scattering in a discrete networks composed of an infinite array of interacting elements coupled locally to a finite chainlet, consisting of N degrees of freedom (Burioni *et al.*, 2005; Miroshnichenko and Kivshar, 2005a) [see Fig. 8(c)]. Each degree of freedom provides with an additional local path for scattering wave to propagate, which may lead to a variety of interference phenomena. This finite chainlet can be considered as an approximation of a complex N -level system, such as a quantum dot, for example. Miroshnichenko and Kivshar (2005a) revealed that, in general, there are exactly N total reflection and $N - 1$ total transmission resonances [see Fig. 8(d)]. Each

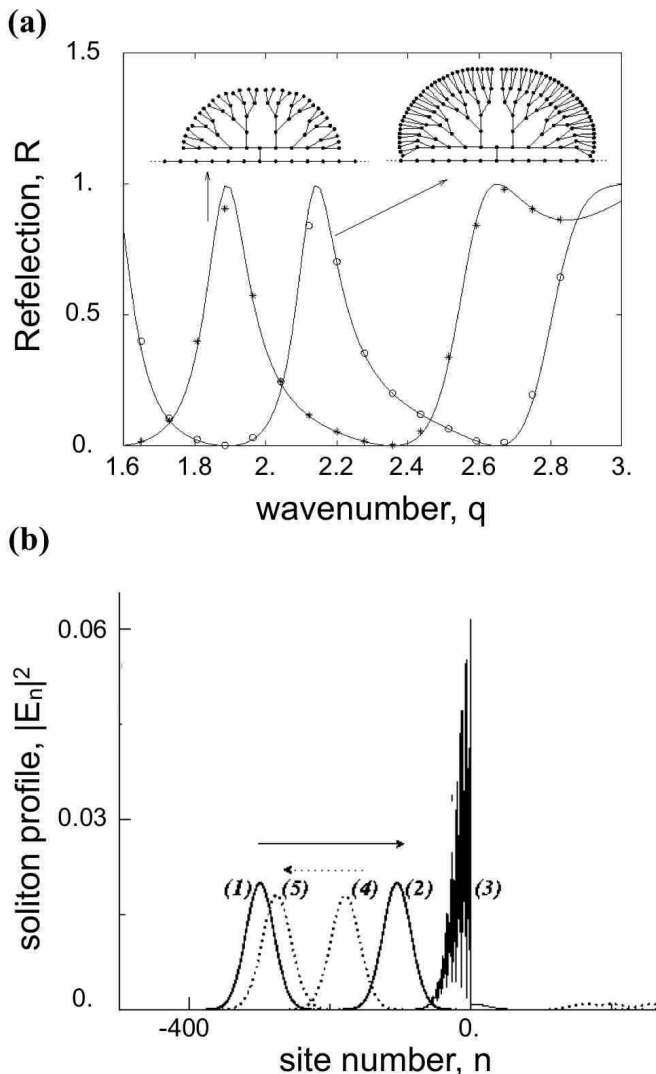


FIG. 9 Resonant reflection of a soliton in topological networks (a) The reflection coefficient versus wavenumber k for two Cayley trees of length $M = 5$ (line) and $M = 6$ (line) attached to the discrete array. Empty circles and stars correspond to direct numerical simulations of the soliton propagation. (b) Example of the soliton reflection by a Fano-like defect. From Burioni *et al.* (2005).

frequency of the total reflection corresponds to eigenfrequency of the N -level subsystem, and each total transmission corresponds to eigenfrequency of the $(N-1)$ -level subsystem, indicated in Fig. 8(c). In other words, at resonances some particular eigenstates of the side-coupled chainlet are excited. It allows us to make some intriguing analogy by considering the scattering by a finite chainlet as a playing on 'Fano-flute', where each note corresponds to resonantly excited eigenstate.

1. Resonant reflection of solitons

Many other inhomogeneous networks were considered to design various topological filters (Burioni *et al.*, 2005, 2006). One can even plant Cayley trees into a discrete array and gather very well pronounced Fano resonances [see Fig. 9(a)]. It was demonstrated that the results of the plane wave analysis are valid for soliton scattering as well (Miroshnichenko *et al.*, 2003; Wulf and Skalozub, 2005), (Burioni *et al.*, 2005, 2006), where all elements of the discrete networks are nonlinear. A soliton can be considered as a superposition of linear plane waves with wavenumbers from some interval, determining its spectral width Δk_S . The presence of a nonlinearity leads to interaction between various plane waves, which may affect the scattering process.

There are two characteristic time scales important for scattering of solitons. One of them is the interaction time of the soliton with the defect τ_{int} , which is inversely proportional to its spectral width Δk_S and velocity v . Another one corresponds to dispersion of plane waves inside the soliton τ_{disp} (Miroshnichenko *et al.*, 2003). For fast propagating solitons the interaction time is much smaller than dispersion $\tau_{\text{int}} \ll \tau_{\text{disp}}$. As a result, under this condition the soliton can be considered as a set of noninteracting plane waves. The scattering of soliton can be described as a scattering of each wave component governed by the linear model. Therefore, it is possible to achieve resonant transmission and backscattering (Fano resonance) of solitons by various defects (Miroshnichenko *et al.*, 2003), (Burioni *et al.*, 2005, 2006) [see Fig. 9(b)]. In the opposite limit, when the interaction between soliton and the defect is much larger than dispersion $\tau_{\text{int}} \gg \tau_{\text{disp}}$, the wave-wave interaction becomes very important during scattering process. Since this interaction may lead to dephasing between individual plane waves, the interference phenomena will be affected, in particular the Fano resonance, as it relies on keeping the phase coherence in the course of the scattering process.

2. Light scattering in quadratic waveguide arrays

Another interesting example is the light scattering in array of channel waveguides with quadratic nonlinearity generated by periodic poling of several waveguides (Miroshnichenko *et al.*, 2005a). When the matching conditions are satisfied, the fundamental-frequency (FF) mode with the frequency ω can generate parametrically the second-harmonic (SH) wave with the frequency 2ω [see Fig. 10(a)], so that such a structure with several poled waveguides may behave as a nonlinear defect with localized quadratic nonlinearity (Iwanow *et al.*, 2004). The waveguide array can be described by a discrete model of weakly coupled linear waveguides with several waveguides having a quadratic nonlinear response (Iwanow *et al.*, 2004; Miroshnichenko *et al.*,

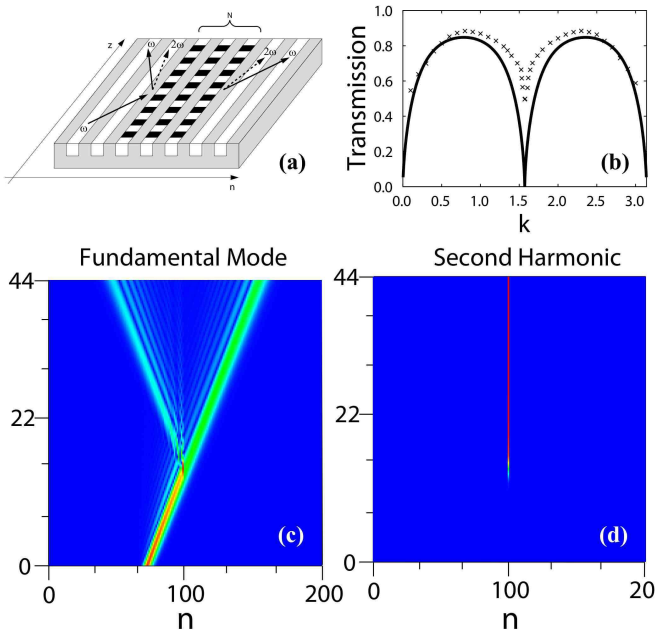


FIG. 10 (Color online) Light scattering in array of channel waveguides with quadratic nonlinearity. (a) Schematic view of a one-dimensional array of channel waveguides with nonlinear defects, created by periodic poling. Arrows indicate the scattering process. (b) Comparison of the transmission coefficients of the plane waves (solid line) and Gaussian beam (crosses). Bottom: Example of the Gaussian beam scattering by single nonlinear defect showing the resonant reflection part of the beam of the fundamental frequency (c), and resonantly excitation of the second harmonic (d). Adapted from Miroshnichenko *et al.* (2005a).

2005a), which is very similar to the Fano-Anderson model (4). The fundamental mode in this case can be considered as a continuum of propagating states, while the generated second harmonic can be either extended or effectively localized depending on the phase matching condition (Miroshnichenko *et al.*, 2005a). In the latter case excited second harmonic will act as a discrete state in the continuum, leading to the appearance of the Fano resonance in the transmission [see Fig. 10(b)]. Results of the direct numerical simulations of the Gaussian beam scattering are in a good agreement with the plane wave analysis [see Fig. 10(b)]. Figures 10(c,d) show evolution of the fundamental and second harmonic of the Gaussian beam scattering at the resonance. One may clearly see that part of the fundamental harmonic of the Gaussian beam is been resonantly reflected by a single nonlinear defect in the middle [see Fig. 10(c)]. Due to the fact that the spectral width of the Gaussian beam is larger than the width of the resonance some part of the beam still propagates through the defect. During the scattering the second harmonic is been resonantly excited [see Fig. 10(d)]. The interesting feature is that when two parts of the beam scattered away from the defect and do not interact with it anymore, the second harmonic persists being highly excited in a self-sustain form. It can

be used as a very effective method for second harmonic generation in optics by means of the Fano resonance.

IV. SCATTERING BY TIME-PERIODIC POTENTIALS

A. General remarks

With the development of the ultrahigh-intensity lasers much attention was devoted to the problem of wave scattering by various time-periodic potentials. They appear to be very attractive due several reasons: they can be relatively easy generated, and what is more important they provide with an opportunity to dynamically tune scattering properties. Many interesting effects were demonstrated in comparison to the static scattering potentials (Emmanouilidou and Reichl, 2002; Li and Reichl, 1999; Martinez and Reichl, 2001). The most peculiar one is the possibility of total resonant reflection of waves (Bagwell and Lake, 1992). The analysis of some simplified problems reveals the analogy to the Fano resonance. Indeed, the underlying physics of this phenomenon is that a time-periodic scattering potential induces several harmonics. In general, these harmonics can be either inside or outside the propagation spectrum, generating "open" and "closed" channels, respectively. The presence of such dynamically generated channels is equivalent to a local increase of spatial dimensionality, discussed in the previous Section. In other words, each channel generates an alternative pathway for the scattering wave to propagate. Open channels correspond to continua, and closed ones to discrete states of Fano's approach. As a result, it may lead to resonant interference effects in terms of the Fano resonances.

Below the detailed example of scattering by time-periodic scattering potential originated from a nonlinearity in a spatially homogeneous system will be considered. The approach is quite general, and can be easily applied to similar problems.

B. Scattering by Discrete Breathers

Discrete Breathers (DBs) are known as time-periodic and spatially localized solutions of nonlinear discrete systems (Aubry, 1997; Flach and Willis, 1998; MacKay and Aubry, 1994). They originate from a peculiar interplay between nonlinearity and discreteness. They are similar to solitons in nonlinear systems, with an extra property being periodic in time with the frequency Ω_b . The spatial discreteness leads to finite frequency spectrum of small amplitude plane waves ω_k . Due to nonlinearity the frequency of the DB Ω_b and its localization length are amplitude-dependent, making them tunable. One of the necessary condition for a DB to exist is that all multiples of the breather frequency should lie outside the propagation band of small amplitude plane waves $n\Omega_b \neq \omega_k$. Otherwise, spurious resonances will lead to delocalization of DB (Flach and Willis, 1998).

The tunability of DBs allows to escape all those resonances, and, consequently, to stabilize the DB state. DBs were detected and studied experimentally in interacting Josephson junction systems (Binder *et al.*, 2000; Trías *et al.*, 2000), coupled nonlinear optical waveguides (Eisenberg *et al.*, 1998), lattice vibration in crystals (Swanson *et al.*, 1999), anti-ferromagnetic structures (Schwarz *et al.*, 1999), micro-mechanical cantilever arrays (Sato *et al.*, 2003), Bose-Einstein condensates loaded on optical lattices (Eiermann *et al.*, 2004), and many others.

It has been recently theoretically demonstrated that scattering of small amplitude plane waves by DBs may exhibit Fano-like asymmetric profiles, with total suppression of the transmission $T = 0$ (Flach *et al.*, 2003a,b; Kim and Kim, 2000, 2001; Lee and Kim, 2000b; Miroschnichenko *et al.*, 2005c). One of the crucial condition allowing a total reflection in these systems is the existence of so-called closed channels in addition to the open ones. In general, each harmonic of the DB generates a scattering channel, which is closed due nonresonant condition of the DB (Flach *et al.*, 2003a). Scattering waves may propagate in the open channel, while they decay in closed ones. One may consider each closed channel as a side-coupled defect in the Fano-Anderson model. As a result, in general, the scattering potential generated by a D may lead to existence of the Fano-resonances in the transmission coefficient. Below we will demonstrate the applicability of this kind of analogy on a particular example.

We will perform our analysis wave scattering by DBs in the discrete nonlinear Schrödinger equation (DNLS) (Flach *et al.*, 2003b), which has been used frequently to study breather properties due to its tractable form.

The equations of motion for the DNLS are given by

$$i\dot{\Psi}_n = C(\Psi_{n+1} + \Psi_{n-1}) + |\Psi_n|^2\Psi_n, \quad (18)$$

where n is an integer labeling the lattice sites, Ψ_n is a complex scalar variable and C describes the nearest neighbor interaction (hopping) on the lattice. The last term in (18) corresponds to the Kerr type nonlinearity. For small amplitude waves $\Psi_n(t) = \epsilon e^{i(\omega_k t - kn)}$ the dispersion relation

$$\omega_k = -2C \cos k \quad (19)$$

follows from Eq.(18).

One of the peculiarities of the DNLS equations is that they support DB solutions with the single harmonic due to gauge invariance of the equations (18) of the following form

$$\hat{\Psi}_n(t) = \hat{A}_n e^{-i\Omega_b t}, \quad \hat{A}_{|n| \rightarrow \infty} \rightarrow 0, \quad (20)$$

where the time-independent amplitude \hat{A}_n can be taken real valued, and the breather frequency $\Omega_b \neq \omega_k$ is some function of the maximum amplitude \hat{A}_0 . The spatial localization is given by an exponential law $\hat{A}_n \sim e^{-\lambda|n|}$

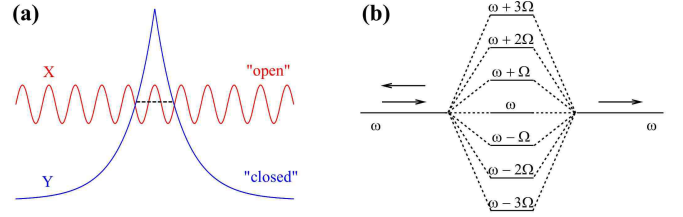


FIG. 11 (Color online) Spectral representation of time-periodic scattering potentials. (a) Schematic view of the open channel X and closed channel Y from the Eqs. (24-25). The dashed line indicates the localized state of the closed channel Y inside the open channel X ; (b) Schematic view of the virtual states, generated by number of harmonics of the time-periodic scattering potential.

where $\cosh \lambda = |\Omega_b|/2C$. Thus the breather can be approximated as a single-site excitation if $|\Omega_b| \gg C$. In this case the relation between the single-site amplitude \hat{A}_0 and Ω_b becomes $\Omega_b = \hat{A}_0^2$. In the following, breather amplitudes for $n \neq 0$, i.e. $\hat{A}_{n \neq 0} \approx 0$ will be neglected, since $\hat{A}_{\pm 1} \approx (C/\Omega_b)\hat{A}_0 \ll A_0$.

By perturbing the breather solution with small fluctuations $\phi_n(t)$

$$\Psi_n(t) = \hat{\Psi}_n(t) + \phi_n(t) \quad (21)$$

and substituting this into (18) gives, after linearization, the following set of equations:

$$i\dot{\phi}_n = C(\phi_{n+1} + \phi_{n-1}) + \Omega_b \delta_{n,0} (2\phi_0 + e^{-2i\Omega_b t} \phi_0^*) \quad (22)$$

with $\delta_{n,m}$ being the Kronecker symbol. As one may see, a DB generates a scattering potential that consists of two parts: a static one, which depends on the breather intensity only 'DC' $\sim \Omega_b = \hat{A}_0^2$, and dynamical one, which depends on time as well 'AC' $\sim \Omega_b e^{-2i\Omega_b t}$. Note here, that in the dynamical part of the scattering potential the complex conjugation of the scattering amplitude ϕ^* is also involved. By using the substitution

$$\phi_n(t) = X_n e^{i\omega t} + Y_n^* e^{-i(2\Omega_b + \omega)t}, \quad (23)$$

it is possible to eliminate the time dependence in (22)

$$\begin{aligned} -\omega X_n &= C(X_{n+1} + X_{n-1}) + \Omega_b \delta_{n,0} (2X_0 + Y_0^*) \\ (2\Omega_b + \omega) Y_n &= C(Y_{n+1} + Y_{n-1}) + \Omega_b \delta_{n,0} (2Y_0 + X_0), \end{aligned}$$

where X_n and Y_n are complex amplitudes. The form of Eq. (24) suggests that the DB scattering potential can be decomposed onto two interacting channels X_n and Y_n . For scattering waves the frequency ω should be chosen from the propagation band ω_k . As a result, the channel X_n supports extended waves, while for Y_n channel does not, since it's carrying frequency $-(2\Omega_b + \omega_q)$ is outside the propagation band ω_k (Flach *et al.*, 2003b) [see Fig. 11(a)]. It allows to name them as open channel X_n and closed channel Y_n .

Instead of solving (24), it is useful to consider more general set of equations

$$\begin{aligned} -\omega_k X_n &= C(X_{n+1} + X_{n-1}) - \delta_{n,0}(V_x X_0 + V_a X_1) \\ (\Omega + \omega_k) Y_n &= C(Y_{n+1} + Y_{n-1}) - \delta_{n,0}(V_y Y_0 + V_a X_0), \end{aligned} \quad (25)$$

which can be reduced to Eq. (24) with the following parameters $\Omega = 2\Omega_b$ and $V_x = V_y = 2V_a = -2\Omega_b$. In the present form, one may clearly see the analogy between the system (25) and the Fano-Anderson model (6), where the open channel X_n correspond to a continuum, and the closed channel Y_n corresponds to a discrete level (side-coupled defect). Indeed, for decoupled system (25) with $V_a = 0$ the closed channel Y_n possesses exactly one localized eigenstate

$$Y_n = Y e^{-\lambda|n|}. \quad (26)$$

with corresponding eigenfrequency

$$\omega_L^{(y)} = -\Omega + \sqrt{V_y^2 + 4C^2}. \quad (27)$$

The transmission coefficient can be computed by using the transfer matrix approach (Tong *et al.*, 1999) with the boundary conditions $X_{N+1} = \tau e^{ik}$, $X_N = \tau$, $Y_{N+1} = D/\kappa$, $Y_N = D$ for the right end and $X_{-N-1} = 1 + \rho$, $X_{-N} = e^{ik} + \rho e^{-ik}$, $Y_{-N-1} = F$, $Y_{-N} = \kappa F$ for the left one. Here τ and ρ are the transmission and reflection amplitudes with $T = |\tau|^2 = 1 - |\rho|^2$. F and D describe the exponentially decaying amplitudes in the closed Y -channel, where the degree of localization is connected with the coefficient $\eta \equiv e^\lambda$

$$\eta = \frac{1}{2C} \left[\Omega + \omega_k + \sqrt{(\Omega + \omega_k)^2 - 4C^2} \right]. \quad (28)$$

The transmission coefficient can be written as (Flach *et al.*, 2003b)

$$\begin{aligned} T &= \frac{4 \sin^2 k}{\left(2 \cos k - a - \frac{d^2 \eta}{2 - b\eta} \right)^2 + 4 \sin^2 k}, \\ a &= \frac{-\omega_k + V_x}{C}, \quad b = \frac{\Omega + \omega_k + V_y}{C}, \quad d = \frac{V_a}{C}. \end{aligned} \quad (29)$$

From Eq. (29) one may see that transmission coefficient vanishes, when the condition

$$2 - b\eta = 0 \quad (30)$$

is satisfied. After some algebra this condition may be simplified to the following one

$$\omega_k = \omega_L^{(y)}, \quad (31)$$

which has a very clear physical meaning: total reflection takes place when a local mode, originating from the closed Y -channel, resonates with the plane wave spectrum ω_k of the open X -channel. The only condition is that the interaction between these channels is nonzero

$V_a \neq 0$. Remarkably, the resonance position does not depend on the actual value of V_a , so there is no renormalization. The existence of local modes which originate from the X -channel for nonzero V_x and possibly resonate with the closed Y -channel is evidently not of any importance. This resonant total reflection is exactly the Fano resonance, as it is unambiguously related to a local state resonating and interacting with a continuum of extended states. The fact that the resonance is independent of V_a is due to the assumed local character of the coupling between the local mode (originating from the Y -channel) and the open channel. If this interaction has some finite localization length by itself, then the resonance condition (31) may be renormalized. A more physical formulation for the condition of absence of significant renormalization of the position of the resonance is that the wavelength of the propagating wave is large compared to the extension of the space region where the channel coupling occurs (Flach *et al.*, 2003a).

The analysis above clearly demonstrates that the scattering by a DB should exhibit the Fano resonances. Moreover, it gives us a recipe to find the position of the resonance. Namely, one should calculate the localized states of closed channels decoupled from the open one (Flach *et al.*, 2003a,b). When this coupling is weak enough, the Fano resonances will take place exactly at the eigenfrequencies of those localized states. For stronger coupling one should expect the renormalization of the position of the resonances, but still this kind of analysis sheds a light on the origin of those resonances in rather complicated systems. In general, there is an infinite number of harmonics of the DB, which generate an infinite number of closed channels. Not all of them contribute to the scattering process, and it is possible use a finite number of them.

The approach described above is quite generic and can be applied to the scattering through any type of oscillating barriers, self-induced (like DBs) or parametrically driven (by external forces) (Bagwell and Lake, 1992; Boese *et al.*, 2000; Emmanouilidou and Reichl, 2002; Kim, 2002; Li and Reichl, 1999; Longhi, 2006; Martinez and Reichl, 2001). All of them produce similar scattering potentials with an open and a number of closed channels for small amplitude scattering waves. The oscillating frequency generates a set of virtual states [see Fig. 11(b)] given a possibility for various interference phenomena, in particular, the resonant destructive inference, i.e. the Fano resonances.

C. Possible applications

Below we will consider two physical realizations where the Fano resonances can be experimentally observed in the scattering by DBs.

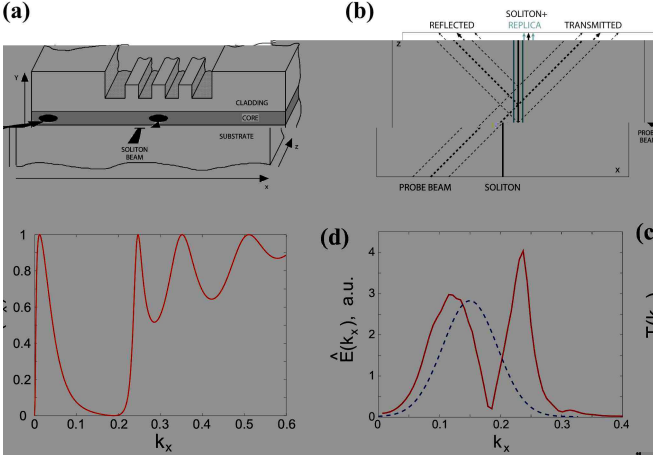


FIG. 12 (Color online) Light scattering by optical solitons. (a) Sketch of the scattering setup by an optical soliton in a one-dimensional waveguide array; The soliton beam is sent along the z -axis, while the probe beam propagates in the xz -plane at some angle to the soliton. (b) top view of the scattering process; (c) transmission coefficient vs k_x for the plane waves under oblique incidence. There is total suppression of the transmission near $k_x \approx 0.181$; (d) Fourier spectrum of the incident (dashed line) and transmitted (solid line) beams. One may clearly see the absence of the resonant frequency [see plot (c)] in the spectrum. Adapted from Flach *et al.* (2005).

1. Light scattering by optical solitons

The first example is the resonant light scattering by optical solitons in a slab waveguide with inhomogeneous refractive index core (Flach *et al.*, 2006, 2005). The soliton is generated in a nonlinear planar waveguide by a laser beam injected into the slab along the z -direction [see Fig. 12(a)]. The soliton beam is confined in the y -direction by the total internal reflection mechanism. The localization in x -direction is achieved by the balance between linear diffraction and an instantaneous Kerr-type nonlinearity. The analogy with the discussed above scattering problem by time-periodic potentials comes from the possibility to interpret the spatial propagation along the z -direction as an artificial time (Agrawal, 1995). Thus, the propagation constant of the soliton can be considered as the frequency of the breather. The evolution of the soliton envelope function satisfies the nonlinear Schrödinger equation (NLS), continuous analog of the Eq. (18) (Flach *et al.*, 2005). The analysis of the scattering problem as very similar to discussed above one. Figure 12(c) shows the dependence of the transmission coefficient for oblique incident light for various k_x wavenumber. It indicates the existence of the Fano resonance for plane waves at $k_x \approx 0.181$, where the transmission coefficient vanishes. This result has been confirmed by direct numerical simulations of the small-amplitude wavepacket scattering by an optical soliton (Flach *et al.*, 2006) [see Fig. 12(b)]. The Fourier spectrum of the transmitted wavepacket reveals that the resonant wavenumber

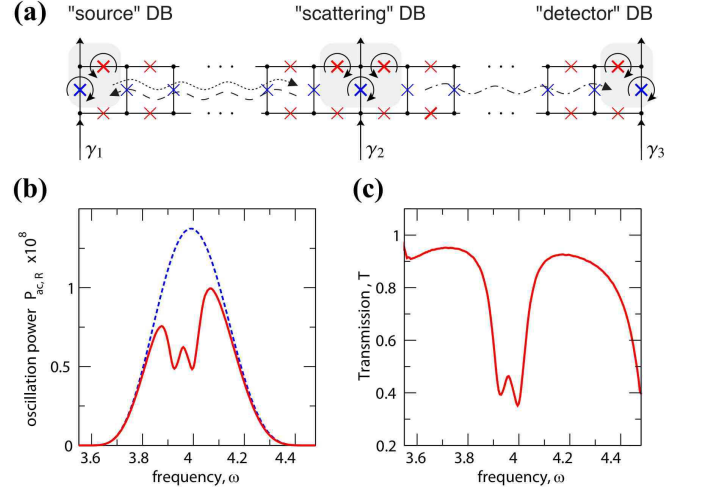


FIG. 13 (Color online) Plasmon scattering by discrete breathers in Josephson junction ladders. (a) Schematic setup for measuring plasmon scattering by a DB in JjLs with the use of controlled bias currents γ_i . (b) oscillating power $P_{ac,R}$ at the right end with (red solid line) and without (blue dashed line) DB; (c) transmission coefficient T , derived from (b) by using Eq. (32). Adapted from Miroshnichenko *et al.* (2005c).

$k_x \approx 0.181$ was filtered out from the initial wavepacket [see Fig. 12(d)]. Such a spectral hole burning effect can be used a characteristic feature for detection of the Fano resonance in real experimental setup.

2. Plasmon scattering in Josephson junction ladders

The second example is the plasma wave scattering by DBs in Josephson junction ladders (JJLs). JJLs are formed by an array of small Josephson junctions that are arranged along the spars and rungs of a ladder [see Fig. 13(a)]. Each junction consists of two small weakly coupled superconducting islands. The dynamical state of a junction is described by the phase difference $\phi(t)$ (Josephson phase) of the superconducting order parameters of the two islands. When the difference does not vary in time $\phi(t) = const$, the junction is in the superconducting state. Otherwise, the junction is in a resistive state with a nonzero voltage drop $V \propto \dot{\phi}(t)$. As it was demonstrated experimentally JJLs support dynamic localized states (or simply DBs) (Binder *et al.*, 2000; Trías *et al.*, 2000). A breather is characterized by a few junctions being in the resistive state $\langle \dot{\phi} \rangle \neq 0$ while the others reside in the superconducting state $\langle \dot{\phi} \rangle = 0$. The frequency of a DB is proportional to the average voltage drop across the resistive junctions $\Omega_b \propto \langle \dot{\phi} \rangle$. Miroshnichenko *et al.* (2005c) have recently proposed an interesting experimental setup to measure the Fano resonances in the transmission line. Linear waves are generated in a JJL with open ends by applying locally a time-periodic current $\gamma_1(t) = \gamma_{ac} \cos(\omega t)$. The local current acts as a local parametric drive. It excites a tail of junctions that oscil-

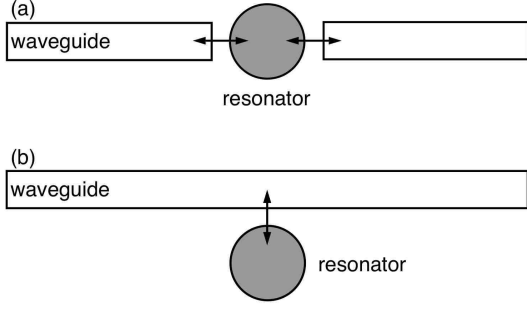


FIG. 14 Schematic for (a) a waveguide directly coupled to a cavity and (b) a waveguide side-coupled to a cavity.

late with frequency ω . This tail extends into the ladder and decays exponentially in space. To monitor the linear wave propagation in the system the time-averaged oscillation power $P_{ac,n} = \langle \dot{\phi}_n^2 \rangle$ is used. The transmission coefficient can be obtained by relating the oscillation power at the right boundary with and without presence of a DB in the system

$$T = \frac{P_{ac,R}(\text{with DB})}{P_{ac,R}(\text{without DB})}. \quad (32)$$

Figures 13(b,c) show the presence of the resonant suppression of the transmission coefficient for particular frequencies ω . Analysis in Ref. (Miroshnichenko *et al.*, 2005c) reveals that they are exactly Fano resonances, originated from the localized states of the closed channels of the scattering DB.

V. LIGHT PROPAGATION IN PHOTONIC DEVICES

A. General remarks

Optical microcavity structures are of great current interests for device applications, and many of these structures involved coupling of one or several cavities to a waveguide. Such waveguide-cavity systems can naturally exhibit Fano resonances with high quality factors, and they can be used for optical modulations and switching. The on/off switching functionality can be realized by shifting the resonant frequency either toward or away from the signal frequency.

The basic geometry of a waveguide-cavity system that demonstrate a sharp Fano resonance has been introduced and analyzed in Refs. (Haus and Lai, 1991; Xu *et al.*, 2000), and it consists of a waveguide coupled to a cavity (or resonator). In general, two-port photonic devices based upon waveguide-resonator interaction can be presented in two geometries, as shown in Figs. 14(a,b). The first configuration is based on a direct-coupling geometry (Marin Soljačić and Joannopoulos, 2002), and the second geometry is a waveguide side coupled with a single-mode cavity (Xu *et al.*, 2000; Yanik *et al.*, 2003a).

Such structures can be made tunable by adding some cavities with nonlinear response or by employing an external control. Below, we review the basic properties of the simplest waveguide-cavity systems, and also discuss several generalizations including all-optical switching structures based on the concepts of Fano resonances.

B. Green's function formalism

The Green's function approach (Mingaleev and Kivshar, 2002a,b) allows to obtain very accurate results in comparison to the time-consuming direct numerical finite-difference time-domain (FDTD) simulations, even for rather complex geometries of the waveguide-cavity systems. To derive the corresponding equations, we take into account the explicit temporal dependencies which will allow us to study the pulse propagation and scattering.

We consider a photonic crystal created by a periodic square lattice of infinite cylindrical rods parallel to the z axis. We neglect the material dispersion and assume the dielectric constant $\epsilon(\vec{r})$ to be periodic in two transverse directions, $\vec{r} = (x, y)$. The evolution of the E -polarized electric field propagating in the (x, y) plane is governed by the scalar wave equation

$$\nabla^2 E_z(\vec{r}, \tau) - \frac{1}{c^2} \partial_\tau^2 [\epsilon(\vec{r}) E_z(\vec{r}, \tau)] = 0, \quad (33)$$

where $\nabla^2 = \partial_x^2 + \partial_y^2$. We assume that the light field propagating in such structures can be separated into fast and slow components, $E_z(\vec{r}, \tau) = e^{-i\omega\tau} E(\vec{r}, \tau|\omega)$, where $E(\vec{r}, \tau|\omega)$ is a slowly varying envelope of the electric field, i.e. $\partial_\tau^2 E(\vec{r}, \tau|\omega) \ll \omega \partial_\tau E(\vec{r}, \tau|\omega)$. This allows to simplify Eq. (33) to the following form

$$\left[\nabla^2 + \epsilon(\vec{r}) \left(\frac{\omega}{c} \right)^2 \right] E(\vec{r}, \tau|\omega) \simeq -2i\epsilon(\vec{r}) \frac{\omega}{c^2} \frac{\partial E(\vec{r}, \tau|\omega)}{\partial \tau} \quad (34)$$

Both, the straight waveguide and side-coupled cavity are created by introducing defect rods into a perfect two-dimensional periodic structure, as shown in Fig. 14(a). Therefore, the dielectric constant can be represented as a sum of two components, describing the periodic and defect structures $\epsilon(\vec{r}) = \epsilon_{pc} + \delta\epsilon$. We employ the Green's function of the two-dimensional periodic structure without defects, and rewrite Eq. (34) in the integral form

$$E(\mathbf{x}, \tau|\omega) = \int d^2\mathbf{y} G(\mathbf{x}, \mathbf{y}|\omega) \hat{L} E(\mathbf{y}, \tau, \omega), \quad (35)$$

where we introduce the linear operator

$$\hat{L} = \left(\frac{\omega}{c} \right)^2 \delta\epsilon(\vec{r}) + 2i\epsilon(\vec{r}) \frac{\omega}{c^2} \frac{\partial}{\partial \tau}, \quad (36)$$

and consider the time evolution of the slowly varying envelope as a perturbation to the steady state.

The defect rods introduced into the periodic structure can formally be described as follows:

$$\delta\epsilon(\vec{r}) = \sum_{n,m} \left[\delta\epsilon_{m,n}^{(0)} + \chi^{(3)} |E(\mathbf{x}, \tau|\omega)|^2 \right] \theta(\mathbf{x} - \mathbf{x}_{n,m}), \quad (37)$$

where we use the θ -function to describe the position of a defect rod at site n, m , where $\theta(\mathbf{x}) = 1$ for \mathbf{x} inside the defect rods, and $\theta(\mathbf{x}) = 0$ otherwise, and $\delta\epsilon_{m,n}^{(0)}$ is the variation of the dielectric constant of the defect rod

(m, n). Importantly, this approach allows us to incorporate a nonlinear response in a straightforward manner, which is assumed to be of the Kerr type being described by the term $\chi^{(3)} |E|^2$.

Substituting Eq. (37) into the integral equation (35) and assuming that the electric field does not change inside the dielectric rods, we can evaluate the integral at the right hand side of Eq. (35) and derive a set of *discrete nonlinear equations*

$$i\sigma \frac{\partial}{\partial \tau} E_{n,m} - E_{n,m} + \sum_{k,l} J_{n-k,m-l}(\omega) (\delta\epsilon_{k,l}^{(0)} + \chi^{(3)} |E_{k,l}|^2) E_{k,l} = 0, \quad (38)$$

for the amplitudes of the electric field $E_{n,m}(\tau|\omega) = E(\mathbf{x}_{n,m}, \tau|\omega)$ calculated at the defect rods. The parameters σ and $J_{k,l}(\omega)$ are determined by using the corresponding integrals of the Green's function, where the whole information about the photonic crystal dispersion is now hidden in their specific frequency dependencies, which can be found in Refs. (Mingaleev and Kivshar, 2001; Mingaleev *et al.*, 2006). In this way, the Green's function needs to be calculated only once for a given photonic structure, e.g. by employing the approach outlined in Ref. (Ward and Pendry, 1998), and then it can be used to study any photonic circuit in that structure.

For the simple system when the photonic crystal has a waveguide side coupled to a single defect see Fig. 15(a)], the problem describes a discrete system studied earlier [see Fig. 15(b)], and the transmission demonstrates a Fano resonance for reflection [see Fig. 15(c)], analyzed in details in Refs. (Mingaleev *et al.*, 2006; Miroshnichenko *et al.*, 2005b).

In a general case, the effective interaction between defect rods is long-range (Mingaleev and Kivshar, 2002b; Mingaleev *et al.*, 2000) and, we should have $L > 1$. However, the coupling strength decays exponentially with the distance and, as a result, for coupled-resonators optical waveguides the specific discrete arrays with nearest-neighbor interactions (at $L = 1$) gives already an excellent agreement with direct FDTD simulations (Mingaleev and Kivshar, 2002b).

C. Waveguide-cavity systems

1. Defects in the waveguide

These two basic geometries shown in Figs. 14(a,b) can be further improved by placing partially reflecting elements into the waveguides (Fan, 2002; Khelif *et al.*, 2003); these elements can allow creating sharp and asymmetric response line shapes. In such systems, the trans-

mission coefficient can vary from 0% to 100% in a frequency range narrower than the full width of the resonance itself.

To illustrate the effect of defects, Fan (Fan, 2002) simulated the response of the structure shown in Fig. 16(a) using a FDTD scheme with the perfectly matched layer boundary conditions. A pulse is excited by a monopole source at one end of the waveguide. The transmission coefficients are then calculated by Fourier transforming the amplitude of the fields at the other end, and are shown as a solid line in Fig. 16(b). In comparison, the transmission spectra for the same structure, except without the two small cylinders in the waveguide, is shown by a dashed line.

Importantly, no detailed tuning of either the resonant frequency or the coupling between the cavity and the waveguide is required to achieve the asymmetric line shapes. Also, since the reflectivity of the partially reflecting elements need not to be large, the underlying physics here differs from typical coupled-cavity systems, and resembles the Fano resonances involving interference between a continuum and a discrete level.

2. Sharp bends as Fano resonances

One of the most fascinating properties of photonic crystals is their ability to guide electromagnetic waves in narrow waveguides created by a sequence of line defects, including light propagation through extremely sharp waveguide bends with nearly perfect power transmission (Lin *et al.*, 1998; Mekis *et al.*, 1996). It is believed that the low-loss transmission through sharp waveguide bends in photonic crystals is one of the most promising approaches to combine several devices inside a compact nanoscale optical chip.

Interestingly, high transmission through sharp bends in photonic crystal waveguides can be described by a simple model of the Fano resonance where

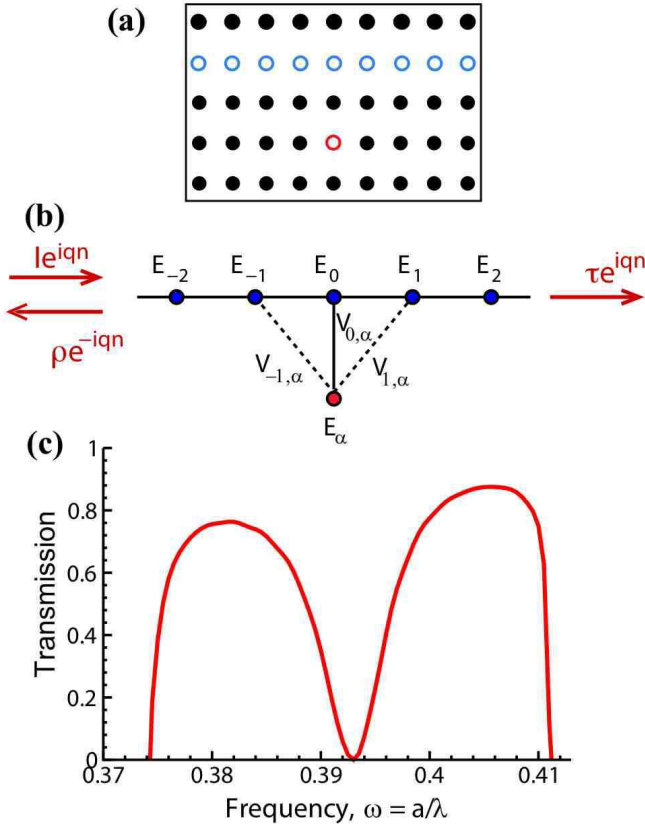


FIG. 15 Schematic view of (a) photonic crystal waveguide with an isolated side-coupled cavity, and (b) effective discrete system. (c) Typical profile of the Fano resonance.

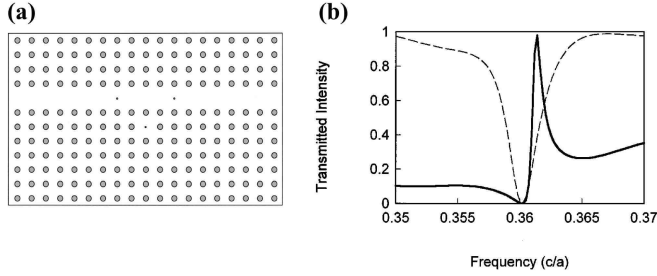


FIG. 16 Light propagation in photonic crystal waveguide with side-coupled cavity. (a) Photonic crystal waveguide formed by removing a single row of rods. Within the line defect there are two smaller rods. A point defect, created by reducing the radius of a single rod, is placed away from the waveguide. (b) Transmission spectra through the structure (a) with (solid) and without (dashed) of the two defects in the waveguide. From Fan (2002).

the waveguide bend plays a role of a specific localized defect (Miroshnichenko and Kivshar, 2005b). Miroshnichenko and Kivshar (2005b) derived effective discrete equations for two types of the waveguide bends in two-dimensional photonic crystals and obtained exact analytical solutions for the resonant transmission and re-

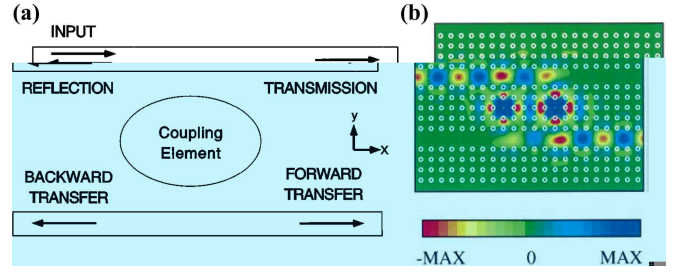


FIG. 17 (Color online) Add-drop filter. (a) Schematic diagram of two waveguides coupled through an element which supports a localized resonant state. (b) Electric field pattern of the photonic crystal at the resonant frequency. The white circles indicate the position of the rods. From Fan *et al.* (1998).

flection. This approach seems to be useful in getting a deeper insight into the physics of resonant transmission.

3. Add-drop filters

The Fano resonance can be employed for a variety of photonic devices based on the resonant tunneling. In particular, if two waveguides interact through a coupling element which supports a localized mode, a channel add-drop filter can be realized via the resonant tunneling between the waveguides (Fan *et al.*, 1998, 1999; Soljačić *et al.*, 2003). The schematic diagram of a generic coupled system of this kind is shown in Fig. 17(a). At the Fano resonance, the propagating state excites the resonant modes, which in turn decay into both waveguide. The transmitted signal in the first waveguide is made up of the input signal and the signal which originates from the decay of the localized states. In order to achieve complete transfer, these two components must be made to interfere destructively. The reflected amplitude, on the other hand, originates entirely from the decay of the localized states. Hence, at least two states are needed for the decaying amplitudes to cancel in the backward direction.

This concept was developed by Fan *et al.* (1998) for the propagation of electromagnetic waves in two-dimensional photonic crystal. To realize this concept, they used two photonic crystal waveguides and two coupled single-mode high- Q cavities, as shown in Figure 17(b). The photonic crystal is made of a square lattice of high-index dielectric rods, and the waveguides are formed by removing two rows of dielectric rods, and the cavities are introduced between the waveguides by reducing the radius of two rods. Each coupling splits the frequency of the even and odd states, but with opposite sign. An accidental degeneracy, caused by an exact cancellation between the two coupling mechanisms, is enforced by reducing the dielectric constant of four specific rods in the photonic crystal. The cancellation could equally have been accomplished by reducing the size of

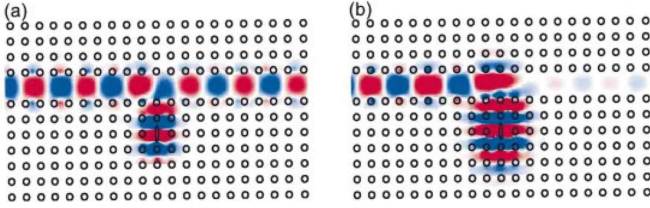


FIG. 18 (Color online) Electric field distributions in the photonic crystal for (a) high and (b) low transmission states. Red and blue represent large positive or negative electric fields, respectively. The same color scale is used for both panels. The black circles indicate the positions of the dielectric rods. From Yanik *et al.* (2003a).

the rods instead of their dielectric constant.

Figure 17(b) shows that the field pattern when the transmission is close to 100% over the entire spectrum, except at the resonant frequency, where it drops to 0%. The forward transferred signal shows a Lorentz-like line shape with a maximum close to 99% at resonance. The quality factor is larger than 1000. The backward transferred signal is almost completely absent over the entire frequency range.

This type of four-port photonic crystal systems can be employed for optical bistability, being particularly suitable for integration with other active devices on a chip (Soljačić *et al.*, 2003). A similar concept can be employed for the realization of all-optical switching action in a nonlinear photonic crystal cross-waveguide geometry with instantaneous Kerr nonlinearity, in which the transmission of a signal can be reversibly switched on and off by a control input (Yanik *et al.*, 2003b).

D. All-optical switching and bistability

A powerful principle that could be explored to implement all-optical transistors, switches, and logical gates is the concept of optical bistability. The use of photonic crystals enables the system to be of a size on the order of the wavelength of light, consume only a few milliwatts of power, and have a recovery and response time smaller than 1 ps. Several theoretical and experimental studies explored the nonlinear Fano resonances for designing optimal bistable switching in nonlinear photonic crystals (Cowan and Young, 2003; Maes *et al.*, 2008; Marin Soljačić and Joannopoulos, 2002; Mingaleev and Kivshar, 2002b; Mingaleev *et al.*, 2007, 2006; Yanik *et al.*, 2003a). A photonic crystal provides an optimal control over the input and output and facilitates further large-scale optical integration.

The main idea of using the Fano resonance for all-optical switching and bistability is quite simple: One should introduce an element with nonlinear response and achieve nonlinearity-induced shift of the resonant frequency, as was discussed above for discrete models. Thus, by employing *nonlinear Fano resonances* we can achieve

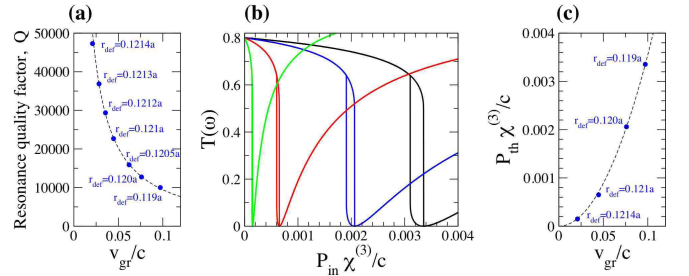


FIG. 19 (Color online) Ultra-low all-optical switching in the slow-light regime. (a) Quality factor Q vs. group velocity v_g at resonance for the waveguide-cavity structure. (b) Nonlinear bistable transmission at the frequencies with 80% of linear light transmission vs. the incoming light power for different values of the rod radius; (c) Switch-off bistability threshold vs. the group velocity at resonance. From Mingaleev *et al.* (2007).

bistability in many of the device structures suggested on the photonic-crystal platform. For example, for the side-coupled geometry shown in Fig. 14(b), one could take advantage of the interference between the propagating wave inside the waveguide and the decaying wave from the cavity, to greatly enhance achievable contrast ratio in the transmission between the two bistable states. This approach was realized by Yanik *et al.* (2003a) who demonstrated that such a configuration can generate extremely high contrast between the bistable states in its transmission with low input power.

One of the great advantages in using nonlinear photonic-crystal cavities is the enhancement of nonlinear optical processes, including nonlinear Fano resonance (Bravo-Abad *et al.*, 2007; Soljacic and Joannopoulos, 2004). Such enhancement can be very efficient in the regime of the slow-light propagation, that was demonstrated experimentally with the smallest achieved group velocity $c/1000$ (Gersen *et al.*, 2005; Jacobsen *et al.*, 2005; Notomi *et al.*, 2001; Vlasov *et al.*, 2005). Because of this success, the interest to the slow-light applications based on photonic-crystal waveguides is rapidly growing, rising the problems of a design of different types of functional optical devices which would efficiently operate in the slow-light regime.

Recently, Mingaleev *et al.* (2007) have studied the resonant transmission of light through a photonic-crystal waveguide coupled to a nonlinear cavity, and demonstrated how to modify the structure geometry for achieving bistability and all-optical switching at ultra-low powers in the slow-light regime. This can be achieved by placing a side-coupled cavity between two nearest defects of a photonic-crystal waveguide assuming that all the defect modes and the cavity mode have the same symmetry. In this structure the quality factor grows inversely proportional to the group velocity of light at the resonant frequency and, accordingly, the power threshold required

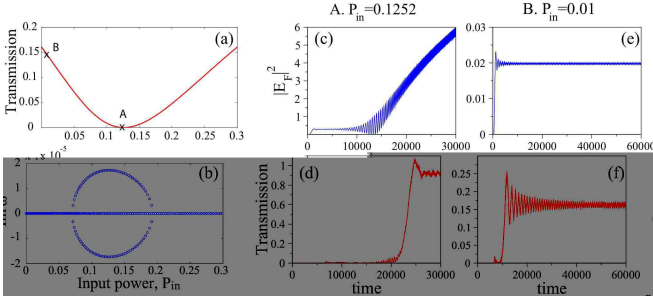


FIG. 20 (Color online) Dynamical instability of the nonlinear Fano resonance. (a) Nonlinear transmission coefficient, and (b) imaginary part of eigenvalues of the stability problem vs input power. It is demonstrated here that in the vicinity of the nonlinear Fano resonance the plane wave excitation becomes dynamically unstable. Temporal evolution of (c,e) the field inside the side-coupled cavity, and (d,f) transmission coefficient for two different values of the input power values, indicated in plot (a). Near the resonance the dynamics of the field inside the nonlinear cavity demonstrates the development of a modulation instability in time. Adapted from Miroshnichenko *et al.* (2009).

for all-optical switching vanishes as a square of the group velocity (see Fig. 19).

Numerically obtained dependence $Q(v_{gr}) \sim 1/v_{gr}$ is shown in Fig. 19(a), and it is in an excellent agreement with the theoretical predictions. Since the bistability threshold power of the incoming light in waveguide-cavity structures scales as $P_{th} \sim 1/Q^2$ (Mingaleev *et al.*, 2006), a rapid vanishing of $P_{th} \sim v_g^2$ when the resonance frequency approaches the band edge are observed, as shown in numerical calculations summarized in Figs. 19(b,c).

By now, several experimental observations of optical bistability enhanced through Fano interferences have been reported (Weidner *et al.*, 2007; Yang *et al.*, 2007). In particular, Yang *et al.* (2007) employed a high- Q cavity mode ($Q = 30000$) in silicon photonic crystal and demonstrated Fano-resonance based bistable states and switching with switching thresholds of $185\mu\text{W}$ and 4.5 fJ internally stored cavity energy that might be useful for scalable optical buffering and logic.

It is important to note, that the nonlinear Fano resonance is generally dynamically unstable under the plane wave excitation (Miroshnichenko *et al.*, 2009). It means that near the resonance the intensity of the scattered wave starts to grow in time, leading to modulational instability, while far from resonance it converges to steady-state solution (see Fig. 20). However, as it was demonstrated by Miroshnichenko *et al.* (2009) this instability can be marginally suppressed for temporal Gaussian pulses excitations, providing with an effective method of recovering the bistable transmission.

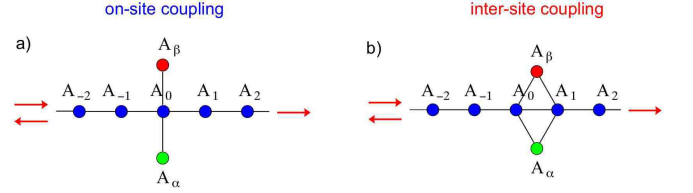


FIG. 21 (Color online) Two types of the geometries of a photonic-crystal waveguide side coupled to two nonlinear optical resonators. Light transmission and bistability are qualitatively different for (a) on-site and (b) inter-site locations of the resonator along waveguide. Adapted from Mingaleev *et al.* (2008).

E. Fano-Feshbach resonances

A very important effect associated with the Fano resonances in double-resonator photonic structures can be linked to the electromagnetically-induced transparency (EIT) (Fleischhauer *et al.*, 2005). The coupled-resonator-induced transparency (CRIT) structures have been introduced in 2004 (Maleki *et al.*, 2004; Smith *et al.*, 2004; Suh *et al.*, 2004), although the early work (Opatrný and Welsch, 2001) suggested already an idea of macroscopic double-resonator optical system exhibiting the EIT-like effect. Recently, the CRIT effect has been observed experimentally in the system of two interacting microresonators (glass spheres of about $400\mu\text{m}$ in diameter) with the whispering-gallery modes (Naweed *et al.*, 2005), in a cavity with at least two resonant modes (Franson and Hendrickson, 2006), and in the integrated photonic chips with two microring resonators (Tomita *et al.*, 2009; Xu *et al.*, 2006). Providing an efficiently tunable ‘transparency on an optical chip’, such CRIT devices are considered as a crucial step towards the development of integrated all-optical chips (Boyd and Gauthier, 2006).

To explain the origin of CRIT resonances, we characterize the light transmission by the transmission and reflection coefficients which can be presented in the form

$$T(\omega) = \frac{\sigma^2(\omega)}{\sigma^2(\omega) + 1}, \quad R(\omega) = \frac{1}{\sigma^2(\omega) + 1}, \quad (39)$$

where the detuning function $\sigma(\omega)$ may have quite different type of frequency dependence for different types of waveguide-cavity structures. Zero transmission (total reflection) corresponds to the condition $\sigma(\omega) = 0$, while perfect transmission (zero reflection) corresponds to the condition $\sigma(\omega) = \pm\infty$.

For the waveguide-cavity structure shown in Fig. 14(b), we obtain (Mingaleev *et al.*, 2006)

$$\sigma(\omega) \simeq \frac{(\omega_{\alpha} - \omega)}{\gamma_{\alpha}}, \quad (40)$$

where ω_{α} is the eigenfrequency of the localized cavity mode of an isolated cavity α . The spectral width γ_{α}

of the resonance is determined by the overlap integral between the cavity mode and the guided mode at the resonant frequency.

To find $\sigma(\omega)$ for the two-cavity structure, one can apply a variety of methods but the simplest approach is based on the transfer-matrix technique (Fan, 2002). When two cavities are separated by the distance $d = 2\pi m/k(\omega_t)$, where $k(\omega)$ is the waveguide's dispersion relation, m is any integer number, and the frequency ω_t is defined below, and there is no direct coupling between the cavities, we obtain

$$\sigma(\omega) \simeq \frac{(\omega_\alpha - \omega)(\omega_\beta - \omega)}{\Gamma(\omega_t - \omega)}, \quad (41)$$

with the total resonance width $\Gamma = \gamma_\alpha + \gamma_\beta$ and the frequency of perfect transmission $\omega_t = (\gamma_\alpha\omega_\beta + \gamma_\beta\omega_\alpha)(\gamma_\alpha + \gamma_\beta)^{-1}$, lying in between the two cavity frequencies, ω_α and ω_β , of zero transmission.

In the case when the cavities α and β are identical, we obtain a single-cavity resonance and the only effect of using two cavities is the doubling of the spectral width, $\Gamma = 2\gamma_\alpha$, of the resonant reflection line, as it is illustrated in Fig. 22(a). However, introducing even the smallest difference between two cavities leads to the opening of an extremely narrow resonant transmission line on the background of this broader reflection line, as it is illustrated in Fig. 22(c). Indeed, for small difference between cavities we may rewrite Eq. (41) in the vicinity of the resonant transmission frequency, $\omega_t = \omega_\alpha + \delta\omega/2$, as $\sigma(\omega) \approx \Gamma_t/(\omega - \omega_t)$, with the line width $\Gamma_t = \delta\omega^2/8\gamma_\alpha$, which can easily be controlled by tuning the frequency difference $\delta\omega$. The quality factor of this transmission line, $Q_t = \omega_t/2\Gamma_t \approx 4\gamma_\alpha\omega_\alpha/\delta\omega^2$, grows indefinitely when $\delta\omega$ vanishes. As mentioned above, this effect is the all-optical analogue of the electromagnetically-induced transparency and is now often referred as the effect of coupled-resonator-induced transparency (Smith *et al.*, 2004).

In contrast, the inter-coupling between two cavities, as shown in Fig. 21(b) manifests itself in a qualitatively new effect of coupled-resonator-induced reflection (CRIR): for small detuning $\delta\omega = \omega_\beta - \omega_\alpha$, one of the resonant reflection frequencies shifts very close to the perfect transmission frequency, ω_t , producing a narrow resonant reflection line, as is illustrated in Fig. 22(d). The frequency of this line is always close to the frequency ω_α of the cavity mode, while its spectral width is determined by the frequency difference $\delta\omega$, growing indefinitely as $\delta\omega$ vanishes (Landobasa Y. Mario and Chin, 2006; Mingaleev *et al.*, 2008).

It should be emphasized that despite such a qualitative difference in their spectral manifestations, both CRIT and CRIR effects have the same physical origin which can be attributed to the Fano-Feshbach resonances (Feshbach, 1958, 1962; Mies, 1968) which are known to originate from the interaction of two or more resonances (e.g., two Fano resonances) in overlapping regime, where the spectral widths of resonances are comparable to or

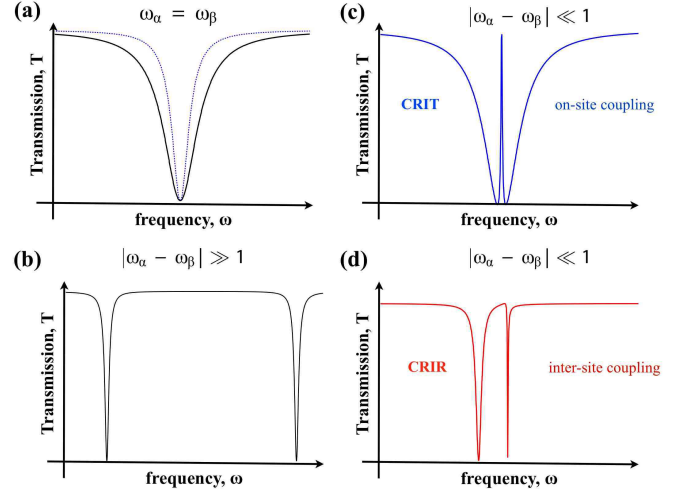


FIG. 22 (Color online) Typical transmission curves for four different cases (a) two identical side-coupled defects $\omega_\alpha = \omega_\beta$ (solid). Transmission for single side-coupled cavity is shown by dashed; (b) two side-coupled cavities with larger detuned eigenfrequencies $|\omega_\alpha - \omega_\beta| \gg 1$; (c,d) two side-coupled cavities with slightly detuned eigenfrequencies $|\omega_\alpha - \omega_\beta| \ll 1$ for (c) on-site coupling and (d) inter-site coupling. From Mingaleev *et al.* (2008).

larger than the frequency separation between them. In a general situation it leads to a drastic deformation of transmission spectrum and formation of additional resonances with sharp peaks. The Fano-Feshbach resonances are associated with a collective response of multiple interacting resonant degrees of freedom, and they have numerous evidences in quantum mechanical systems (Magunov *et al.*, 2003; Raoult and Mies, 2004).

Finally, we mention that the interaction between two Fano resonances (Hino, 2001; Miroshnichenko, 2009) can be employed to stop and store light coherently, with an all-optical adiabatic and reversible pulse bandwidth compression process (Yanik and Fan, 2004; Yanik *et al.*, 2004). Such a process overcomes the fundamental bandwidth delay constraint in optics and can generate arbitrarily small group velocities for any light pulse with a given bandwidth, without any coherent or resonant light-matter interactions. The mechanism can be realized in a system consisting of a waveguide side coupled to tunable resonators, which generates a photonic band structure that represents a classical EIT analogue (Maes *et al.*, 2005; Yanik *et al.*, 2004).

F. Guided resonances in photonic crystal slabs

Scattering of light on photonic crystal slabs leads to another class of Fano resonances associated with the presence of guided resonances in the periodic structures. Indeed, a photonic crystal slab consists of a two-dimensionally periodic index contrast introduced into a

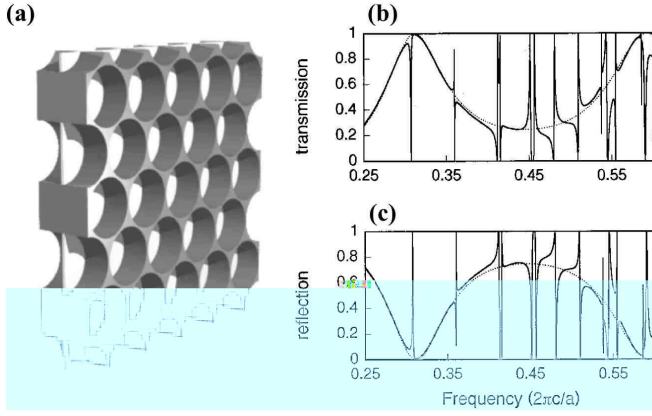


FIG. 23 Light scattering by photonic crystal slabs. (a) Geometry of the photonic-crystal film. (b) Transmission and (c) reflection spectra. The solid lines are for the photonic crystal structure, and the dashed lines are for a uniform dielectric slab with a frequency-dependent dielectric constant. Adapted from Fan and Joannopoulos (2002).

high-index guiding layer Fig. 23(a). Such modulated structures support in-plane guided modes that are completely confined by the slab without any coupling to external radiations (Magnusson and Wang, 1992). In addition to in-plane waveguiding, the slabs can also interact with external radiations in complex and interesting ways (Fan and Joannopoulos, 2002; Fan *et al.*, 2003; Koshino, 2003). Of particular importance is the presence of guided resonances in the structures. The guided resonances can provide an efficient way to channel light from within the slab to the external environment. In addition, the guided resonances can significantly affect the transmission and reflection of externally incident light, resulting in complex resonant line shapes which can be linked with Fano resonances.

Fan and Joannopoulos (2002) calculated the transmission and reflection coefficients at various k points for the structure shown in Fig. 23(a), the calculated spectra for the s-polarized incident wave are shown in Figs. 23(b,c). The spectra consist of sharp resonant features superimposed upon a smoothly varying background. The background resembles Fabry-Perot oscillations when light interacts with a uniform dielectric slab. To clearly see this, the background is fit to the spectra of a uniform slab, which are shown as dashed lines in Figs. 23(b,c). The uniform slab has the same thickness as the photonic crystal. resonances can be described theoretically by employing the Fano-type formulas, the fitting with the only parameter, the effective dielectric constant, agrees completely with the numerical simulations (see also Ref. (Koshino, 2003)).

By introducing a nonlinear layer into the slab with a periodic lateral structure, we can generate a bistable transmission for significant intensity ranges, due to Fano resonances, achieving a strong frequency-dependent transparency variation related to the transfer via guided

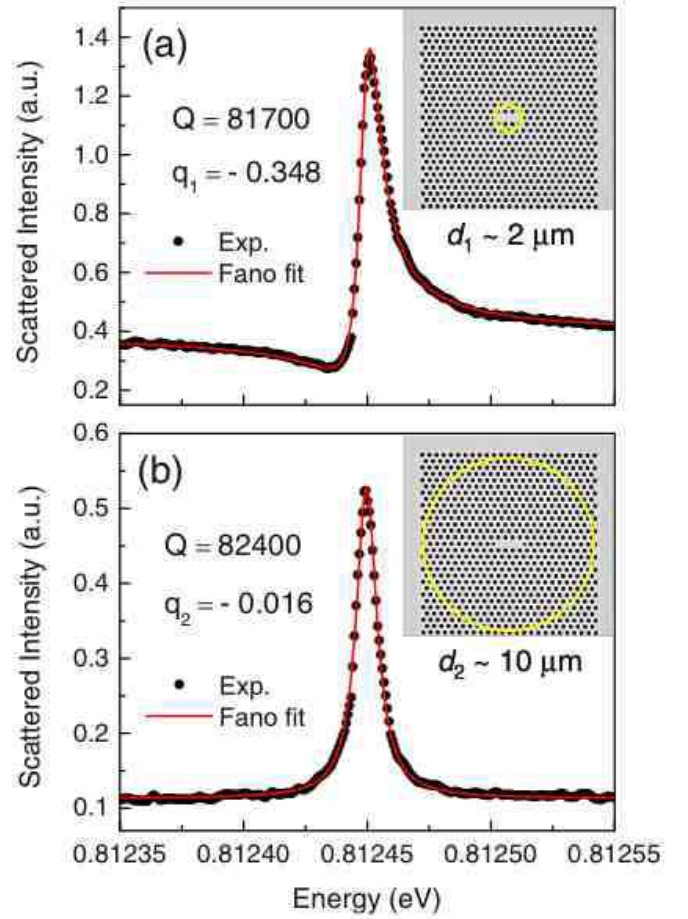


FIG. 24 (Color online) Measured scattering spectra (dots) and fitting by Fano formula (solid lines) of photonic crystal nanocavity for two different excitation conditions: (a) by tightly focused, and (b) slightly defocused laser beam of diameters d_1 and d_2 , respectively, indicated by circles. Note here, that the actual profiles are inverted ones because of the use of crossed polarized detection. From Galli *et al.* (2009).

modes. A self-consistent simulation tool which allows for the computation of multivalued transmission has been developed by Lousse and Vigneron (2004), and it explained the peculiar shape of the hysteresis loops associated with nonlinear Fano resonances.

Complex resonant line shapes due to Fano resonances were observed experimentally in several settings (Chen *et al.*, 2009; Grillet *et al.*, 2006; Harbers *et al.*, 2007; Qiang *et al.*, 2008; Yang *et al.*, 2008). In particular, Grillet *et al.* (2006) observed Fano resonances in the optical transmission spectrum of a chalcogenide glass photonic crystal membrane and demonstrated, for the first time, the suppression of optical transmission by over 40 dB, the strongest reported so far and a remarkable result for a dielectric structure just 330 nm thick. The resulting insights gained will allow further work towards engineering very sharp resonances and, combined with the large intrinsic nonlinearity of the chalcogenide glasses, should allow the

demonstration of optical bistability in a photonic-crystal mirror.

Recently, it was experimentally demonstrated that the shape of the Fano resonance in the light scattering from high-Q planar photonic crystal nanocavity can be controlled by varying the waist of the Gaussian beam (Galli *et al.*, 2009). For tightly focused beam with the spot diameter $d_1 \approx 2\mu\text{m}$ a strong asymmetric Fano resonances was observed with the asymmetry parameter $q_1 = -0.348$ [see Fig. 24(a)]. On the other hand, for slightly defocused Gaussian beam with the spot diameter $d_2 \approx 10\mu\text{m}$ the symmetric Fano resonance was observed with $q_2 = -0.016$ [see Fig. 24(b)]. In this geometry the light reflected from the nanocavity mimics the scattering via the discrete level, while the light reflected from the photonic crystal pattern, can be considered as the scattering to the continuum. The interference of these two reflected components gives rise a birth the Fano resonance. The variation of the Fano profile with the increase of the excitation area can be understood as the enhancement of the scattering to the continuum, leading to the decrease of the asymmetry parameter q . Indeed, the variation of the asymmetry parameter $q_1/q_2 \sim 22$ is proportional to the variation of the excitation areas $(d_2/d_1)^2 \sim 25$. Thus, by changing the excitation conditions it is possible to tune the Fano resonance in the scattering by photonic crystal nanocavity.

G. Light scattering by spherical nanoparticles

Light scattering by an obstacle is one of the fundamental problems of electrodynamics, see, e.g., monographs (Bohren and Huffman, 1998; Born and Wolf, 1999; van der Hulst, 1981). It was first described by Lord Rayleigh and is characterized by a sharp increase in scattering intensity with a rise in light frequency (Rayleigh, 1871a,b,c). It explains why we can enjoy the blue sky during day time (the intensely scattered blue component of the sunlight) and, scarlet sunrises and sunsets at dawn and dusk (the weakly scattered red component). Lord Rayleigh's studies were generalized by Gustav Mie who obtained the complete analytical solution of the Maxwell's equations for the scattering of electromagnetic radiation by a spherical particle valid for any ratio of diameter to the wavelength (Mie, 1908).

A common belief is that the general Mie solution transforms into that of Rayleigh when particles are small. However, recent studies of resonant scattering by small particles with weak dissipation rates (Bashevoy *et al.*, 2005; Tribelsky and Luk'yanchuk, 2006) have revealed new and unexpected features, namely giant optical resonances with an inverse hierarchy (the quadrupole resonance is much stronger than the dipole one, etc.) , a complicated near-field structure with vortices, unusual frequency and size dependencies, which allow to name such a scattering anomalous. Tribelsky *et al.* (2008) revealed that the physical picture of this anomalous scattering is

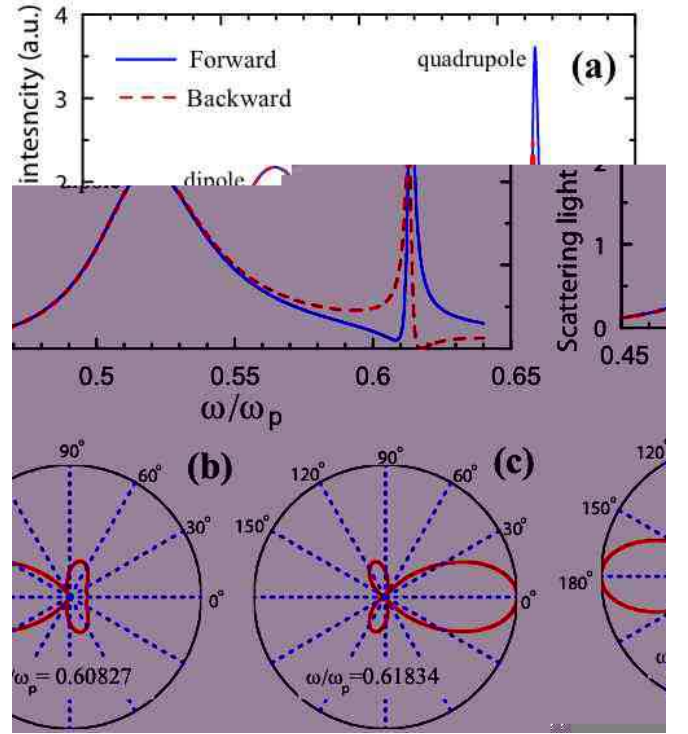


FIG. 25 (Color online) Exact Mie solution of the light scattering by a plasmonic nanoparticle. The radius of the nanoparticle is much smaller than the light wavelength $a/\lambda = 0.083$. (a) Frequency dependence of the scattering light intensity in the vicinity of the dipole and quadrupole resonances. In the latter case both forward (solid lines) and backward (dashed lines) scattering profiles exhibit asymmetric Fano resonances; (b,c) The angular dependence of the light scattering in the vicinity of the quadrupole resonance. The plasmonic frequency is normalized to $\omega_p a/c = 1$. Adapted from Luk'yanchuk *et al.* (2008).

analogous to the physics of Fano resonances. This analogy sheds a new light to the phenomenon. It allows to employ powerful methods developed in the theory of the Fano resonances (such as, e.g., the Feshbach-Fano partitioning theory) to describe the resonant light scattering. It also easily explains certain features of the anomalous scattering and related problems, namely sharp changes in the scattering diagrams upon small changes in ω (see Fig. 25). Tribelsky *et al.* (2008) analytically obtained an asymmetric profile of the resonance lines by analyzing the exact Mie solution of the light scattering problem by a spherical nanoparticle (Miroshnichenko *et al.*, 2008).

Figure 25 demonstrates light scattering by a potassium colloidal nanoparticle immersed in a KCl crystal, calculated with a realistic dependence $\epsilon(\omega)$ fitting actual experimental data (Luk'yanchuk *et al.*, 2008; Tribelsky *et al.*, 2008). A small variation of the incident light frequency in the vicinity of the quadrupole resonance drastically changes the scattering pattern (see Fig. 25), resulting in asymmetric Fano-like profiles for

intensities of the forward and backward scattered light. In this case, excited localized plasmons (polaritons) are equivalent to the discrete levels in the Fano's approach, while the radiative decay of these excitations is similar to tunneling to the continuum. In general, it may provide with significant suppression of the scattering along any given direction. Note, that in accordance with the theoretical expression obtained from the Mie formula, the points of destructive interference for the forward and backward scattering lie on different sides of the corresponding resonant peaks.

H. Plasmonic nanocavities and tunable Fano resonance

Recent progress in the fabrication and visualization of nano-sized structures have given rise a birth to a novel and rapidly emerging field of nanoplasmonics. The optical properties of metals are governed by coherent oscillations of conduction-band electrons, known as plasmons (Bohm and Pines, 1951). The interaction between light and metallic nanoparticles is mostly dominated by charge-density oscillations on the closed surfaces of the particles, called localized surface plasmon resonances (LSPs). The studies of LSPs in noble-metal nanoparticles, such as gold and silver, have expanded their applications from various surface-enhanced spectroscopies (Moskovits, 1985) to novel nanometer optical devices and waveguides (Barnes *et al.*, 2003; Ozbay, 2006). One of the most important properties of LSPs is the possibility of strong spatial localization of the electron oscillations, combined with their high frequencies varying from UV to IR ranges. LSPs have the ability to strongly scatter, absorb, and squeeze light into nanometer scales, producing huge enhancement of electromagnetic fields. Such unique properties of nanomaterials are essential for the development of novel material functions with potential technological and medical applications with specific optical, magnetic, and reactivity properties.

Plasmonic nanostructures can be considered as a physical realization of coupled oscillator systems at the nanoscale. The energies and linewidths of the LSPs depend mostly on the nanoparticle geometries, such as size and shape. Thus, the spectral tunability of LSPs has been widely investigated. As it was suggested by Hao *et al.* (2007), a more promising geometries for fine tuning are rings and disk-like shapes. In such structures the dipole-like resonance can be tuned into the near-infrared region by changing the width of metallic ring, for example. One of the important issue of the nanoplasmonic is the effect of symmetry breaking, which allows to excite higher-order multipolar modes leading to a larger electromagnetic field enhancements. The symmetry breaking can be easily achieved in metallic ring/disk cavity structure by displacing the disk with respect to the center of the ring. The plasmon resonances of ring/disk cavity system can be understood

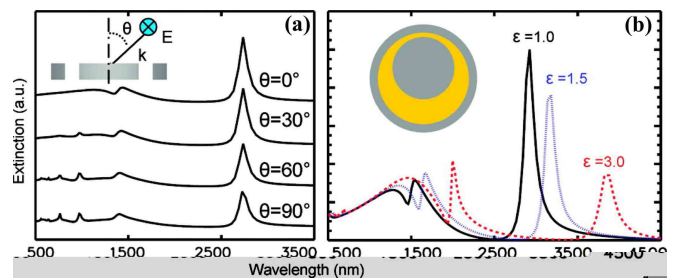


FIG. 26 (Color online) A metallic nanostructure consisting of a disk inside a thin ring supports superradiant and very narrow subradiant modes. Symmetry breaking in this structure enables a coupling between plasmon modes of differing multipolar order, resulting in a tunable Fano resonance: (a) extinction spectra as a function of incident angle θ ; (b) effect filling the cavity with a dielectric material on the extinction spectrum or permittivity $\epsilon = 1$ (solid line), $\epsilon = 1.5$ (dashed line), and $\epsilon = 3$ (dotted line). Adapted from Hao *et al.* (2008).

as the interaction or hybridization of the single ring and disk cavity plasmons. This hybridization leads to a low energy symmetric plasmon and high energy anti-symmetric plasmon (Hao *et al.*, 2007). The latter one is superradiant, i.e. it strongly radiates because disk and ring dipolar plasmons are aligned and oscillate in phase. The low energy symmetric plasmon is subradiant because of opposite alignment of dipolar moments. It turns out that in symmetry-broken structure, the quadrupole ring resonance couples to superradiant high energy anti-symmetric disk-ring dipole mode (Hao *et al.*, 2008). The direct coupling interferes with the dispersive coupling between the quadrupolar ring mode and the superradiant mode, resulting in Fano resonance in the extinction spectrum (see Fig. 26). By varying the incident angle the shape of the Fano resonance can be altered from asymmetric to a symmetric one.

Another examples of nanoplasmonic structures supporting the asymmetric Fano resonance are metallic nanoshell near a metallic film (Le *et al.*, 2007), and heterogeneous dimers composed of a gold and silver nanoparticles (Bachelier *et al.*, 2008). Both structures represent a highly tunable plasmonic Fano resonance, accompanied by large local electric field enhancements. Thus, the strong response of LSP resonances may be effectively used for biological and medical sensing applications.

A novel type of the nonlinear Fano resonance has been found in hybrid molecules composed of semiconductor and metal nanoparticles (Zhang *et al.*, 2006). The latter ones support surface plasmons with continuous spectrum, while the former ones support discrete interband excitations. Plasmons and excitons become strongly coupled via Förster energy transfer. At high light intensities, the absorption spectrum demonstrates sharp asymmetric profile, which originates from the coherent interparticle Coulomb interaction, and can be understood in terms of the nonlinear Fano resonance.

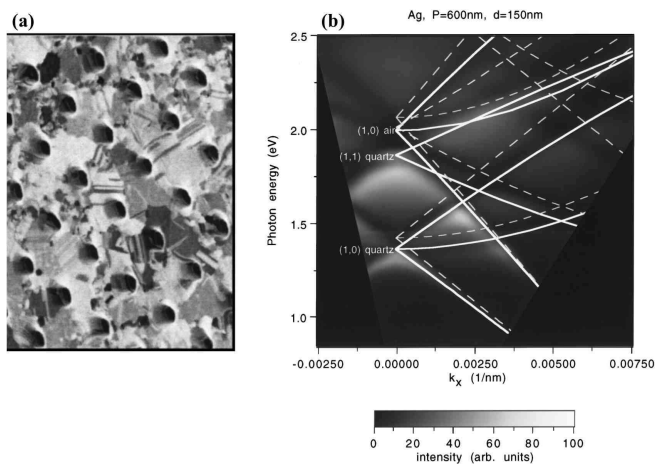


FIG. 27 Light scattering by metallic gratings. (a) Focused ion beam image of a two-dimensional hole array in a polycrystalline silver film. (b) Observed transmission intensity as a function of photon energy and k_x with predicted energy dispersion of surface plasmon-polaritons (solid) and loci of Wood's anomaly (dashed lines). From Ghaemi *et al.* (1998).

I. Extraordinary transmission of light through metallic gratings

The scattering by metallic gratings was the subject of extensive research for over a century. One of the important early achievements of the optics of metallic gratings was the discovery and understanding of the Wood's anomalies (Rayleigh, 1907; Wood, 1902, 1935). One type of anomaly is due to excitation of surface plasmon-polaritons propagating on the the metallic surface. Another one is the diffractive anomaly, when a diffracted order becomes tangential to the plane of the grating. It is characterized by a rapid variation of the diffracted order intensity, corresponding to the onset or disappearance of a particular spectral order (Wood, 1935). This resonant behaviour of the Wood's anomaly can be understood in terms of the coupling of the incoming waves with the surface-bound states of periodic arrays (Fano, 1936, 1937, 1938, 1941; Hessel and Oliner, 1965). Thus, by considering a surface-bound state as a discrete level and scattered waves as a continuum the Wood's anomaly can be interpreted as the Fano resonance (Billaudeau *et al.*, 2009).

It was demonstrated that a periodic thin-film metallic grating, formed from a two-dimensional array of holes, the transmitted fraction of the incident light can exceed the open fraction of the array for certain wavelengths (Ebbesen *et al.*, 1998; Ghaemi *et al.*, 1998). The enhancement in the transmitted zero-order beam is reported to be several orders of magnitude larger than that from pure metallic slab without holes. This phenomenon has been called extraordinary transmission through periodic arrays of subwavelengths holes in metallic films.

The common understanding of the extraordinary transmission is due to resonant excitation

of surface plasmon-polaritons by incoming radiation (Ghaemi *et al.*, 1998; van der Molen *et al.*, 2005). In addition to the resonant enhancement of the transmission the resonant suppression was observed as well. It was demonstrated that these transmission minima correspond exactly to loci of Wood's anomaly (see Fig. 27) (Ghaemi *et al.*, 1998). According to experimental observations, each extraordinary transmission is accompanied by resonant suppression resulting in asymmetric lineshapes, which can be perfectly fitted by the Fano formula (de Abajo, 2007). Moreover, it was theoretically demonstrated by Spevak *et al.* (2009) that periodically modulated ultrathin metal films may exhibit resonant suppression of the transmittance, emphasizing the Wood's anomaly effect. Thus, the extraordinary resonant scattering of light by modulated metal film can be described in terms of the Fano resonance, revealing the interference nature of the phenomenon.

Kobyakov *et al.* (2009) suggested to use active layers to simultaneously enhance both transmittance and reflectance at the resonance in subwavelength periodic planar bimetallic grating by exciting gain-assisted surface plasmons.

VI. CHARGE TRANSPORT THROUGH QUANTUM DOTS

A. General remarks

In recent decades charge transport through quantum dots (QD) has been extensively studied both theoretically and experimentally (Altshuler *et al.*, 1991; Hanson *et al.*, 2007; Kastner, 1992; Koch and Lübbig, 1992; Reimann and Manninen, 2002). One of the reasons of that interest is the further miniaturization of electronic device components. A comprehensive picture of a big variety of underlying physical phenomena has emerged (see e.g. Aleiner *et al.* (2002); Alhassid (2000) and references therein). The finite size of the dot is responsible for a dense but discrete set of single particle levels. Confinement of electrons in small quantum dots leads to the necessity of taking into account their Coulomb repulsion. As a result, at temperatures below the charging energy the Coulomb blockade emerges (Aleiner *et al.*, 2002; Alhassid, 2000). At even lower temperatures the phase coherence of the excitations in the quantum dot is preserved during the scattering, and additional interference phenomena appear, depending on the coupling strength to the leads. In view of the enormous literature available, we will briefly introduce the main physics, and focus on results which are directly related to the finding of destructive interferences and Fano resonances.

B. From a single electron transistor to quantum interference

A quantum dot is a small confinement region for electrons (typically almost two-dimensional) with leads coupled to it. The manufacturing of a huge variety of geometries is easily possible. In the simplest case two leads are used, and a voltage V is applied, resulting in a current of electrons which enter the dot through one lead, and eventually exit into the second lead. Various gate voltages can be additionally applied, e.g. V_g which controls the energy of the electrons in the dot relative to the leads, and others which control the strength of the coupling between the leads and the dot. Here we will consider only situations where the applied voltage V between the two leads is small so that the energy eV is smaller than all other relevant energy scales. This is also called the equilibrium case, at variance to the non-equilibrium case which is also frequently studied.

Let us consider a closed dot with linear size L , when the leads are decoupled. If one neglects the contribution from Coulomb interaction, the spectrum of many body states in a quantum dot can be obtained from the solution of the single particle problem. The single particle level spacing $\Delta_{sp} = \pi\hbar^2/m^*L^2$ (Alhassid, 2000). The effective mass of an electron in GaAs is rather low: $m^* = 0.067m_e$ (Alhassid, 2000). For $L = 100nm$ one obtains $\Delta_{sp} \approx 2K$, while for $L = 500nm$ the spacing is reduced to $\Delta_{sp} \approx 90mK$. Adding one electron to the closed dot therefore leads to an energy increase of the order of Δ_{sp} . Now take Coulomb interaction into account. If the number of electrons in the dot is N , then the charging energy of adding one additional electron is $E_c \sim Ne^2/L$. Therefore, for large values of N , and not too small values of L , $E_c \gg \Delta_{sp}$. Note that typical dot sizes are of the order $100nm - 1\mu m$. N can strongly vary, with values $N \sim 10^2 - 10^3$. Characteristic values of the charging energy are in the range $E_c \sim 100 - 400K$ ($12 - 50meV$). Therefore, for all practical purposes, $E_c \gg \Delta_{sp}$.

The number of electrons in a quantum dot is defined by minimizing the energy of the dot with respect to N . This energy is given by (Alhassid, 2000)

$$E(N) = -NeV_g + N^2e^2/2C, \quad (42)$$

where C is the total capacitance between the dot and its surroundings. Apart from special values of the gate voltage, there will be a given electron number N with smallest energy, and changing the number of electrons will cost an amount about one charging energy E_c . For particular values of the gate voltage $V_g^{(n)}$ however degeneracies between $E(N)$ and $E(N+1)$ appear.

Consider an experimental geometry shown in Fig.28. If the coupling to the leads is weak enough and the temperature $kT < E_c$ the Coulomb blockade regime sets in. As long as $V_g \neq V_g^{(n)}$ the charging energy prevents lead electrons from entering the dot, and the conductance G is practically zero. However, when $V_g = V_g^{(n)}$, the degeneracy between N and $N+1$ electron states on the

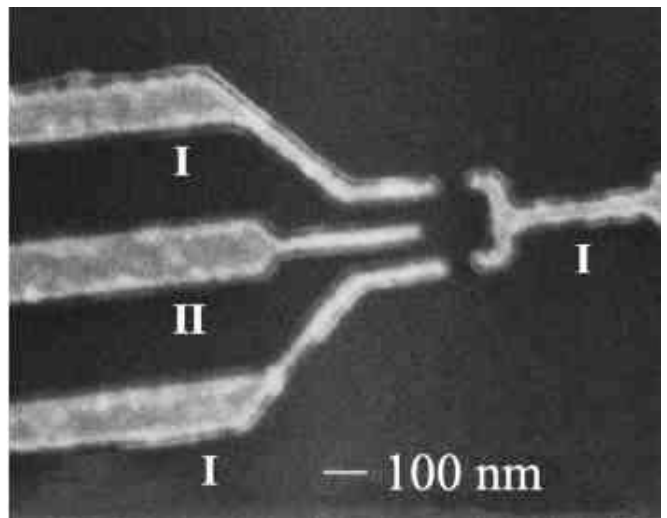


FIG. 28 Electron micrograph of a single electron transistor based on a GaAs/AlGaAs heterostructure. The split gates (I) define the tunnel barriers and the additional gate electrode (II) adjusts the potential energy on the quantum dot. From Göres *et al.* (2000).

dot sets in. Therefore, electrons can pass through the dot one by one, and the conductance takes the universal value $G = 2e^2/h$ (here the factor 2 accounts for spin degeneracy). Note that the Coulomb interaction is treated in a mean-field type way, therefore no phase coherence of dot electrons is required.

Lowering the temperature further, the phase coherence of the dot electrons becomes essential (see e.g. Aikawa *et al.* (2004); Ji *et al.* (2000)). Note that the typical electron mean free path can be of the order of $10\mu m$, one-two orders of magnitude larger than the dot size. It may also be possible to reduce *decoherence* effects within some suitable range by *increasing* the coupling of the dot to the leads, which may lead to a shorter residence time of electrons inside the dot and therefore to less scattering. With the option of having several channels which electrons can use to pass through the dot, phase coherence will lead to interference effects, and therefore to possible Fano resonances.

If a magnetic field is added, orbital and spin effects have to be considered as well. The Zeeman energy $E_z = g\mu_B H$ sets another temperature scale. Depending on the Lande factor g , which can vary strongly from sample to sample, the corresponding Zeeman energy E_z is of the order of $100 - 200mK$ for $B = 1T$. Allowing the electrons to traverse the dot along different pathes, an Aharonov-Bohm phase shift ϕ occurs due to a nonzero magnetic flux penetrating the area S enclosed by them (Altshuler *et al.*, 1980): $\phi = \frac{e}{h}BS$. With $S = L^2$ we find for $L = 100nm$ that $\phi/2\pi = 0.38B/T$, and for $L = 1\mu m$ that $\phi/2\pi = 38B/T$.

Therefore, for $L = 100nm$ and $B = 1T$ it follows $E_z \ll \Delta_{sp}$. Then at low temperatures $kT < E_z$ of the order of $T \sim 50 - 100mK$ and at a magnetic field $B \sim 1T$

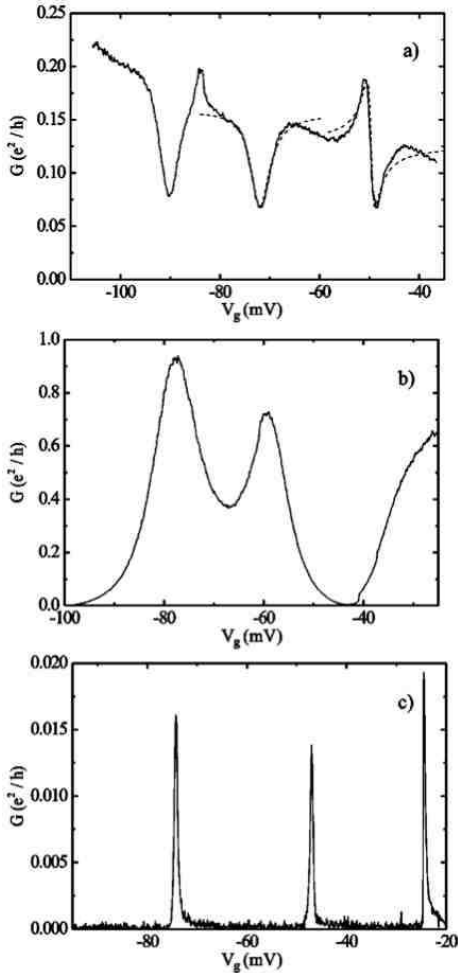


FIG. 29 Conductance versus gate voltage. Comparison of conductance measurements in the (a) Fano regime, (b) intermediate regime, and (c) Coulomb blockade regime. From (c) to (a) the lead-dot coupling increases. Fits to the Fano formula (1) are shown for the center and right resonances in (a). The respective asymmetry parameters are $q = -0.03$ and $q = -0.99$. From Göres *et al.* (2000).

the Coulomb blocked dot has a well defined spin: either $|S_z| = 1/2$, or $S_z = 0$. Changing the gate voltage and reaching the next degeneracy $E(N) = E(N + 1)$, an electron with a well-defined spin is allowed to enter the dot - either spin up or spin down. The allowed spin value alternates as one further tunes the gate voltage to the next degeneracy. If the phase coherence of electrons is preserved during the scattering, one may again expect interference phenomena - but this time, depending on the chosen value of V_g , only electrons with spin up (respectively spin down) will interfere along different channels. Increasing the coupling to the leads may cause spin-selective destructive interference for a given spin species, while the other spin species is freely passing through. The orbital effect of the magnetic field leads to an additional phase shift of the order of 0.8π , independent of applied gate voltages.

For $L = 1\mu\text{m}$ the single particle spacing $\Delta_{sp} \approx 20\text{mK}$. Therefore at $B = 1\text{T}$ it follows $E_z \gg \Delta_{sp}$. Then at temperatures $T \sim 50 - 100\text{mK}$ the Coulomb blocked dot is magnetized, but electrons which enter the dot can have any spin, preventing spin-selective destructive interference. The orbital effect of the magnetic field is huge with a 2π phase shift every 25mT upon changing the magnetic field.

Before proceeding, let us briefly mention related studies of the Kondo effect in transport through quantum dots. In the Coulomb blockade, the number of electrons on the dot is well defined, and either even or odd. Assuming a ground state only, the total electronic spin is either $1/2$ (odd number of electrons) or zero (even number). In the absence of a magnetic field and for odd numbers of electrons, the whole dot could be viewed as some magnetic impurity with spin $1/2$, which scatters conduction electrons passing from one lead to another. That calls for an analogy with the well known Kondo effect which is observed in the low temperature properties of the conductivity of electrons in metals with magnetic impurities (Hewson, 1993). The resistivity in metals usually drops with lowering the temperature, since the number of phonons, which are responsible for electron scattering due to electron-phonon interaction, decreases. At around 30K a minimum in the resistivity appears for some metals, and subsequently the resistivity increases again with further lowering the temperature. This increase is due to scattering of electrons by magnetic impurities, and originates from an exchange interaction of the conduction electron spin with the spin of the magnetic impurity. The exchange interaction sets an energy and temperature scale (the Kondo temperature T_K), which is typically of the order of $T_K \sim 100\text{mK} - 1\text{K}$, similar to the Zeeman energy of an electronic spin $1/2$ in a magnetic field of 1 Tesla. For temperatures $T < T_K$ the impurity spin is screened by a cloud of renormalized conduction electrons. The Kondo temperature depends sensitively on the coupling strength (hybridization) Γ between the conduction electrons and the magnetic impurities. For weak coupling T_K is exponentially small in $-1/\Gamma$. This analogy stirred ideas to observe the Kondo effect in the conductance of electrons through quantum dots. For that low temperatures have to be used, and the coupling of the leads to the dot has to be increased (in order to increase T_K). An enormous amount of theoretical studies was performed (Aleiner *et al.*, 2002). Experimental results showed a deviation from the Coulomb blockade regime for strong lead-dot coupling (see below). The relation to theoretical models based on Kondo mechanisms is still debated (see e.g. Aleiner *et al.* (2002); Ji *et al.* (2000)).

C. From Coulomb blockade to Fano resonances

A number of experimental studies report on the observation of Coulomb blockade in various quantum dot realizations on the basis of AlGaAs heterostruc-

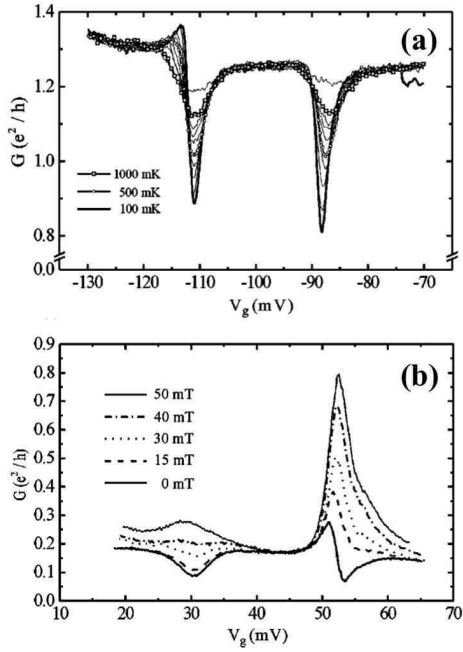


FIG. 30 Conductance versus gate voltage. (a) Temperature dependence of the conductance for two Fano resonances. (b) Conductance as a function of the gate voltage for various magnetic fields applied perpendicular to the two-dimensional electron gas. Adapted from Göres *et al.* (2000).

tures (Cronenwett *et al.*, 1998; Goldhaber-Gordon *et al.*, 1998a, 2001, 1998b; Göres *et al.*, 2000; Kobayashi *et al.*, 2002; Schmid *et al.*, 1998). The charging energies are in the range $E_c \sim 100 - 300K$. Temperatures were as low as $30mK$, applied magnetic fields up to 1T, and higher. Therefore, the Zeeman energy E_z is 2-3 orders of magnitude lower than the charging energy E_c . The Coulomb blockade is usually observed in the case of weak coupling between the leads and the dot. In Fig. 29 the results of Göres *et al.* (2000) are shown, which correspond to the setup in Fig. 28. For weak lead-dot coupling (c) the Coulomb blockade regime is nicely observed (temperatures are around $100mK$, and the drain source voltage $V_{ds} \approx 5\mu V \ll V_g$). With increasing coupling the sharp peak structure is smeared out (b), which has been discussed in relation to the Kondo effect. Even further increasing the coupling, Fano resonances are observed in the strong coupling case (a). A fitting yields asymmetry parameters $q = -0.03$ and $q = -0.99$ for the center and right resonances, respectively. Note that also the peaks in (c) separating Coulomb blockades with different numbers of electrons on the dot, are clearly asymmetric. The same authors studied the temperature and weak magnetic field dependence of the Fano profiles in the strong coupling regime for even larger absolute values of the gate voltage, shown in Fig. 30.

The fitting of the resonances in Fig. 30(a) yields an almost linear decrease of the linewidth Γ with temperature, reaching values of $2meV$ at $100mK$. The depth of the Fano resonance increases with decreasing temper-

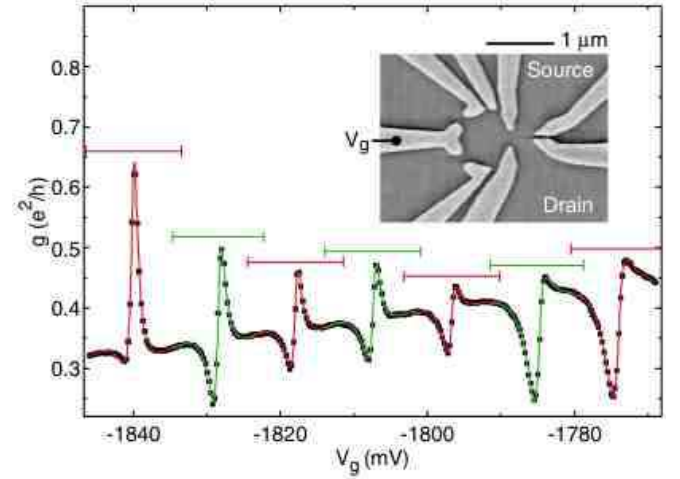


FIG. 31 Channel conductance data (squares) and fits (curves) vs gate voltage in the Fano regime. Bars show fitting ranges. Inset: SEM image of a similar sample. From Johnson *et al.* (2004).

ature, making the Fano resonance sharper and deeper at low temperatures. The Fano resonances show very strong dependence on the value of a weak applied magnetic field Fig. 30(b). Note that the largest applied fields are at $50mT$, which corresponds to a Zeeman energy of the order of $10mK$ or less.

The origin of the observed Fano resonances is interferences of electrons along several channels (paths) traversing the quantum dot. When the lead-dot coupling is weak, the background conductance is very small [see Fig. 29(c)]. Still an asymmetric line shape is observed. The Fano resonance (dip) may either be hard to be detected with that background, or simply be absent, since essentially only one path is active. Another possibility is that the antiresonance is extremely narrow (weak coupling to a dot state). Since the Fano resonances are well observed at large lead-dot coupling, phase coherence of electrons passing through the dot is therefore established, and is further increased with lowering the temperature.

The dramatic change of the resonance shape at weak magnetic fields is attributed to a suppression of the coupling into the dot states (Göres *et al.*, 2000). That leads to an enhancement of the asymmetry parameter q , and respectively to a shifting of the Fano resonance (dip) out of the window of available gate voltages. The alternative explanation of losing phase coherence of traversing electrons does not account for the extremely low-field scale at which the change occurs (Göres *et al.*, 2000). In a similar way one can exclude orbital Aharonov-Bohm effects, since the expected phase shifts are of the order of $\phi \leq 0.12$.

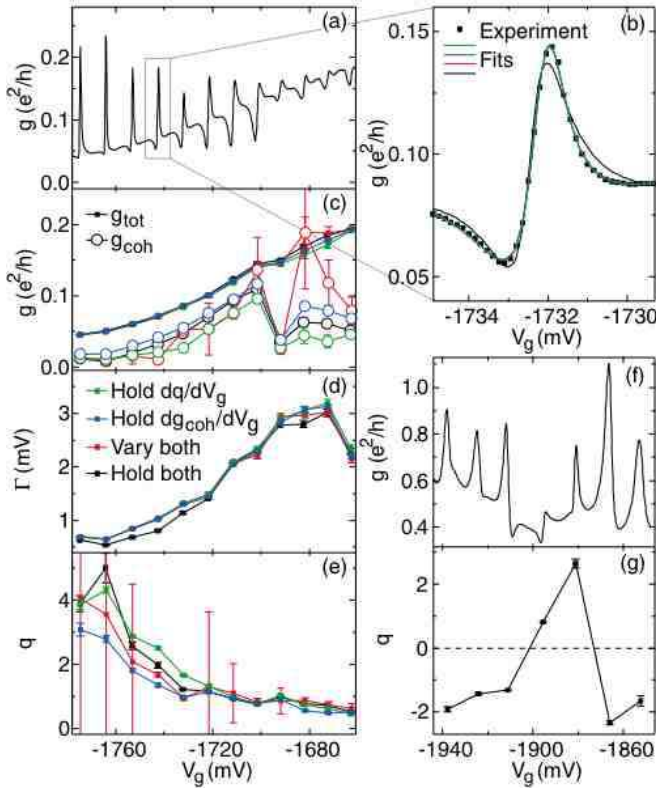


FIG. 32 Tunable Fano interferometer. (a) Experimental data with 12 Fano resonances. (b) Fits of one resonance using different fitting parameters. (c)-(e) g_{tot} , g_{coh} , Γ , and q from (a). (f) Data exhibiting reversals of q . (g) Extracted q values. From Johnson *et al.* (2004).

D. From Fano interferometers to Aharonov-Bohm interferometers

In the above described experiments, the quantum dot design allowed essentially only to control the lead-dot coupling. To further advance in the tunability of Fano resonances with quantum dots, interferometer devices have been manufactured. In addition to a small quantum dot, which can be traversed by electrons, a second region (second dot, or additional channel, or additional arm) is coupled in a controlled way. Therefore, the coupling to a second channel can be tuned systematically. Of course there may be already several channels involved in the traversing of electrons through the primary dot.

Impressive results have been obtained by Johnson *et al.* (2004) in designing a tunable Fano interferometer which consists of a quantum dot and an additional tunnel-coupled channel (see Fig.31).

A sequence of several Fano resonances was observed, and well fitted with the Fano formula (1). Moreover, Johnson *et al.* (2004) performed careful fittings of various resonance shapes as shown in Fig.32. In panel (a) another set of resonances is observed. Upon variation of the gate voltage the asymmetry of the resonance shape clearly changes, as also seen in panel (e). In addition, also the

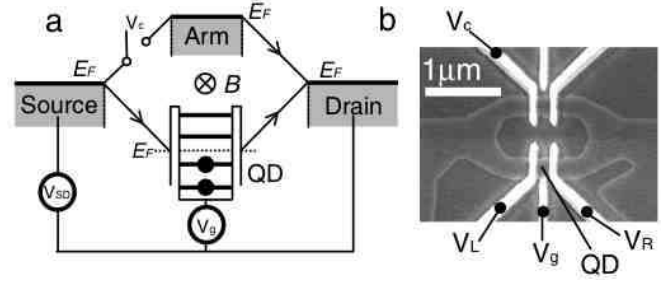


FIG. 33 An Aharonov-Bohm ring with an embedded QD in one of its arms. (a) Schematic representation of the experimental setup. (b) Scanning electron micrograph of the fabricated device. From Kobayashi *et al.* (2002).

line width Γ is changing (panel (d)). In another gate voltage window (panel (f)) these changes are even more drastic. Indeed, the fit yields a change of the sign of q with V_g (panel (g)). Note, that according to (1) at $q = 0$ a symmetric resonant reflection, with no resonant transmission, is predicted. Indeed, around the value $V_g \approx -1900\text{mV}$ the conductance in panel (f) shows practically a dip only.

Yet another twist was taken by Kobayashi *et al.* (2002) with a qualitatively similar geometry but an additional magnetic field penetrating the interferometer area and turning it into an Aharonov-Bohm (AB) device (see Fig.33). The current through the quantum dot and the additional arm (channel) can be controlled independently. Magnetic fields were around 1 Tesla. With the arm switched off, a series of Coulomb blockade peaks is observed (see Fig.34).

When making the arm transmittable, clear interference effects are observed through asymmetric Fano line-shapes (see Fig.34). In that system, the discrete level and the continuum are spatially separated, allowing to control Fano interference via the magnetic field piercing the ring as shown in Fig.35. The line shape changes periodically with the AB period $\sim 3.8\text{mT}$, which agrees with the expected value using the ring dimension (Kobayashi *et al.*, 2002). As magnetic field B is swept, an asymmetric line shape with negative q continuously changes to a symmetric one and then to an asymmetric one with positive q . Kobayashi *et al.* (2002) argue, that due to the breaking of time reversal symmetry in the presence of a magnetic field, the matrix elements defining q are not real as usually assumed, but complex, therefore leading to complex q values. This confirms theoretical investigations for the noninteracting single particle AB interferometer case (Aharony *et al.*, 2002, 2003; Entin-Wohlman *et al.*, 2002a,b; Sasada and Hatano, 2005).

E. From strong correlations to spin filters

An enormous bulk of theoretical literature on various facets of the conductance properties of quantum dots is available. We will discuss some of these results be-

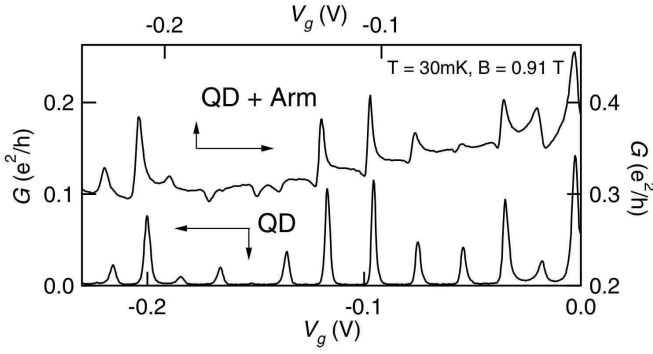


FIG. 34 Coulomb oscillation at $V_c = -0.12V$ with the arm pinched off, and asymmetric Coulomb oscillation at $V_c = -0.086V$ with the arm transmissible. Here $T = 30mK$ and $B = 0.91T$. Adapted from Kobayashi *et al.* (2002).

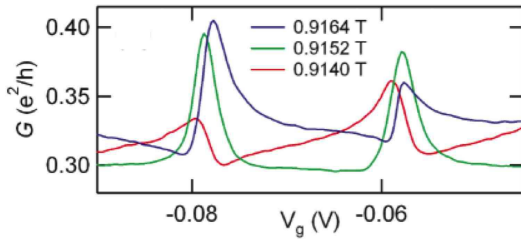


FIG. 35 Conductance of (a) two Fano peaks at $30mK$ and selected magnetic fields, (b) one Fano peak vs V_g and B , (c) Same as (b) but for larger windows of V_g variations. The white line represents the AB phase as a function of V_g . From Kobayashi *et al.* (2002).

low. Let us remind the reader about some characteristic scales. The Coulomb energy (charging energy) of quantum dots is of the order of $50meV$ ($380K$). The Kondo temperature in a typical metal with magnetic impurities is of the order of $10\mu eV$ ($100mK$), comparable to the Zeeman energy of a spin $1/2$ electron in a magnetic field of around 1 Tesla. Therefore, when operating at temperatures of the order of the Zeeman energy, the charge on a typical quantum dot is extremely well fixed by the number of electrons. The next question is whether a conductance electron, when penetrating the quantum dot, is able to efficiently interact with an excess spin $1/2$ particle for odd electron numbers, or whether it will usually follow a path which avoids strong exchange interaction. These, partly open, issues make it sometimes hard to judge the relevance of many interesting theories.

1. Correlations

The simplest model, which keeps the effect of Coulomb interactions and correlations, uses exactly one level from the quantum dot, adds links to leads (left and right), and takes Coulomb interaction of spin up and spin down electrons into account - but only on the dot (see Fig.36a).

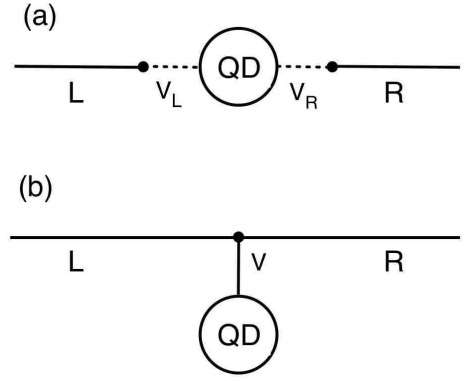


FIG. 36 Schematic representation of (a) a serial model of leads and a quantum dot (43)-(44), and (b) a T-shape model of leads and a side-coupled quantum dot (45).

The resulting Hamiltonian has the following form:

$$H_s = H_D + H_W, \quad H_D = \epsilon_d \sum_{\sigma} n_{\sigma} + U n_{\uparrow} n_{\downarrow}, \quad (43)$$

$$H_W = \sum_{k\sigma r} \epsilon_{kr} c_{k\sigma r}^{\dagger} c_{k\sigma r} + (V_r c_{k\sigma r}^{\dagger} d_{\sigma} + H.c.). \quad (44)$$

Here $n_{\sigma} = d_{\sigma}^{\dagger} d_{\sigma}$ measures the number of electrons on the quantum dot level, which interact with each other with strength U . The left and right leads are denoted by $r = L(R)$. The level energy ϵ_d is measured from the Fermi energy of the leads. The lead states are chosen in the momentum representation. All fermionic creation and annihilation operators $c, c^{\dagger}, d, d^{\dagger}$ obey the standard anticommutation relations.

2. Interferences

There are many ways to incorporate interference and multiple paths, in order to reach Fano resonances. One of the simplest ones is a T-shaped scheme, which is a small change of the above model by *side-coupling* the quantum dot to the quantum wire (leads) (see Fig.36b):

$$H_T = -t \sum_{n,\sigma} (c_{n,\sigma}^{\dagger} c_{n-1,\sigma} + c_{n,\sigma}^{\dagger} c_{n+1,\sigma}) + \sum_{\sigma} \epsilon_{d,\sigma} n_{\sigma} + \sum_{\sigma} (V d_{\sigma}^{\dagger} c_{0,\sigma} + V^* c_{0,\sigma}^{\dagger} d_{\sigma}) + U n_{\uparrow} n_{\downarrow}. \quad (45)$$

The lead states are chosen in the coordinate representation. Interference is possible because electrons can directly pass from the left to the right, but can also visit the side dot and exit again. These two paths are enough for destructive interference.

Another possibility is to extend the serial dot scheme (43)-(44) by adding a direct path (arm) for electrons to transit from the left to the right leads (Hofstetter *et al.*, 2001):

$$H_{AB} = H_s + H_a, \quad H_a = \sum_{kq\sigma} W e^{i\phi} c_{k\sigma R}^{\dagger} c_{q\sigma L} + H.c. \quad (46)$$

The phase ϕ models a magnetic flux which is encompassed by the loop of the direct path and the path via the quantum dot.

The Hamiltonians (43)-(44),(45) belong to the class of Anderson Hamiltonians (Anderson, 1961). Thus the thermodynamic properties of both models are similar, e.g. the average number of (spin up and spin down) electrons on the dot $\langle n_\sigma \rangle$. However, the transport properties depend crucially on the chosen geometry. Note that changing the dot level ϵ_d is qualitatively similar to varying the gate voltage of a quantum dot. The dot level is capable of accepting at most one spin up and one spin down electron.

Wiegmann and Tsvelick (1983) obtained analytical results for $\langle n_\sigma \rangle$ assuming a linearized spectrum of lead electrons, which is not a crucial constraint, as long as the lead electron bands are partially filled (ideally half-filling), and as long as the temperature is much smaller than the distance from the Fermi energy to the band edges. In addition, there exist various numerical methods to compute $\langle n_\sigma \rangle$ approximately.

With standard scattering matrix approaches, as well as using the Friedel sum rule ((Hewson, 1993; Langreth, 1966)), the conductance of the serial dot scheme (43)-(44) at zero temperature can be expressed in the following way ((Glazman and Raikh, 1988; Ng and Lee, 1988)):

$$g_\sigma = \left(\frac{2V_L V_R}{V_L^2 + V_R^2} \right)^2 \sin^2 \pi \langle n_\sigma \rangle . \quad (47)$$

Hofstetter *et al.* (2001) studied Fano resonances in transport through the the AB interferometer model (46) at zero temperature. The schematic view of the AB interferometer is similar to Fig.33(a). For zero AB phase $\phi = 0$, and the direct path being switched off $W = 0$, there are three states of a Coulomb blockade to be expected upon variation of the gate voltage ϵ_d : the dot contains either zero, one, or two electrons, with sharp transitions between them. We remind again, that the empty dot is almost not conducting (Coulomb energy too large), and the dot filled with two electrons as well (Pauli principle). When there is one electron on the dot, a second can enter while the first leaves. Despite of applying a magnetic field, model (46) is invariant under spin reversal (because the bare dot levels are not Zeeman splitted). This may be not easy to be achieved in an experiment. Therefore, when there is one electron on the dot, it can have either spin up or spin down, and on average $\langle n_\sigma \rangle = 1/2$ in that case. For $\epsilon_d > 0$ (Fermi energy is placed at zero) the dot is empty, and the conductance is zero. When $-U < \epsilon_d < 0$, one electron can enter the dot, but not two. Then additional electrons can tunnel through, giving maximal conductance. Finally, for $\epsilon_d < -U$, two electrons occupy the dot, and the conductance is zero again. This broad region of almost perfect conductance is due to spin exchange processes on the quantum dot level, and can be therefore related to the discussed above Kondo effect. Indeed, in Fig.37 this is

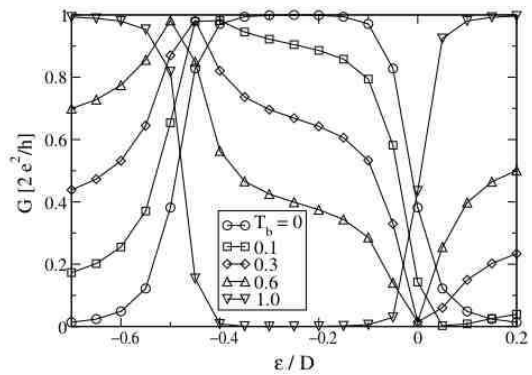


FIG. 37 Conductance as a function of ϵ_d for different values of background transmission T_b . The AB phase $\phi = 0$. From Hofstetter *et al.* (2001).

observed for $T_b = 0$ with $T_b = 4x/(1+x)^2$ being the background transmission probability, where $x = \pi^2 W^2 N_L N_R$, and $N_{L,R}$ is the density of states in the left (right) lead. With increasing T_b the curves change dramatically. Most importantly, a Fano resonance is appearing in the studied energy window, qualitatively similar to experimental observations (Kobayashi *et al.*, 2002). For the considered model the resonance location is shifting towards $-U/2$, and its width tends to $-U$, as T_b further increases Fig.37. A variation of the AB phase ϕ in some intermediate T_b regime yields the possibility to change the sign of the asymmetry parameter q .

3. Spin filters

When a magnetic field is applied to the AB interferometer setup in Fig.33(a), it is reasonable to consider also its action on the quantum dot region itself, which leads to a Zeeman splitting of the dot level. This is incorporated in the side dot model (45) with specifying

$$\epsilon_{d,\uparrow} = \epsilon_d + \Delta/2 , \quad \epsilon_{d,\downarrow} = \epsilon_d - \Delta/2 , \quad (48)$$

where Δ is the Zeeman energy up to which the single particle level is splitted for spin down and spin up electrons. It is easy to incorporate the AB phase shift as well, we will discuss it below.

For $U = 0$ (45) is reduced to the Fano-Anderson model (6), and the transmission is computed within the one-particle picture for an electron moving at the Fermi energy ϵ_F :

$$-\epsilon_F \phi_i = t(\phi_{n-1} + \phi_{n+1}) + V^* \varphi \delta_{n0}, \quad (49)$$

$$-\epsilon_F \varphi = -\epsilon_{d,\sigma} \varphi + V \phi_0, \quad (50)$$

where ϕ_n refers to the amplitude of a single particle at site n in the conducting channel and φ is the amplitude at the side dot. With the help of the Friedel sum rule ((Hewson, 1993; Langreth, 1966)) one arrives at (Torio *et al.*, 2004)

$$g_\sigma = \cos^2 \pi \langle n_\sigma \rangle . \quad (51)$$

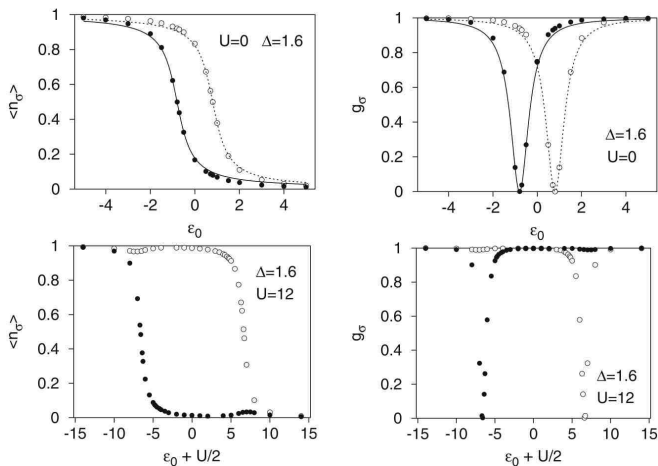


FIG. 38 Left plots: $\langle n_\sigma \rangle$ versus ϵ_d for a finite splitting $\Delta = 1.6$, $U = 0$ (top) and $U = 12$ (bottom). The black (white) dots represent the numerical results for the spin up (spin down) occupation number. Right plots: g_σ versus ϵ_d for finite splitting $\Delta = 1.6$, $U = 0$ (top) and $U = 12$ (bottom). The conductance is computed numerically for spin up (black dots) and spin down (white dots) electrons. The solid and the dashed lines on the top figures represent the exact results of Eq. (51). Adapted from Torio *et al.* (2004).

This relation has a geometric origin and actually holds for arbitrary U (at zero temperatures). For a nonzero magnetic field $\Delta \gg \Gamma$ the two Fano resonances for spin up and spin down electrons are energetically separated. Therefore, the current through the channel is completely polarized at $\epsilon_F = \epsilon_{d,\uparrow}$ and $\epsilon_F = \epsilon_{d,\downarrow}$. The AB phase can be easily included into the model (45) similar to (46). Remarkably it will not change the position of the resonances (cf. also (9)), since the position of the Fano resonance is entirely determined by the matching condition between the dot level(s) and the Fermi energy.

The obtained spin filter will operate at temperatures $kT \ll \Delta$. For a field of a few Tesla that implies temperatures less than $100mK$. While that is possible in principle, two more problems appear. First, to control such a spin filter, one would have to control the gate voltage on the scale of μeV (because the spin polarized Fano resonances are separated in the gate voltage by the same amount of the Zeeman energy). Second, as discussed above, Coulomb interactions have to be taken into account.

For nonzero U and Δ , the results for the mean number of particles on the dot, and for the spin-resolved conductance, have been obtained by Torio *et al.* (2004), and are shown in Fig.38. The main outcome is, that the presence of a strong Coulomb interaction is shifting the two Fano resonances for spin up and spin down electrons further apart. Therefore, the current through the channel is completely polarized at $\epsilon_F = \epsilon_{d,\uparrow} + U$ and $\epsilon_F = \epsilon_{d,\downarrow}$. For $U \gg \Delta$ the distance between the two spin polarized Fano resonances is of the order of the charging energy (and not the Zeeman energy). At the same time, the

Kondo regime is completely suppressed. For $\epsilon_F < \epsilon_{d,\downarrow}$, the dot level is empty, and electrons pass directly from the left to the right lead (background transmission). For $\epsilon_F = \epsilon_{d,\downarrow}$ the dot is opening for spin down electrons. A Fano resonance appears, and its width is determined solely by $\Gamma = 2|V|^2/|v_F|$ where $v_F = d\epsilon/dq|_{\epsilon_F}$ is the Fermi velocity. For $\epsilon_{d,\downarrow} < \epsilon_F < \epsilon_{d,\uparrow} + U$ the dot level is filled with one spin down electron, and does not contribute to the conductance, leading to direct transmission from left to right leads. For $\epsilon_F = \epsilon_{d,\uparrow} + U$ the dot is opening for spin up electrons. A Fano resonance appears, with the same width as for the previous case. Finally, for $\epsilon_F > \epsilon_{d,\uparrow} + U$, the dot is filled with two electrons and does not contribute to the conductance, leading to direct transmission from left to right leads.

For typical quantum dots with $L \approx 100nm$ and $B \approx 1T$, the spin filter effect is expected to be active for temperatures below $100mK$, with a distance between the spin polarized Fano resonances of the order of $20 - 50meV$. To observe it, one needs to monitor experimentally the spin-resolved flow of electrons with a spatial resolution less than the dot dimension.

F. More

Gurvitz and Levinson (1993) obtained resonant reflection and transmission within a generalized description of a conducting channel (with several transverse modes) with a single impurity.

Extensions of the theoretical models in order to include many dot levels were performed by Stefanski *et al.* (2004) for very large ($0.1eV$) charging energies. Two dots with rather small charging energies ($1meV$) were discussed by Stefanski (2003). A series of authors considered the limit $U \rightarrow \infty$ (Bulka and Stefanski, 2001; Kang *et al.*, 2001; Kang and Shin, 2000). It remains to be clarified, whether such models can be used to discuss temperature effects on transport properties through quantum dots.

Lee and Bruder (2006) extended the spin filter model by including spin-orbit interactions and extending the side dot into a side ring with many levels. Estimates of Kondo temperatures, and general temperature effects, have been discussed by Aligia and Salguero (2004). Lobos and Aligia (2008) included Rashba spin-orbit coupling into the consideration of AB interferometers (see also Chi *et al.* (2007); Gong *et al.* (2008); Sanchez and Serra (2006); Serra and Sáanchez (2007)). Spin inversion devices in a quasi-two-dimensional semiconductor wave guide under sectionally constant magnetic fields and spin-orbit interactions were discussed by Cardoso and Pereyra (2008).

Experimental progress was reported by Neel *et al.* (2007) through contacting the tip of a low-temperature scanning tunneling microscope with individual cobalt atoms adsorbed on Cu(100), where Fano resonances have been observed.

Single-molecule devices attracted attention recently.

There one sandwiches various molecules between gold electrodes and studies their conductance properties. Impressive Fano resonances (with the background transmission dropping by several orders of magnitude) were reported recently by Finch *et al.* (2009). The additional influence of Andreev reflection at low temperatures, when the metallic contacts turn superconducting, was studied by Kormányos *et al.* (2009).

Since Fano resonances rely on phase coherence of electrons traversing the structure along different paths, several authors investigated the influence of phonons on decoherence in quantum dots (Pastawski *et al.*, 2002; Torres *et al.*, 2006). Clerk *et al.* (2001) studied the possibility to extract phase decoherence properties from measurements on the q -factor of the Fano resonance.

VII. MORE

As was mentioned in Introduction, there exist many manifestations of Fano resonances in different fields. In this Section we mention several most recent results, which either very close conceptually to the problems discussed above or can be described by the similar models, even being associated with a completely different physics.

A. Matter wave scattering in Bose-Einstein condensates

First, we discuss the Fano physics associated with the transport properties of ultracold atoms and applications in the fields of matter-wave interferometry (Schumm *et al.*, 2005) or quantum information processing with neutral atoms (Jaksch *et al.*, 1999; Pachos and Knight, 2003). Over the last couple of years, it has been shown that optical lattices, generated by counter-propagating laser beams and providing a periodic potential modulation for the atoms, introduce many interesting and potentially useful effects by modifying single atom properties and enhancing correlations between atoms. When atoms are scattered across a localized Bose-Einstein condensate (BEC) in an optical lattice, the dramatic effects of scattering resonances can be observed, with either full transparency or total reflection (Vicencio *et al.*, 2007). These effects can be interpreted by employing the physics of a tunable Fano-like resonance, and they may lead to interesting applications for blocking and filtering atom beams (Vicencio *et al.*, 2007).

We follow Ref. (Vicencio *et al.*, 2007) and consider a BEC on a lattice, where interactions between atoms are present only in a very localized region (see Fig. 39). Such a situation could be realized experimentally by combining optical lattices with atom-chip technology (Hänsel *et al.*, 2001; Ott *et al.*, 2001) or in optical microlens arrays (Dumke *et al.*, 2002). Specifically, the system is described by the discrete nonlinear Schrödinger (DNLS) equation, a classical variant of the Bose-Hubbard

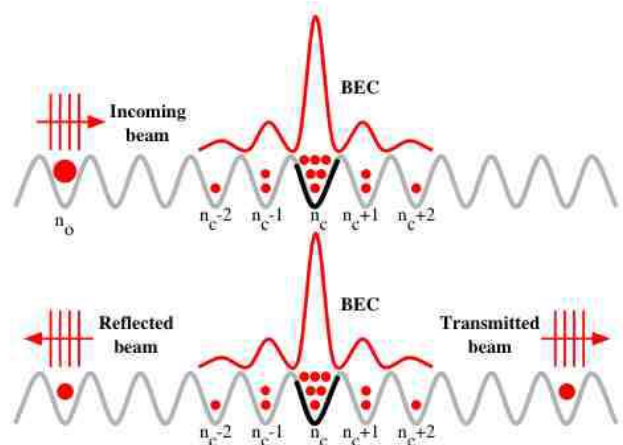


FIG. 39 (Color online) Scattering scheme in an optical lattice. The incoming, reflected, and transmitted beams of atoms are represented as plane waves. The atoms interact only around $n = n_c$, where the BEC is centered. From Vicencio *et al.* (2007).

model appropriate for a BEC in a periodic potential in the tight binding limit (Morsch and Oberthaler, 2006). With interactions being present only on site number n_c , we write in dimensionless form

$$i \frac{d\Psi_n}{dt} = -(\Psi_{n+1} + \Psi_{n-1}) - \gamma |\Psi_{n_c}|^2 \Psi_{n_c} \delta_{n,n_c}, \quad (52)$$

where Ψ_n is a complex amplitude of the BEC field at site n and $-\gamma = U/J$ is the interaction strength on site n_c , where J is the tunneling energy between the lattice sites and U is on-site interaction energy per atom. This simple model reflects generic features of BECs in a one-dimensional optical lattice with inhomogeneous scattering length. Furthermore, this model could be realized quantitatively in a deep optical lattice with tight transverse confinement (Smerzi and Trombettoni, 2003).

The model (52) is similar to the models discussed above in application to the scattering by discrete breathers (18) and photonic structures (38). It supports an exact localized solution $\Psi_n(t) = b x^{|n-n_c|} \exp(-iE_b t)$, where $x = -\frac{1}{2}(E_b + g)$ with $g = \gamma b^2$, b is the condensate amplitude and $E_b = -(4 + g^2)^{1/2}$ is the chemical potential.

The scattering of propagating atoms with the energy $E_k = -2 \cos k$ by this localized BEC can be studied analytically, in a full analogy with the optics. The transmission $T(k)$ is shown in Fig. 40 for three values of g (solid curves). As g increases, the width and the position of the resonance increase. Furthermore, the more localized the BEC becomes, the stronger it reflects the atom beam off resonance. By tuning the nonlinear parameter g , we can thus choose the amount of the beam which passes through the BEC. Off resonance (for larger values of k), we can select the percentage of the incoming beam that is transmitted for a defined quasi-momentum. Therefore, the actual setup can be used as a 100% blockade or as a

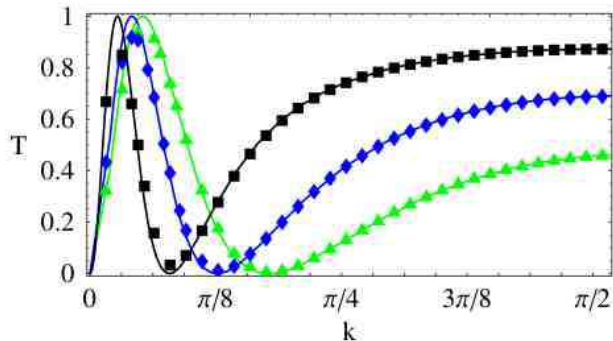


FIG. 40 (Color online). Transmission T versus momentum k . Lines: analytic solution, symbols: real time numerical simulations of Eq. (52) using wave packets for $g = 0.36$ (line and boxes), $g = 0.6$ (line and diamonds), and $g = 0.9$ (line and triangles). From Vicencio *et al.* (2007).

selective filter.

The analytical results have been confirmed by numerical simulation of Eq. (52) with the atom beam of a Gaussian profile. The results are shown in Fig. 40 by the symbols for three different values of the parameter g . The agreement between theory and simulations is almost perfect, but some disagreement is observed for small values of k where the group velocity is very small and the numerical computation of T is unreliable.

Conceptually similar schemes based on the resonant scattering associated with the effective Fano resonance discussed above have been suggested in many other settings. For example, Micheli *et al.* (Micheli *et al.*, 2004; Micheli and Zoller, 2006) proposed a scheme utilizing quantum interference to control the transport of atoms in one-dimensional optical lattices by a single impurity atom. In this scheme [see Fig. 41(a)], an atomic quantum gas interacts with a single internal atomic state, representing bosonic or fermionic modes, controlled by an atomic spin-1/2 impurity. The quantum gas is confined by tight trapping potentials (e.g., an optical or magnetic trap), so that only the motional degrees along the z axis in Fig. 1(a) are relevant. In the z direction the motion is confined to the left by a trapping potential (e.g., a blue sheet of light), while the atomic impurity restricts the motion of the gas to the right due to collisional interactions of the quantum gas with the impurity. The atom representing the impurity can, for example, be a different atomic species in a tight trapping potential. Thus the impurity atom plays the role of single-atom mirror confining the quantum gas in an atomic cavity. This allows one to amplify the state of the qubit, and provides a single-shot quantum nondemolition measurement of the state of the qubit. In view of the analogy between state amplification via this type of blocking mechanism and readout with single electron transistors used in solid state systems, this setup can be referred to as a single atom

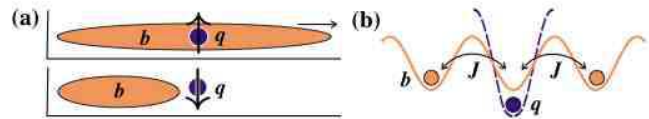


FIG. 41 (Color online) Single atom transistor. (a) A spin 1/2 impurity used as a switch: in one spin state it is transparent to the probe atoms, but in the other it acts as a single atom mirror. (b) Implementation of the SAT as a separately trapped impurity q with probe atoms b in an optical lattice. From Micheli *et al.* (2004).

transistor (SAT).

As a variant of the configuration of Fig. 41(a) Micheli *et al.* (Micheli *et al.*, 2004; Micheli and Zoller, 2006) considered the case where the quantum gas is loaded in an optical lattice, as illustrated in Fig. 41(b). In this case the gas could be loaded initially, for example, in a Mott insulating state, i.e., where large repulsion of the gas atom leads to a filling of the lattice sites with exactly one atom per lattice site. The cat state will thus correspond to a superposition of the Mott phase and the melted Mott phase, i.e., a quasi-condensate of atoms obtained by expansion of the atomic gas. In this case the distinguishing features of the two entangled quantum phases are the observation or nonobservation of interference fringes as signatures of the Mott and BEC phase, when the atomic gas is released in a single experiment.

A remarkable feature of the SAT is its resistance to both two- and three-body loss processes on the impurity site (Micheli *et al.*, 2004). Also, parallels may be drawn between the SAT and other systems coupled to fermionic and bosonic modes. These include the readout of a single photon in cavity quantum electrodynamics, electron counting statistics, and the transport of electrons past impurities such as quantum dots (although these particles are normally initially present on both sides of the impurity).

B. Detection of Efimov states via quantum interference

In 1970th V. Efimov predicted that a three-body quantum system can support weakly bound states (trimer) under conditions when none of the three constituting pairs are bound (Efimov, 1970, 1971). Efimov trimer states appear in the limit where the two-body interaction is too weak to support a two-body bound state (dimer). The number of bound states in which the three particles can exist is infinite. Efimov derived an effective potential-energy curve for such a system as a function of a three-particle 'hyperradius', which is proportional to the root-mean-square distance of the three particles from their centre of mass (Efimov, 1971). By solving time-independent Schrödinger equation, the allowed energy levels follow on iteratively from each

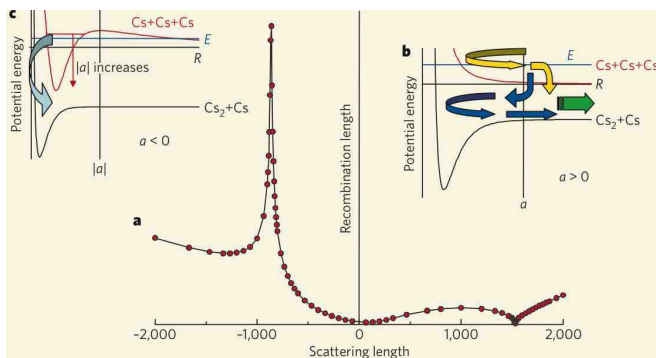


FIG. 42 (Color online) Observation of the Efimov states. (a) The theoretical rate of the three-body recombination process $Cs+Cs+Cs \rightarrow Cs_2+Cs$, obtained from numerical solutions of the three-body Schrödinger equation (D’Incao and Esry, 2006; Esry and Greene, 2006) and plotted as a function of the two-body scattering length a (in units of the Bohr radius a_0). Insets (b,c) the three-body potentials responsible for these features: the potential before recombination of three incident atoms at energy E (blue line) is shown in red; that after recombination, in black. The resonance positions change with the scattering length (shown by the arrow), tuning the system in and out of resonance and yielding a series of peaks in the recombination length. From Esry and Greene (2006).

other according to the rule $E_{n+1} = E_n \exp(-2\pi/s_0)$, where s_0 is a constant related to the strength of the so-called effective dipole moment with a value slightly greater than one (D’Incao and Esry, 2006; Efimov, 1971; Esry and Greene, 2006; Jensen and Fedorov, 2003). Thus, the binding energies decrease exponentially as n increases. Surprisingly, such trimer states should exist regardless of the nature of the two-body interaction, and, thus, are generic in few-body systems and now is being seen as central to Bose-Einstein condensation and other ultracold phenomena in dilute atomic gases. These trimer states do not have a classical analogue, because the binding mechanism is purely quantum mechanical. Recently, the first experimental observation of Efimov states has been reported in ultracold cesium trimers (Kraemer *et al.*, 2006), by measuring the three-body recombination process $Cs+Cs+Cs \rightarrow Cs_2+Cs$. The fingerprint of Efimov trimers in this system appears as resonant enhancement and suppression of three-body collisions as a function of the two-atom interaction strength (Esry and Greene, 2006; Kraemer *et al.*, 2006), with typical asymmetric profiles. Mazumdar *et al.* (2006) explained this asymmetric response in terms of the Fano resonance, suggesting that the asymmetry can be used as a diagnostic tool for the Efimov effect. Indeed, the very weak bounding and large spacial spread of the Efimov states (discrete levels) lead to strong overlap with the continuum states, resulting in possibilities for constructive and destructive interference phenomena.

Figures 42(a-c) show the theoretical rate of the three-body recombination process $Cs+Cs+Cs \rightarrow Cs_2+Cs$,

obtained from numerical solutions of the three-body Schrödinger equation (D’Incao and Esry, 2006; Esry and Greene, 2006) and plotted as a function of the two-body scattering length a (in units of the Bohr radius a_0). Predicted by the theory, the interference minimum at $a > 0$ and the resonance maximum at $a < 0$ were observed experimentally by Kraemer *et al.* (2006) in their studies of caesium recombination. For positive a , the transition between the two potentials takes place a by one of two paths (blue and yellow pathways). Minima and maxima in the recombination rate arise from quantum-mechanical interference between these two paths in the outgoing channel (green arrow) leading to the asymmetrical Fano profiles.

C. Transport through carbon nanotubes

During last decades, carbon nanotubes have been studied extensively because of their unconventional properties (Saito *et al.*, 1998). For applications to nanoscale electronic devices, researchers have fabricated various forms of carbon nanotubes to engineer their physical properties, including new morphologies such as X- and T-shaped junctions (Terrones *et al.*, 2000). These developments offer interesting opportunities to study phasecoherent transport in novel geometries. In the closed or unitary geometry, the conductance generally exhibits the Fano line shape (Kobayashi *et al.*, 2002). Similar to other systems discussed in this paper, the Fano effect arises from the coherent interference between a narrow localized level (quantum dot) and a continuum energy spectrum (the arm without a quantum dot). Carbon nanotubes are excellent objects for observing phase coherence phenomena and Fano effects, and there are many theoretical studies and experimental signatures of the Fano effect in different types of carbon nanotubes (Babic and Schonenberger, 2004; Hu *et al.*, 2006; Kim *et al.*, 2005, 2003; Yi *et al.*, 2003; Zhang and Chandrasekhar, 2006; Zhang *et al.*, 2004), including the studies of the direct transport through a single quantum dot (Göres *et al.*, 2000).

In particular, Fano resonances are very pronounced in the transport properties of a multiply connected carbon nanotubes shown in Fig. 43(b), where a single tube is branched off into two smaller arms and then they merge into one. Both π -bonding and π^* (π anti)-bonding electron transport channels show resonant tunneling through discrete energy levels in the finite arms (Kim *et al.*, 2005). The width of the resonant tunneling peaks in the π channel is broad and the transmission probability is fairly uniform as a function of energy. The π^* channel, on the other hand, has a more interesting structure of either broad or narrow resonant tunneling.

The conductance as a function of the incident electron energy is displayed in Fig. 43 for a fixed length. To examine the structure of the conductance in detail, total conductance is decomposed into two nonmixing contri-

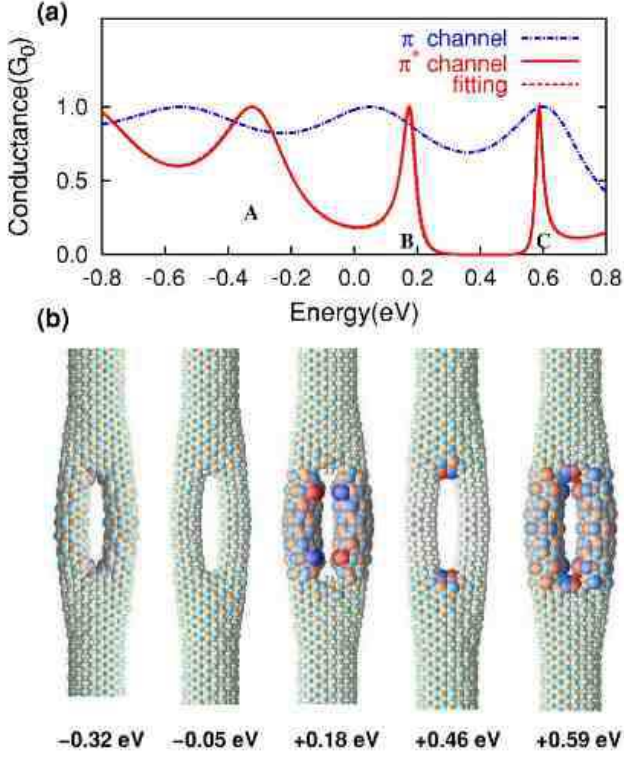


FIG. 43 (Color online) Conductance and wave functions calculated numerically in Ref. (Kim *et al.*, 2005). In (a), the full numerical calculation for π^* (solid line) is indistinguishable from the fit with the multiple Fano resonance formula (dashed line). In (b), the dark spheres indicate \pm signs and the size of the spheres is the amplitude of the wave function. From Kim *et al.* (2005).

contributions of π and π^* channels, $G = G_0(T_\pi + T_{\pi^*})$, where T_π and T_{π^*} are the transmission probabilities of the two. Kim *et al.* (2005) found that T_π always has peaks of magnitude one and varies very slowly as a function of energy, whereas T_{π^*} always has both broad and narrow peaks of magnitude one, and the line shape is highly asymmetric, especially for narrow peaks. T_π has no zeroes within the interested energy window while T_{π^*} is featured with zeroes near the narrow asymmetric peaks [see an example in Fig. 43(a)]. Coherent interference between a very broad level and its narrow neighboring level is evident in the asymmetric Fano-type line shapes of the π^* transport channel, and the corresponding transmission probability is featured with both zero and unity.

To confirm the concept of the Fano resonances, Kim *et al.* (2005) fitted the curve of T_{π^*} with the multilevel generalization of the Greens function formula. The curve fitting is practically indistinguishable from the π^* -channel conductance indicating that the simple model with the multilevel transmission formula is valid for explaining the Fano resonance structures and the transmission zeroes.

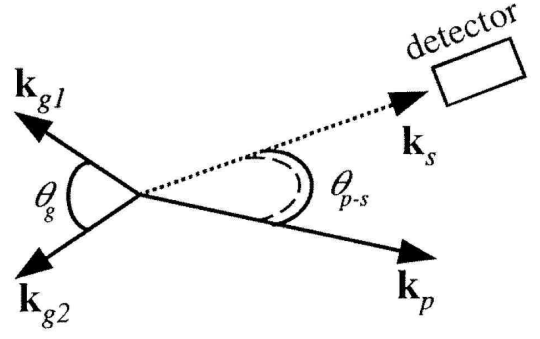


FIG. 44 Planar wavevector diagram illustrating the phase-matching condition for RFWM. From Teodoro and McCormack (1999).

D. Resonant four-wave mixing induced autoionization

Four-wave mixing is one of the most important phenomena in optics, which involves the interaction of three laser beams to produce a nonlinear polarization via the cubic electric susceptibility $\chi^{(3)}$. The induced polarization acts as the source of a fourth coherent light beam, detected as the signal. Four-wave mixing can be considered as the formation and scattering from laser-induced gratings. The grating is formed by two laser beams, called grating beams, with wavevector \mathbf{k}_g . The third probe beam with the wavevector \mathbf{k}_p is then scattered off the laser-induced grating and produces the fourth scattered beam, which is detected as the four-wave mixing signal. Due to the energy conservation, the frequency of the signal beam must be equal to the frequency of the probe beam $\omega_s \equiv \omega_p$. Momentum conservation results in a phase-matching condition for the signal wavevector

$$|\mathbf{k}_s| = |\mathbf{k}_{g1} - \mathbf{k}_{g2} + \mathbf{k}_p| = \omega_p/c, \quad (53)$$

and the Bragg-scattering angular condition

$$\frac{\omega_p}{\omega_g} = \frac{\sin(\theta_g/2)}{\sin(\theta_{p-s}/2)}, \quad (54)$$

where θ_g is the angle between two grating beams, and θ_{p-s} is the angle between the probe and signal beams (see Fig. 44).

In general, the four-wave mixing process can take place in any material. When the frequency of the incident laser beams matches the transition resonances of the medium, a drastic enhancement of the signal intensity can be observed. Such processes are called resonant four-wave mixings (RFWMs), and used as spectroscopic and diagnostic tools for probing stable and transient molecular species. Armstrong and Wynne (1974) studied experimentally four-wave mixing involving an autoionizing resonances in alkali-metal atomic vapor. In their experiment a two-photon transition between two bound states of the metal was excited, followed by single-photon absorption to the autoionizing level. The

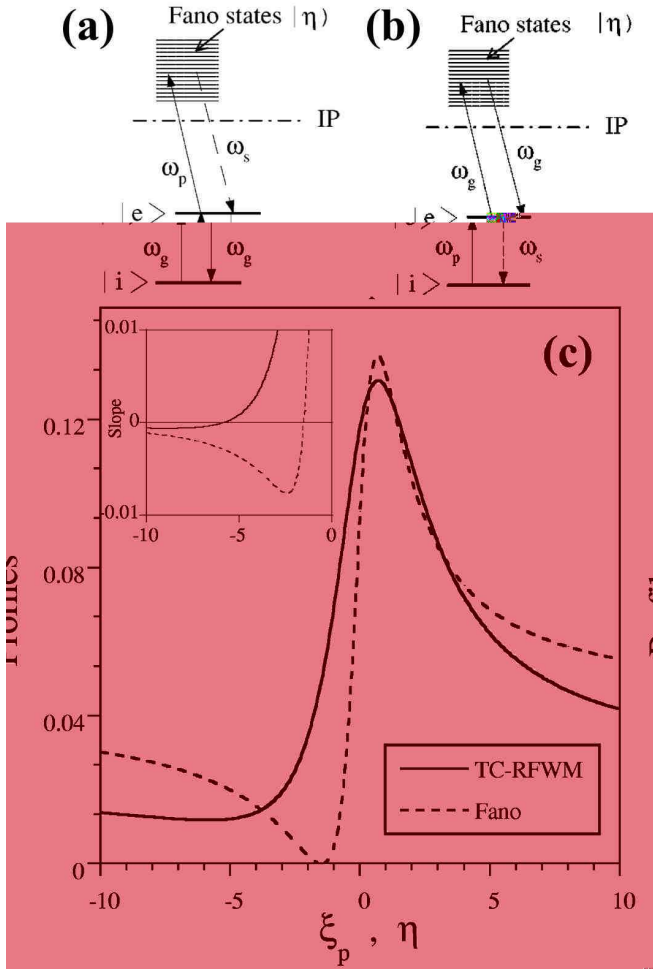


FIG. 45 Two-color resonant four-wave mixing. (a) Nonparametric and (b) parametric TC-RFWM process. Autoionizing level (Fano state) above the ionization potential (IP) is indicated by $|\eta\rangle$, $|i\rangle$ and $|e\rangle$ are ground and intermediate states, respectively. (c) Comparison of TC-RFWM and Fano profiles. Inset: the slopes of two profiles. It clearly indicates the separation between the slope zeros corresponding to profiles minima. This might be of crucial importance in analyzing observed lineshapes. From Teodoro and McCormack (1998).

detected signal demonstrated a characteristic asymmetric response. Using the Fano formalism, the authors derived an expression for the line-shape and fitted it with the Fano formula (Armstrong and Wynne, 1974), which allows to obtain the width and asymmetry parameter for the autoionizing states (Agarwal and Lakshmi, 1983; Alber and Zoller, 1983; Armstrong and Beers, 1975; Crance and Armstrong, 1982a,b; Haan and Agarwal, 1987; Meier *et al.*, 1995). Thus, this form of RFWM can be considered as one of the techniques to study autoionizing levels.

A double resonant version of RFWM is called two-colour RFWM (TC-RFWM) when two optical fields have frequencies resonant with two different transitions. It

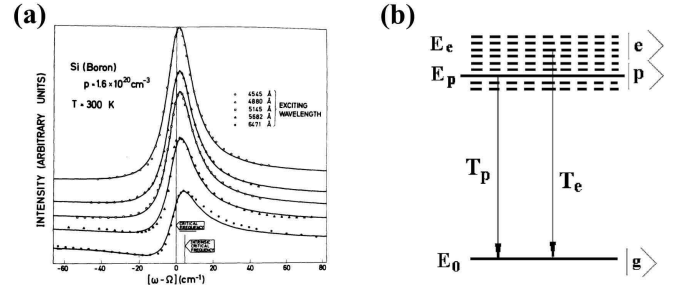


FIG. 46 Fano resonance in Raman scattering of heavily doped semiconductors. (a) Raman scattering vs scattering wavelength for p -type Si. The solid lines are theoretical fits, with the Fano formula (1), to experimental results (discrete points). From Cerdeira *et al.* (1973a). (b) Schematic illustration of the ground $|g\rangle$, electronic continuum $|e\rangle$, and optical phonon $|p\rangle$ states with corresponding transitions involved in a Fano resonance. From Jin and Xu (2007).

provides with a variety of excitation schemes, which are very useful for high-resolution spectroscopy. In Figure 45 possible TC-RFWM excitation schemes are shown, where the grating beams are in the resonance with the lower transition [see Fig. 45(a)], and vice-versa [see Fig. 45(b)]. Because of the presence of autoionizing states in overall FWM process, in both cases TC-RFWM exhibits asymmetric profiles, which can up to certain extent be approximated by the Fano formula [see Fig. 45(c)]. Unlike the Fano profile, the TC-RFWM spectral lines have no zero. It can be interpreted due to dephasing during nonlinear parametric conversions, which is the key difference to the standard linear Fano resonance. Nevertheless, TC-RFWM provides with an efficient way to coherently control the signal lineshape (McCormack *et al.*, 1998).

E. Raman scattering of heavily doped semiconductors

It is worth noting that asymmetric lineshapes were also observed in Raman spectra of heavily doped semiconductors (Bechstedt and Peuker, 1975; Bell *et al.*, 1973; Cerdeira *et al.*, 1973a; Chandrasekhar *et al.*, 1978; Hopfield *et al.*, 1967; Magidson and Beserman, 2002) and high- T_c superconductors (Friedl *et al.*, 1990; Limonov *et al.*, 1998, 2000; Misochko *et al.*, 2000). Although, almost every asymmetric profile of these spectra can be nicely fitted by the Fano formula (Aleshkin *et al.*, 2007; Belitsky *et al.*, 1997; Cardona, 1983; Cardona *et al.*, 1974; Cerdeira *et al.*, 1973b; Hase *et al.*, 2006b; Jin and Xu, 2007; Jin *et al.*, 2001; Lee *et al.*, 2006; Menéndez and Cardona, 1985), a suitable theory for a quantitative description of all cases is still lacking. The general qualitative understanding is the following. The absorbed photon can initiate two kind of processes. The first one is the inter- or intra-band electronic transition from the ground state

to the continuum. The second process is the transition to the intermediate state followed by the one-phonon Raman emission and electron transition to either the initial ground state or to the excited donor state. Thus, the interference of two processes may, indeed, result in the Fano resonance.

There are many other systems where the Fano resonance was observed and studied in details, but they are out of the scope of this Review. To name a few, the resonant phonon transport between two crystalline media in the presence of a weakly bounded intermediate layer due to nonlocal interaction (Kosevich, 1997, 2008; Kosevich *et al.*, 2008).

VIII. CONCLUSIONS

This Review offers a bird-eye view on the Fano resonances in various physical systems. All examples presented here share the same basic feature - coexistence of resonant and nonresonant paths for scattering wave to propagate. It results in constructive and destructive interference phenomena, producing, in general, asymmetric lineshapes, first quantitatively described by Ugo Fano. It turns out to be a very common situation in complex systems. This makes the Fano resonance a generic phenomenon. The proper understating of it allows to explain or predict the behaviour of a system under consideration. The characteristic features of the Fano resonance are asymmetric profile or resonant suppression of the response of the system. Several detailed examples considered in this Review demonstrate that regardless the complexity of the system it is always possible to decompose it onto two interacting parts - resonant and nonresonant ones. In some cases it is obvious due to topology (a waveguide with side-coupled cavity, for example), but in some cases it becomes very tricky like scattering by discrete breathers. But, nevertheless, all systems supporting the Fano resonance can be mapped to the Fano-Anderson model. This model is very simple and provides with the core understanding of the phenomenon. It can be considered as a guideline for explanation of the Fano resonance in the particular system.

The interference origin makes the Fano resonance a very common effect in the scattering of waves, which could be of different nature. And we hope that the Reader is now able to answer the question: "Physics without Fano resonances?!".

The work has been supported by the Australian Research Council through the Discovery and Center of Excellence projects.

References

- de Abajo, F. J. G., 2007, "Colloquium: Light scattering by particle and hole arrays," *Rev. Mod. Phys.* **79**, 1267.
- Agarwal, G. S., and P. A. Lakshmi, 1983, "Effect of spontaneous emission and recombination on the four-wave mixing profiles involving autoionizing resonances," *Phys. Rev. A* **28**, 3430–3437.
- Agrawal, G., 1995, *Nonlinear Fiber Optics* (Academic, San Diego).
- Aharony, A., O. Entin-Wohlman, B. I. Halperin, and Y. Imry, 2002, "Phase measurement in the mesoscopic Aharonov-Bohm interferometer," *Phys. Rev. B* **66**, 115311.
- Aharony, A., O. Entin-Wohlman, and Y. Imry, 2003, "Measuring the Transmission Phase of a Quantum Dot in a Closed Interferometer," *Phys. Rev. Lett.* **90**, 156802.
- Aikawa, H., K. Kobayashi, A. Sano, S. Katsumoto, and Y. Iye, 2004, "Observation of "Partial Coherence" in an Aharonov-Bohm Interferometer with a Quantum Dot," *Phys. Rev. Lett.* **92**, 176802.
- Alber, G., and P. Zoller, 1983, "Harmonic generation and multiphoton ionization near an autoionizing resonance," *Phys. Rev. A* **27**, 1373–1388.
- Aleiner, I. L., P. W. Brouwer, and L. I. Glazman, 2002, "Quantum effects in Coulomb blockade," *Phys. Rep.* **358**, 309 – 440.
- Aleshkin, V. Y., A. V. Antonov, L. V. Gavrilenko, and V. I. Gavrilenko, 2007, "Fano resonance study in impurity photocurrent spectra of bulk GaAs and GaAs quantum wells doped with shallow donors," *Phys. Rev. B* **75**, 125201.
- Alhassid, Y., 2000, "The statistical theory of quantum dots," *Rev. Mod. Phys.* **72**, 895–968.
- Aligia, A. A., and L. A. Salguero, 2004, "Magnetotransport through a quantum wire side coupled to a quantum dot," *Phys. Rev. B* **70**, 075307.
- Altshuler, B. L., D. Khmel'nitzkii, A. I. Larkin, and P. A. Lee, 1980, "Magnetoresistance and Hall effect in a disordered two-dimensional electron gas," *Phys. Rev. B* **22**, 5142–5153.
- Altshuler, B. L., P. A. Lee, and R. A. Webb, 1991, *Mesoscopic Phenomena in Solids* (Springer, North-Holland, Amsterdam).
- Anderson, P. W., 1961, "Localized Magnetic States in Metals," *Phys. Rev.* **124**, 41–53.
- Aoki, K., H. Yamawaki, and M. Sakashita, 1996, "Observation of Fano interference in high-pressure ice VII," *Phys. Rev. Lett.* **76**, 784–786.
- Armstrong, J. A., and J. J. Wynne, 1974, "Autoionizing States of Sr Studied by the Generation of Tunable Vacuum uv Radiation," *Phys. Rev. Lett.* **33**, 1183–1185.
- Armstrong, L., and B. L. Beers, 1975, "Comment Concerning the Study of Autoionizing States Using Parametric Generation," *Phys. Rev. Lett.* **34**, 1290–1291.
- Armstrong, L., C. E. Theodosiou, and M. J. Wall, 1978, "Interference between radiative emission and autoionization in the decay of excited states of atoms," *Phys. Rev. A* **18**, 2538–2549.
- Aubry, S., 1997, "Breathers in nonlinear lattices: Existence, linear stability and quantization," *Physica D* **103**, 201–250.
- Auger, P., 1925a, "Sur l'effet photoélectrique composé," *J. Phys. Radium* **6**, 205–208.
- Auger, P., 1925b, "Sur les rayons secondaires produit dans un gal par. des rayons," *Comptes rendus* **180**, 65.
- Auger, P., 1926 *Ann. Phys. (Paris)* **6**, 183.
- Babic, B., and C. Schonenberger, 2004, "Observation of Fano resonances in single-wall carbon nanotubes," *Phys. Rev. B* **70**, 195408.
- Bachelier, G., I. Russier-Antoine, E. Benichou, C. Jonin, N. D. Fatti, F. Vallée, and P.-F. Brevet, 2008, "Fano Profiles Induced by Near-Field Coupling in Heterogeneous

- Dimers of Gold and Silver Nanoparticles,” *Phys. Rev. Lett.* **101**, 197401.
- Bagwell, P. F., and R. K. Lake, 1992, “Resonances in transmission through an oscillating barrier,” *Phys. Rev. B* **46**, 15329–15336.
- Bandopadhyay, S., B. Dutta-Roy, and H. S. Mani, 2004, “Understanding the Fano resonance through toy models,” *Am. J. Phys.* **72**, 1501–1507.
- Bandrauk, A. D., and J. P. Laplante, 1976, “Fano line shapes in predissociation,” *J. Chem. Phys.* **65**, 2602–2608.
- Bar-Ad, S., P. Kner, M. V. Marquezini, S. Mukamel, and D. S. Chemla, 1997, “Quantum Confined Fano Interference,” *Phys. Rev. Lett.* **78**, 1363–1366.
- Barnes, W. L., A. Dereux, and T. W. Ebbesen, 2003, “Surface plasmon subwavelength optics,” *Nature* **424**, 824–830.
- Bashevoy, M., V. Fedotov, and N. Zheludev, 2005, “Optical whirlpool on an absorbing metallic nanoparticle,” *Opt. Express* **13**, 8372–8379.
- Bechstedt, F., and K. Peuker, 1975, “Theory of interference between electronic and phonon Raman Scattering,” *Physica Status Solidi (b)* **72**, 743–752.
- Becker, U., T. Prescher, E. Schmidt, B. Sonntag, and H. E. Wetzl, 1986, “Decay channels of the discrete and continuum Xe [bold 4]d resonances,” *Phys. Rev. A* **33**, 3891–3899.
- Belitsky, V. I., A. Cantarero, M. Cardona, C. Trallero-Giner, and S. T. Pavlov, 1997, “Feynman diagrams and Fano interference in light scattering from doped semiconductors,” *J. Phys.: Condens. Matter* **9**, 5965–5976.
- Bell, M. I., R. N. Tyte, and M. Cardona, 1973, “Resonant Raman scattering in GaP in the E0 - E0 + [Delta]0 region,” *Solid State Communications* **13**, 1833 – 1837.
- Beutler, H., 1935, “Über Absorptionsserien von Argon, Krypton und Xenon zu Termen zwischen den beiden Ionisierungsgrenzen ${}^2P_3^{2/0}$ und ${}^2P_1^{2/0}$,” *Z. Phys. A* **93**, 177–196.
- Bhatia, A. K., and A. Temkin, 1984, “Line-shape parameters for 1P Feshbach resonances in He and Li^+ ,” *Phys. Rev. A* **29**, 1895–1900.
- Bianconi, A., 2003 (AIP Conf. Proc.), volume 652, 13–18.
- Billaudeau, C., S. Collin, F. Pardo, N. Bardou, and J.-L. Pelouard, 2009, “Tailoring radiative and non-radiative losses of thin nanostructured plasmonic waveguides,” *Opt. Express* **17**, 3490–3499.
- Binder, P., D. Abraimov, A. V. Ustinov, S. Flach, and Y. Zolotaryuk, 2000, “Observation of Breathers in Josephson Ladders,” *Phys. Rev. Lett.* **84**, 745–748.
- Boese, D., M. Lischka, and L. E. Reichl, 2000, “Resonances in a two-dimensional electron waveguide with a single δ -function scatterer,” *Phys. Rev. B* **61**, 5632–5636.
- Bohm, D., and D. Pines, 1951, “A Collective Description of Electron Interactions. I. Magnetic Interactions,” *Phys. Rev.* **82**, 625–634.
- Bohren, C. F., and D. R. Huffman, 1998, *Absorption and Scattering of Light by Small Particles* (Wiley).
- Born, M., and E. Wolf, 1999, *Principles of Optics* (Cambridge University Press, UK, 1999).
- Bortchagovsky, E. G., and U. C. Fischer, 2003 (SPIE), volume 5064, 47–61.
- Boyd, R. W., and D. J. Gauthier, 2006, “Photonics: Transparency on an optical chip,” *Nature* **441**, 701–702.
- Bravo-Abad, J., A. Rodriguez, P. Bermel, S. G. Johnson, J. D. Joannopoulos, and M. Soljacic, 2007, “Enhanced nonlinear optics in photonic-crystal microcavities,” *Opt. Express* **15**, 16161–16176.
- Breit, G., and E. Wigner, 1936, “Capture of Slow Neutrons,” *Phys. Rev.* **49**, 519–531.
- Bulka, B. R., and P. Stefanski, 2001, “Fano and Kondo Resonance in Electronic Current through Nanodevices,” *Phys. Rev. Lett.* **86**, 5128–5131.
- Burioni, R., D. Cassi, P. Sodano, A. Trombettoni, and A. Vezzi, 2005, “Propagation of discrete solitons in inhomogeneous networks,” *Chaos* **15**, 043501.
- Burioni, R., D. Cassi, P. Sodano, A. Trombettoni, and A. Vezzi, 2006, “Topological filters and high-pass/low-pass devices for solitons in inhomogeneous networks,” *Phys. Rev. E* **73**, 066624.
- Cardona, M. (ed.), 1983, *Light Scattering in Solids* (Heidelberg: Springer).
- Cardona, M., F. Cerdeira, and T. A. Fjeldly, 1974, “Sign of the Raman tensor of diamond and zinc-blende-type semiconductors,” *Phys. Rev. B* **10**, 3433–3435.
- Cardoso, J. L., and P. Pereyra, 2008, “Spin inversion devices operating at Fano anti-resonances,” *EPL* **83**, 38001.
- Cerdeira, F., T. A. Fjeldly, and M. Cardona, 1973a, “Effect of Free Carriers on Zone-Center Vibrational Modes in Heavily Doped p -type Si. II. Optical Modes,” *Phys. Rev. B* **8**, 4734–4745.
- Cerdeira, F., T. A. Fjeldly, and M. Cardona, 1973b, “Interaction between electronic and vibronic Raman scattering in heavily doped silicon,” *Solid State Commun.* **13**, 325 – 328.
- Chakrabarti, A., 2006, “Electronic transmission in a model quantum wire with side-coupled quasiperiodic chains: Fano resonance and related issues,” *Phys. Rev. B* **74**, 205315.
- Chandrasekhar, M., J. B. Renucci, and M. Cardona, 1978, “Effects of interband excitations on Raman phonons in heavily doped $n - Si$,” *Phys. Rev. B* **17**, 1623–1633.
- Chen, L., Z. Qiang, H. Yang, H. Pang, Z. Ma, and W. Zhou, 2009, “Polarization and angular dependent transmissions on transferred nanomembrane Fano filters,” *Opt. Express* **17**, 8396–8406.
- Chergui, M., N. Schwentner, and V. Chandrasekharan, 1991, “Fano profiles on multiphonon continua in electronic transitions of matrix-isolated NO,” *Phys. Rev. Lett.* **66**, 2499–2502.
- Chi, F., J.-L. Liu, and L.-L. Sun, 2007, “Fano-Rashba effect in a double quantum dot Aharonov-Bohm interferometer,” *J. Appl. Phys.* **101**, 093704.
- Clark, C. W., 2001, “Obituary: Ugo Fano (1912-2001),” *Nature* **410**, 164–164.
- Clerk, A. A., X. Waintal, and P. W. Brouwer, 2001, “Fano Resonances as a Probe of Phase Coherence in Quantum Dots,” *Phys. Rev. Lett.* **86**, 4636–4639.
- Connerade, J. P., 1998, *Highly Excited Atoms* (Cambridge University Press, UK).
- Cotting, R., J. R. Huber, and V. Engel, 1994, “Interference effects in the photodissociation of FNO,” *J. Chem. Phys.* **100**, 1040–1048.
- Cowan, A. R., and J. F. Young, 2003, “Optical bistability involving photonic crystal microcavities and Fano line shapes,” *Phys. Rev. E* **68**, 046606.
- Crance, M., and L. Armstrong, 1982a, “Fluorescence induced by resonant multiphoton ionisation near an autoionising state,” *J. Phys. B* **15**, 3199–3210.
- Crance, M., and L. Armstrong, 1982b, “Four-wave mixing under double-resonance conditions,” *J. Phys. B* **15**, 4637–4646.
- Cronewett, S. M., T. H. Oosterkamp, and L. P. Kouwen-

- hoven, 1998, “A Tunable Kondo Effect in Quantum Dots,” *Science* **281**, 540–544.
- Davis, L. C., and L. A. Feldkamp, 1977, “Interaction of many discrete states with many continua,” *Phys. Rev. B* **15**, 2961–2969.
- dell’Orto, T., M. D. Ventra, J. Almeida, C. Coluzza, and G. Margaritondo, 1995, “Evidence for a photocurrent Fano resonance in an artificial nanostructure,” *Phys. Rev. B* **52**, R2265–R2268.
- D’Incao, J. P., and B. D. Esry, 2006, “Enhancing the observability of the Efimov effect in ultracold atomic gas mixtures,” *Phys. Rev. A* **73**, 030703.
- Dixit, S. N., and P. Lambropoulos, 1979, “Line-profile considerations of resonant multiphoton ionization,” *Phys. Rev. A* **19**, 1576–1579.
- Druger, S. D., 1977, “Coupling-strength incoherence and the absorption line shape of an isolated resonance in a large molecule,” *J. Chem. Phys.* **67**, 3249–3255.
- Dumke, R., T. Mütter, M. Volk, W. Ertmer, and G. Birkl, 2002, “Interferometer-Type Structures for Guided Atoms,” *Phys. Rev. Lett.* **89**, 220402.
- Ebbesen, T., H. Lezec, H. Ghaemi, T. Thio, and P. Wolf, 1998, “Extraordinary optical transmission through sub-wavelength hole arrays,” *Nature* **391**, 667.
- Efimov, V. N., 1970, “Energy levels arising from resonant two-body forces in a three-body system,” *Phys. Lett. B* **33**, 563–564.
- Efimov, V. N., 1971, “Weakly-bound states of three resonantly-interacting particles,” *Sov. J. Nucl. Phys.* **12**, 589.
- Eichmann, U., T. F. Gallagher, and R. M. Konik, 2003, “Fano Line Shapes Reconsidered: Symmetric Photoionization Peaks from Pure Continuum Excitation,” *Phys. Rev. Lett.* **90**, 233004.
- Eiermann, B., T. Anker, M. Albiez, M. Taglieber, P. Treutlein, K.-P. Marzlin, and M. K. Oberthaler, 2004, “Bright Bose-Einstein Gap Solitons of Atoms with Repulsive Interaction,” *Phys. Rev. Lett.* **92**, 230401.
- Eisenberg, H. S., Y. Silberberg, R. Morandotti, A. R. Boyd, and J. S. Aitchison, 1998, “Discrete Spatial Optical Solitons in Waveguide Arrays,” *Phys. Rev. Lett.* **81**, 3383–3386.
- Emmanouilidou, A., and L. E. Reichl, 2002, “Floquet scattering and classical-quantum correspondence in strong time-periodic fields,” *Phys. Rev. A* **65**, 033405.
- Entin-Wohlman, O., A. Aharony, Y. Imry, and Y. Levinson, 2002a, “The Fano Effect in Aharonov-Bohm Interferometers,” *J. Low Temp. Phys.* **126**, 1251.
- Entin-Wohlman, O., A. Aharony, Y. Imry, Y. Levinson, and A. Schiller, 2002b, “Broken Unitarity and Phase Measurements in Aharonov-Bohm Interferometers,” *Phys. Rev. Lett.* **88**, 166801.
- Esry, B. D., and C. H. Greene, 2006, “Quantum physics: A menage a trois laid bare,” *Nature* **440**, 289–290.
- Fan, S., 2002, “Sharp asymmetric line shapes in side-coupled waveguide-cavity systems,” *Appl. Phys. Lett.* **80**, 908–910.
- Fan, S., and J. D. Joannopoulos, 2002, “Analysis of guided resonances in photonic crystal slabs,” *Phys. Rev. B* **65**, 235112.
- Fan, S., W. Suh, and J. D. Joannopoulos, 2003, “Temporal coupled-mode theory for the Fano resonance in optical resonators,” *J. Opt. Soc. Am. A* **20**, 569–572.
- Fan, S., P. R. Villeneuve, J. D. Joannopoulos, and H. A. Haus, 1998, “Channel Drop Tunneling through Localized States,” *Phys. Rev. Lett.* **80**, 960–963.
- Fan, S., P. R. Villeneuve, J. D. Joannopoulos, M. J. Khan, C. Manolatou, and H. A. Haus, 1999, “Theoretical analysis of channel drop tunneling processes,” *Phys. Rev. B* **59**, 15882–15892.
- Fano, U., 1935a, “On the absorption spectrum of noble gases at the arc spectrum limit,” *Nuovo Cimento* **12**, 154 (A translation edited by G. Pupillo, A. Zannoni, and C. W. Clark, arXiv:cond-mat/0502210).
- Fano, U., 1935b, “Sullo spettro di assorbimento dei gas nobili presso il limite dello spettro d’arco,” *Nuovo Cimento* **12**, 154–161.
- Fano, U., 1936, “Some Theoretical Considerations on Anomalous Diffraction Gratings,” *Phys. Rev.* **50**, 573–573.
- Fano, U., 1937, “On the Anomalous Diffraction Gratings. II,” *Phys. Rev.* **51**, 288–288.
- Fano, U., 1938, “Zur Theorie der Intensitätsanomalien der Beugung,” *Ann. Phys. (Leipzig)* **424**, 393–443.
- Fano, U., 1941, “The theory of anomalous diffraction gratings and of quasi-stationary waves on metallic surfaces (Sommerfeld’s waves),” *J. Opt. Soc. Am.* **31**, 213.
- Fano, U., 1961, “Effects of Configuration Interaction on Intensities and Phase Shifts,” *Phys. Rev.* **124**, 1866–1878.
- Fano, U., 1964, “Exclusion of Parity Unfavored Transitions in Forward Scattering Collisions,” *Phys. Rev.* **135**, B863–B864.
- Fano, U., 1965, “Interaction between Configurations with Several Open Shells,” *Phys. Rev.* **140**, A67–A75.
- Fano, U., 1970, “Quantum Defect Theory of l Uncoupling in H_2 as an Example of Channel-Interaction Treatment,” *Phys. Rev. A* **2**, 353–365.
- Fano, U., 1977, “Effects of Configuration Interaction on Intensities and Phase Shifts,” *Citation Classics* **8**, 219.
- Fano, U., and J. W. Cooper, 1965, “Line Profiles in the Far-uv Absorption Spectra of the Rare Gases,” *Phys. Rev.* **137**, A1364–A1379.
- Fano, U., and J. W. Cooper, 1968, “Spectral Distribution of Atomic Oscillator Strengths,” *Rev. Mod. Phys.* **40**, 441–507.
- Fano, U., and C. M. Lee, 1973, “Variational Calculation of R Matrices. Application to Ar Photoabsorption,” *Phys. Rev. Lett.* **31**, 1573–1576.
- Feneuille, S., S. Liberman, J. Pinard, and A. Taleb, 1979, “Observation of Fano profiles in photoionization of rubidium in the presence of a dc field,” *Phys. Rev. Lett.* **42**, 1404–1406.
- Feshbach, H., 1958, “Unified theory of nuclear reactions,” *Ann. Phys. (N. Y.)* **5**, 357–390.
- Feshbach, H., 1962, “A unified theory of nuclear reactions. II,” *Ann. Phys. (N. Y.)* **19**, 287.
- Finch, C. M., V. M. García-Suárez, and C. J. Lambert, 2009, “Giant thermopower and figure of merit in single-molecule devices,” *Phys. Rev. B* **79**, 033405.
- Flach, S., V. Fleurov, A. Gorbach, and A. Miroshnichenko, 2006, “Resonant light-light interaction in slab waveguides: angular filters and spectral hole burning,” *Proc. SPIE* **5975**, 297–306.
- Flach, S., V. Fleurov, A. V. Gorbach, and A. E. Miroshnichenko, 2005, “Resonant Light Scattering by Optical Solitons,” *Phys. Rev. Lett.* **95**, 023901.
- Flach, S., A. E. Miroshnichenko, and M. V. Fistul, 2003a, “Wave scattering by discrete breathers,” *Chaos* **13**, 596–609.
- Flach, S., A. E. Miroshnichenko, V. Fleurov, and M. V. Fistul, 2003b, “Fano Resonances with Discrete Breathers,” *Phys.*

- Rev. Lett. **90**, 084101.
- Flach, S., and C. R. Willis, 1998, “Discrete breathers,” Phys. Rep. **295**, 181–264.
- Fleischhauer, M., A. Imamoglu, and J. P. Marangos, 2005, “Electromagnetically induced transparency: Optics in coherent media,” Rev. Mod. Phys. **77**, 633.
- Franson, J. D., and S. M. Hendrickson, 2006, “Optical transparency using interference between two modes of a cavity,” Phys. Rev. A **74**, 053817.
- Fransson, J., and A. V. Balatsky, 2007, “Exchange interaction and Fano resonances in diatomic molecular systems,” Phys. Rev. B **75**, 153309.
- Friedl, B., C. Thomsen, and M. Cardona, 1990, “Determination of the superconducting gap in $R\text{Ba}_2\text{Cu}_3\text{O}_7-\delta$,” Phys. Rev. Lett. **65**, 915–918.
- Friedrich, H., and D. Wintgen, 1985a, “Interfering resonances and bound states in the continuum,” Phys. Rev. A **32**, 3231–3242.
- Friedrich, H., and D. Wintgen, 1985b, “Physical realization of bound states in the continuum,” Phys. Rev. A **31**, 3964–3966.
- Galli, M., S. L. Portalupi, M. Belotti, L. C. Andreani, L. O’Faolain, and T. F. Krauss, 2009, “Light scattering and Fano resonances in high-Q photonic crystal nanocavities,” Appl. Phys. Lett. **94**, 071101.
- Ganz, J., M. Raab, H. Hotop, and J. Geiger, 1984, “Changing the Beutler-Fano profile of the Ne ns' autoionizing resonances,” Phys. Rev. Lett. **53**, 1547–1550.
- Gersen, H., T. J. Karle, R. J. P. Engelen, W. Bogaerts, J. P. Korterik, N. F. van Hulst, T. F. Krauss, and L. Kuipers, 2005, “Real-Space Observation of Ultraslow Light in Photonic Crystal Waveguides,” Phys. Rev. Lett. **94**, 073903.
- Ghaemi, H. F., T. Thio, D. E. Grupp, T. W. Ebbesen, and H. J. Lezec, 1998, “Surface plasmons enhance optical transmission through subwavelength holes,” Phys. Rev. B **58**, 6779–6782.
- Glazman, L. I., and M. E. Raikh, 1988, “Resonant Kondo transparency of a barrier with quasilocal impurity states,” JETP Lett. **47**, 452–455.
- Glutsch, S., 2002, “Optical absorption of the Fano model: General case of many resonances and many continua,” Phys. Rev. B **66**, 075310.
- Goldhaber-Gordon, D., J. Göres, M. A. Kastner, H. Shtrikman, D. Mahalu, and U. Meirav, 1998a, “From the Kondo Regime to the Mixed-Valence Regime in a Single-Electron Transistor,” Phys. Rev. Lett. **81**, 5225–5228.
- Goldhaber-Gordon, D., J. Göres, H. Shtrikman, D. Mahalu, U. Meirav, and M. A. Kastner, 2001, “The Kondo effect in a single-electron transistor,” J. Mater. Sci. Eng. B **84**, 17–21.
- Goldhaber-Gordon, D., H. Shtrikman, D. Mahalu, D. Abusch-Magder, U. Meirav, and M. A. Kastner, 1998b, “Kondo effect in a single-electron transistor,” Nature **391**, 156–159.
- Gong, W., Y. Zheng, Y. Liu, F. N. Kariuki, and T. Lü, 2008, “Fano effect in a T-shaped double quantum dot structure in the presence of Rashba spin-orbit coupling,” Phys. Lett. A **372**, 2934–2940.
- Göres, J., D. Goldhaber-Gordon, S. Heemeyer, M. A. Kastner, H. Shtrikman, D. Mahalu, and U. Meirav, 2000, “Fano resonances in electronic transport through a single-electron transistor,” Phys. Rev. B **62**, 2188–2194.
- Grillet, C., D. Freeman, B. Luther-Davies, S. Madden, R. McPhedran, D. J. Moss, M. J. Steel, and B. J. Eggleton, 2006, “Characterization and modeling of Fano resonances in chalcogenide photonic crystal membranes,” Opt. Express **14**, 369.
- Gurvitz, S. A., and Y. B. Levinson, 1993, “Resonant reflection and transmission in a conducting channel with a single impurity,” Phys. Rev. B **47**, 10578–10587.
- Haan, S. L., and G. S. Agarwal, 1987, “Stability of dressed states against radiative decay in strongly coupled bound-continuum transitions,” Phys. Rev. A **35**, 4592–4604.
- Hänsel, W., P. Hommelhoff, T. W. Hänsch, and J. Reichel, 2001, “Bose–Einstein condensation on a microelectronic chip,” Nature **413**, 498–501.
- Hanson, R., L. P. Kouwenhoven, J. R. Petta, S. Tarucha, and L. M. K. Vandersypen, 2007, “Spins in few-electron quantum dots,” Rev. Mod. Phys. **79**, 1217.
- Hao, F., P. Nordlander, M. T. Burnett, and S. A. Maier, 2007, “Enhanced tunability and linewidth sharpening of plasmon resonances in hybridized metallic ring/disk nanocavities,” Phys. Rev. B **76**, 245417.
- Hao, F., Y. Sonnefraud, P. van Dorpe, S. A. Maier, N. J. Halas, and P. Nordlander, 2008, “Symmetry Breaking in Plasmonic Nanocavities: Subradiant LSPR Sensing and a Tunable Fano Resonance,” Nano Lett. **8**, 3983–3988.
- Harbers, R., S. Jochim, N. Moli, R. F. Mahrt, D. Erni, J. A. Hoffnagle, and W. D. Hinsberg, 2007, “Control of Fano line shapes by means of photonic crystal structures in a dye-doped polymer,” Appl. Phys. Lett. **90**, 201105.
- Harmin, D. A., 1985, “Asymmetry of field-induced shape resonances in hydrogen,” Phys. Rev. A **31**, 2984–2990.
- Hase, M., J. Demsar, and M. Kitajima, 2006a, “Photoinduced Fano resonance of coherent phonons in zinc,” Phys. Rev. B **74**, 212301.
- Hase, M., J. Demsar, and M. Kitajima, 2006b, “Photoinduced Fano resonance of coherent phonons in zinc,” Physical Review B (Condensed Matter and Materials Physics) **74**, 212301.
- Haus, H. A., and Y. Lai, 1991, “Narrow-band distributed feedback reflector. design,” J. Lightwave Technol. **9**, 754.
- Heinzmann, U., J. Kessler, and J. Lorenz, 1970, “Wavelength Dependence of the Fano Effect,” Phys. Rev. Lett. **25**, 1325–1325.
- Heller, D. F., and S. Mukamel, 1979, “Theory of vibrational overtone line shapes of polyatomic molecules,” J. Chem. Phys. **70**, 463–472.
- Hessel, A., and A. A. Oliner, 1965, “A New Theory of Wood’s Anomalies on Optical Gratings,” Applied Optics **4**, 1275.
- Hewson, A. C., 1993, *The Kondo Problem to Heavy Fermions* (Cambridge University Press, UK).
- Hino, K.-i., 2001, “Overlap structure of Fano-resonance profiles of excitons in a semiconductor quantum well,” Phys. Rev. B **64**, 075318.
- Hino, K.-i., and N. Toshima, 2005, “Spectral modulation of exciton Fano resonance due to Zener breakdown in strongly biased superlattices,” Phys. Rev. B **71**, 205326.
- Hofstetter, W., J. König, and H. Schoeller, 2001, “Kondo Correlations and the Fano Effect in Closed Aharonov-Bohm Interferometers,” Phys. Rev. Lett. **87**, 156803.
- Holfeld, C. P., F. Loser, M. Sudzius, K. Leo, D. M. Whittaker, and K. Kohler, 1998, “Fano Resonances in Semiconductor Superlattices,” Phys. Rev. Lett. **81**, 874–877.
- Hopfield, J. J., P. J. Dean, and D. G. Thomas, 1967, “Interference between Intermediate States in the Optical Properties of Nitrogen-Doped Gallium Phosphide,” Phys. Rev. **158**, 748–755.
- Hu, F., H. Yang, X. Yang, and J. Dong, 2006, “Electronic

- transport and Fano resonance in carbon nanotube ring systems,” *Phys. Rev. B* **73**, 235437.
- van der Hulst, H. C., 1981, *Light Scattering by Small Particles* (Dover, New York).
- Iwanow, R., R. Schiek, G. I. Stegeman, T. Pertsch, F. Lederer, Y. Min, and W. Sohler, 2004, “Observation of Discrete Quadratic Solitons,” *Phys. Rev. Lett.* **93**, 113902.
- Jacobsen, R., A. Lavrinenko, L. Frandsen, C. Peucheret, B. Zsigri, G. Moulin, J. Fage-Pedersen, and P. Borel, 2005, “Direct experimental and numerical determination of extremely high group indices in photonic crystal waveguides,” *Opt. Express* **13**, 7861–7871.
- Jaksch, D., H.-J. Briegel, J. I. Cirac, C. W. Gardiner, and P. Zoller, 1999, “Entanglement of Atoms via Cold Controlled Collisions,” *Phys. Rev. Lett.* **82**, 1975–1978.
- Janzen, E., G. Grossmann, R. Stedman, and H. G. Grimmeiss, 1985, “Fano resonances in chalcogen-doped silicon,” *Phys. Rev. B* **31**, 8000–8012.
- Jensen, A. S., and D. V. Fedorov, 2003, “Efimov states in asymmetric systems,” *Europhys. Lett.* **62**, 336–342.
- Ji, Y., M. Heiblum, D. Sprinza, D. Mahalu, and H. Shtrikman, 2000, “Phase Evolution in a Kondo-Correlated System,” *Science* **290**, 779–783.
- Jin, K.-j., and S. J. Xu, 2007, “Fano resonance in the luminescence spectra of donor bound excitons in polar semiconductors,” *Appl. Phys. Lett.* **90**, 032107.
- Jin, K.-j., J. Zhang, Z.-h. Chen, G.-z. Yang, Z. H. Chen, X. H. Shi, and S. C. Shen, 2001, “Phonon-induced photoconductive response in doped semiconductors,” *Phys. Rev. B* **64**, 205203.
- Joe, Y. S., A. M. Satanin, and C. S. Kim, 2006, “Classical analogy of Fano resonances,” *Phys. Scr.* **74**, 259.
- Johnson, A. C., C. M. Marcus, M. P. Hanson, and A. C. Gossard, 2004, “Coulomb-Modified Fano Resonance in a One-Lead Quantum Dot,” *Phys. Rev. Lett.* **93**, 106803.
- Kang, K., S. Y. Cho, J.-J. Kim, and S.-C. Shin, 2001, “Anti-Kondo resonance in transport through a quantum wire with a side-coupled quantum dot,” *Phys. Rev. B* **63**, 113304.
- Kang, K., and S.-C. Shin, 2000, “Mesoscopic Kondo Effect in an Aharonov-Bohm Ring,” *Phys. Rev. Lett.* **85**, 5619–5622.
- Kastner, M. A., 1992, “The single-electron transistor,” *Rev. Mod. Phys.* **64**, 849–858.
- Kessler, J., and J. Lorenz, 1970, “Experimental Verification of the Fano Effect,” *Phys. Rev. Lett.* **24**, 87–88.
- Khelif, A., B. Djafari-Rouhani, J. O. Vasseur, and P. A. Deymier, 2003, “Transmission and dispersion relations of perfect and defect-containing waveguide structures in phononic band gap materials,” *Phys. Rev. B* **68**, 024302.
- Kim, B., and K. Yoshihara, 1993, “Multichannel quantum interference in the predissociation of Cs_2 : Observation of q-reversal in a complex resonance,” *J. Chem. Phys.* **99**, 1433–1435.
- Kim, G., S. B. Lee, T.-S. Kim, and J. Ihm, 2005, “Fano resonance and orbital filtering in multiply connected carbon nanotubes,” *Phys. Rev. B* **71**, 205415.
- Kim, J., J.-R. Kim, J.-O. Lee, J. W. Park, H. M. So, N. Kim, K. Kang, K.-H. Yoo, and J.-J. Kim, 2003, “Fano Resonance in Crossed Carbon Nanotubes,” *Phys. Rev. Lett.* **90**, 166403.
- Kim, S. W., 2002, “Floquet scattering in parametric electron pumps,” *Phys. Rev. B* **66**, 235304.
- Kim, S. W., and S. Kim, 2000, “The structure of eigenmodes and phonon scattering by discrete breathers in the discrete nonlinear Schrödinger chain,” *Physica D* **141**, 91–103.
- Kim, S. W., and S. Kim, 2001, “Fano resonances in translationally invariant nonlinear chains,” *Phys. Rev. B* **63**, 212301.
- Kleinpoppen, H., and M. McDowell (eds.), 1976, *Electron and photo interaction with atoms (Festschrift for Professor Ugo Fano)* (Plenum Press, New York).
- Kobayashi, K., H. Aikawa, S. Katsumoto, and Y. Iye, 2002, “Tuning of the Fano Effect through a Quantum Dot in an Aharonov-Bohm Interferometer,” *Phys. Rev. Lett.* **88**, 256806.
- Kobyakov, A., A. R. Zakharian, K. M. Gundu, and S. A. Darmanyan, 2009, “Giant optical resonances due to gain-assisted Bloch surface plasmons,” *Appl. Phys. Lett.* **94**, 151111.
- Koch, H., and H. Lübbig (eds.), 1992, *Single Electron Tunneling and Mesoscopic Devices*, volume 31 of *Springer Series in Electronics and Photonics* (Springer, Berlin).
- Kokoouline, V., C. Drag, P. Pillet, and F. Masnou-Seeuws, 2002, “Lu-Fano plot for interpretation of the photoassociation spectra,” *Phys. Rev. A* **65**, 062710.
- Kolorenc, P., V. Brems, and J. Horacek, 2005, “Computing resonance positions, widths, and cross sections via the Feshbach-Fano R-matrix method: Application to potential scattering,” *Phys. Rev. A* **72**, 012708.
- Kormányos, A., I. Grace, and C. J. Lambert, 2009, “Andreev reflection through Fano resonances in molecular wires,” *Phys. Rev. B* **79**(7), 075119.
- Kosevich, Y. A., 1997, “Capillary phenomena and macroscopic dynamics of complex two-dimensional defects in crystals,” *Prog. Surf. Sci.* **55**(1), 1–57.
- Kosevich, Y. A., 2008, “Multichannel propagation and scattering of phonons and photons in low-dimension nanostructures,” *Physics-Uspekhi* **51**(8), 839–859.
- Kosevich, Y. A., A. Feher, and E. S. Syркин, 2008, “Resonance absorption, reflection, transmission of phonons and heat transfer through interface between two solids,” *Low Temp. Phys.* **34**(7), 575–582.
- Koshino, K., 2003, “Analytic approach to the optical response of one-dimensional photonic crystal slabs,” *Phys. Rev. B* **67**, 165213.
- Kraemer, T., M. Mark, P. Waldburger, J. G. Danzl, C. Chin, B. Engeser, A. D. Lange, K. Pilch, A. Jaakkola, H.-C. Nägerl, and R. Grimm, 2006, “Evidence for Efimov quantum states in an ultracold gas of caesium atoms,” *Nature* **440**, 315–318.
- Kroner, M., A. O. Govorov, S. Remi, B. Biedermann, S. Seidl, A. Badolato, P. M. Petroff, W. Zhang, R. Barbour, B. D. Gerardot, R. J. Warburton, and K. Karrai, 2008, “The nonlinear Fano effect,” *Nature* **451**, 311–314.
- Landobasa Y. Mario, S. D., and M. K. Chin, 2006, “Asymmetric Fano resonance and bistability for high extinction ratio, large modulation depth, and low power switching,” *Opt. Express* **14**, 12770–12781.
- Langreth, D. C., 1966, “Friedel Sum Rule for Anderson’s Model of Localized Impurity States,” *Phys. Rev.* **150**, 516–518.
- Le, F., N. Z. Lwin, N. J. Halas, and P. Nordlander, 2007, “Plasmonic interactions between a metallic nanoshell and a thin metallic film,” *Phys. Rev. B* **76**, 165410.
- Lebech, M., J. C. Houver, D. Doweck, and R. R. Lucchese, 2006, “Molecular Frame Photoelectron Emission in the Presence of Autoionizing Resonances,” *Phys. Rev. Lett.* **96**, 073001.
- Lee, C.-W., 1998, “Identification of the Beutler-Fano formula

- in eigenphase shifts and eigentime delays near a resonance,” *Phys. Rev. A* **58**, 4581–4592.
- Lee, J. D., J. Inoue, and M. Hase, 2006, “Ultrafast Fano Resonance between Optical Phonons and Electron-Hole Pairs at the Onset of Quasiparticle Generation in a Semiconductor,” *Phys. Rev. Lett.* **97**, 157405.
- Lee, M., and C. Bruder, 2006, “Spin filter using a semiconductor quantum ring side coupled to a quantum wire,” *Phys. Rev. B* **73**, 085315.
- Lee, S., and B. Kim, 2000a, “Direct evaluation of the asymmetry parameters for isolated resonances,” *J. Phys. B* **33**, 3441–3448.
- Lee, S.-S., and S. Kim, 2000b, “Phonon scattering by breathers in the discrete nonlinear Schrödinger chain,” *Int. J. Mod. Phys. B* **14**, 1903.
- Lewis, B. R., S. T. Gibson, P. O’Keeffe, T. Ridley, K. P. Lawley, and R. J. Donovan, 2001, “Observation of Completely Destructive Quantum Interference between Interacting Resonances in Molecular Predissociation,” *Phys. Rev. Lett.* **86**, 1478–1481.
- Ley, L., R. Karcher, and R. L. Johnson, 1984, “Localized states at the conduction-band edge of amorphous silicon nitride detected by resonance photoemission,” *Phys. Rev. Lett.* **53**, 710–713.
- Li, W., and L. E. Reichl, 1999, “Floquet scattering through a time-periodic potential,” *Phys. Rev. B* **60**, 15732–15741.
- Limonov, M. F., A. I. Rykov, S. Tajima, and A. Yamanaka, 1998, “Raman Scattering Study on Fully Oxygenated $YBa_2Cu_3O_7$ Single Crystals: $x - y$ Anisotropy in the Superconductivity-Induced Effects,” *Phys. Rev. Lett.* **80**, 825–828.
- Limonov, M. F., S. Tajima, and A. Yamanaka, 2000, “Phononic and electronic Raman spectroscopy of the pseudogap state in underdoped $YBa_2Cu_3O_7 - x$,” *Phys. Rev. B* **62**, 11859–11863.
- Lin, S. Y., E. Chow, V. Hietala, P. R. Villeneuve, and J. D. Joannopoulos, 1998, “Experimental Demonstration of Guiding and Bending of Electromagnetic Waves in a Photonic Crystal,” *Science* **282**, 274–276.
- Lobos, A. M., and A. A. Aligia, 2008, “Effects of Interactions in Transport through Aharonov-Bohm-Casher Interferometers,” *Phys. Rev. Lett.* **100**, 016803.
- Longhi, S., 2006, “Transmission and localization control by ac fields in tight-binding lattices with an impurity,” *Phys. Rev. B* **73**, 193305.
- Lousse, V., and J. P. Vigneron, 2004, “Use of Fano resonances for bistable optical transfer through photonic crystal films,” *Phys. Rev. B* **69**, 155106.
- Luk’yanchuk, B. S., T. C. Chong, L. P. Shi, M. I. Tribelsky, Z. B. Wang, L. Li, C.-W. Qiu, C. J. R. Sheppard, and J. H. Wu, 2008, in *IEEE Photonics and Global*.
- MacKay, R. S., and S. Aubry, 1994, “Proof of existence of breathers for time-reversible or Hamiltonian networks of weakly coupled oscillators,” *Nonlinearity* **7**, 1623.
- Maeda, K., K. Ueda, T. Namioka, and K. Ito, 1992, “High-resolution measurement of Beutler-Fano profiles for autoionizing Rydberg series of Xe,” *Phys. Rev. A* **45**, 527–530.
- Maes, B., P. Bienstman, and R. Baets, 2005, “Switching in coupled nonlinear photonic-crystal resonators,” *J. Opt. Soc. Am. B* **22**, 1778–1784.
- Maes, B., P. Bienstman, and R. Baets, 2008, “Symmetry breaking with coupled Fano resonances,” *Opt. Express* **16**(5), 3069–3076.
- Magidson, V., and R. Beserman, 2002, “Fano-type interference in the Raman spectrum of photoexcited Si,” *Phys. Rev. B* **66**, 195206.
- Magnusson, R., and S. S. Wang, 1992, “New principle for optical filters,” *Appl. Phys. Lett.* **61**, 1022–1024.
- Magunov, A. I., I. Rotter, and S. I. Strakhova, 2003, “Fano resonances in the overlapping regime,” *Phys. Rev. B* **68**, 245305.
- Mahan, G., 1993, *Many-Particle Physics* (New York, Plenum Press).
- Maleki, L., A. B. Matsko, A. A. Savchenkov, and V. S. Ilchenko, 2004, “Tunable delay line with interacting whispering-gallery-moderesonators,” *Opt. Lett.* **29**, 626–628.
- Margulis, V. A., and M. A. Pyataev, 2004, “Fano resonances in a three-terminal nanodevice,” *J. Phys. Condens. Matter* **16**, 4315.
- Marin Soljačić, S. G. J. Y. F., Mihai Ibanescu, and J. D. Joannopoulos, 2002, “Optimal bistable switching in nonlinear photonic crystals,” *Phys. Rev. E* **66**, 055601.
- Marinho, R. R. T., O. Bjorneholm, S. L. Sorensen, I. Hjelte, S. Sundin, M. Bassler, S. Svensson, and A. N. de Brito, 2001, “Interference between direct and resonant channels in near-resonance photoemission in argon,” *Phys. Rev. A* **63**, 032514.
- Martinez, D. F., and L. E. Reichl, 2001, “Transmission properties of the oscillating delta-function potential,” *Phys. Rev. B* **64**, 245315.
- Mazumdar, I., A. R. P. Rau, and V. S. Bhasin, 2006, “Efimov States and their Fano Resonances in a Neutron-Rich Nucleus,” *Phys. Rev. Lett.* **97**, 062503.
- McCormack, E. F., F. D. Teodoro, J. M. Grochocinski, and S. T. Pratt, 1998, “Dynamics of Rydberg states of nitric oxide probed by two-color resonant four-wave mixing spectroscopy,” *J. Chem. Phys.* **109**, 63–71.
- Mehlhorn, W., 1998, “70 years of Auger spectroscopy, a historical perspective,” *J. Electron. Spectrosc. Relat. Phenom.* **93**, 1–15.
- Meier, T., A. Schulze, P. Thomas, H. Vaupel, and K. Maschke, 1995, “Signatures of Fano resonances in four-wave-mixing experiments,” *Phys. Rev. B* **51**, 13977–13986.
- Meijerink, A., and G. Blasse, 1989, “Fano antiresonance in the excitation spectra of the luminescence of divalent europium,” *Phys. Rev. B* **40**, 7288–7291.
- Mekis, A., J. C. Chen, I. Kurland, S. Fan, P. R. Villeneuve, and J. D. Joannopoulos, 1996, “High Transmission through Sharp Bends in Photonic Crystal Waveguides,” *Phys. Rev. Lett.* **77**, 3787–3790.
- Menéndez, J., and M. Cardona, 1985, “Interference effects: A key to understanding forbidden Raman scattering by LO phonons in GaAs,” *Phys. Rev. B* **31**, 3696–3704.
- Micheli, A., A. J. Daley, D. Jaksch, and P. Zoller, 2004, “Single Atom Transistor in a 1D Optical Lattice,” *Phys. Rev. Lett.* **93**, 140408.
- Micheli, A., and P. Zoller, 2006, “Single-atom mirror for one-dimensional atomic lattice gases,” *Phys. Rev. A* **73**, 043613.
- Mie, G., 1908, “Beiträge zur Optik trüber Medien, speziell kolloidaler Metallösungen,” *Ann. Phys. (Leipzig)* **330**, 337–445.
- Mies, F. H., 1968, “Configuration Interaction Theory. Effects of Overlapping Resonances,” *Phys. Rev.* **175**, 164–175.
- Mingaleev, S. F., and Y. S. Kivshar, 2001, “Self-Trapping and Stable Localized Modes in Nonlinear Photonic Crystals,”

- Phys. Rev. Lett. **86**, 5474–5477.
- Mingaleev, S. F., and Y. S. Kivshar, 2002a, “Effective equations for photonic-crystal waveguides and circuits,” *Opt. Lett.* **27**, 231–233.
- Mingaleev, S. F., and Y. S. Kivshar, 2002b, “Nonlinear transmission and light localization in photonic-crystal waveguides,” *J. Opt. Soc. Am. B* **19**, 2241–2249.
- Mingaleev, S. F., Y. S. Kivshar, and R. A. Sammut, 2000, “Long-range interaction and nonlinear localized modes in photonic crystal waveguides,” *Phys. Rev. E* **62**, 5777–5782.
- Mingaleev, S. F., A. E. Miroschnichenko, and Y. S. Kivshar, 2007, “Low-threshold bistability of slow light in photonic-crystal waveguides,” *Opt. Express* **15**, 12380–12385.
- Mingaleev, S. F., A. E. Miroschnichenko, and Y. S. Kivshar, 2008, “Coupled-resonator-induced reflection in photonic-crystal waveguide structures,” *Opt. Express* **16**, 11647–11659.
- Mingaleev, S. F., A. E. Miroschnichenko, Y. S. Kivshar, and K. Busch, 2006, “All-optical switching, bistability, and slow-light transmission in photonic crystal waveguide-resonator structures,” *Phys. Rev. E* **74**, 046603.
- Miroschnichenko, A. E., 2009, “Nonlinear Fano-Feshbach resonances,” *Phys. Rev. E* **79**(2), 026611.
- Miroschnichenko, A. E., S. Flach, A. V. Gorbach, B. S. Luk’yanchuk, Y. S. Kivshar, and M. I. Tribelsky, 2008, “Fano resonances: A discovery that did not happen 100 years ago,” *Opt. Phon. News* **19**, 48.
- Miroschnichenko, A. E., S. Flach, and B. Malomed, 2003, “Resonant scattering of solitons,” *Chaos* **13**, 874–879.
- Miroschnichenko, A. E., Y. Kivshar, C. Etrich, T. Pertsch, R. Iliw, and F. Lederer, 2009, “Dynamics and instability of nonlinear Fano resonances in photonic crystals,” *Phys. Rev. A* **79**, 013809.
- Miroschnichenko, A. E., and Y. S. Kivshar, 2005a, “Engineering Fano resonances in discrete arrays,” *Phys. Rev. E* **72**, 056611.
- Miroschnichenko, A. E., and Y. S. Kivshar, 2005b, “Sharp bends in photonic crystal waveguides as nonlinear Fano resonators,” *Opt. Express* **13**, 3969–3976.
- Miroschnichenko, A. E., Y. S. Kivshar, R. A. Vicencio, and M. I. Molina, 2005a, “Fano resonance in quadratic waveguide arrays,” *Opt. Lett.* **30**, 872–874.
- Miroschnichenko, A. E., S. F. Mingaleev, S. Flach, and Y. S. Kivshar, 2005b, “Nonlinear Fano resonance and bistable wave transmission,” *Phys. Rev. E* **71**, 036626.
- Miroschnichenko, A. E., M. Schuster, S. Flach, M. V. Fistul, and A. V. Ustinov, 2005c, “Resonant plasmon scattering by discrete breathers in Josephson junction ladders,” *Phys. Rev. B* **71**, 174306.
- Misochko, O., M. Hase, K. Ishioka, and M. Kitajima, 2005, “Fano interference with the alternating asymmetry parameter in time-domain experiments,” *JETP Letters* **82**, 426–430.
- Misochko, O. V., K. Kisoda, K. Sakai, and S. Nakashima, 2000, “Dynamics of low-frequency phonons in the $YBa_2Cu_3O_7 - x$ superconductor studied by time- and frequency-domain spectroscopies,” *Phys. Rev. B* **61**, 4305–4313.
- van der Molen, K. L., K. J. K. Koerkamp, S. Enoch, F. B. Segerink, N. F. van Hulst, and L. Kuipers, 2005, “Role of shape and localized resonances in extraordinary transmission through periodic arrays of subwavelength holes: Experiment and theory,” *Phys. Rev. B* **72**, 045421.
- Morsch, O., and M. Oberthaler, 2006, “Dynamics of Bose-Einstein condensates in optical lattices,” *Rev. Mod. Phys.* **78**, 179.
- Moskovits, M., 1985, “Surface-enhanced spectroscopy,” *Rev. Mod. Phys.* **57**, 783–826.
- Naweed, A., G. Farca, S. I. Shopova, and A. T. Rosenberger, 2005, “Induced transparency and absorption in coupled whispering-gallery microresonators,” *Phys. Rev. A* **71**, 043804.
- Neel, N., J. Kroger, L. Limot, K. Palotas, W. A. Hofer, and R. Berndt, 2007, “Conductance and Kondo Effect in a Controlled Single-Atom Contact,” *Phys. Rev. Lett.* **98**, 016801.
- von Neumann, J., and E. Wigner, 1929, “Über merkwürdige diskrete Eigenwerte / On unusual discrete eigenvalues,” *Z. Phys.* **30**, 465–467.
- Ng, T. K., and P. A. Lee, 1988, “On-Site Coulomb Repulsion and Resonant Tunneling,” *Phys. Rev. Lett.* **61**, 1768–1771.
- Nockel, J. U., and A. D. Stone, 1994, “Resonance line shapes in quasi-one-dimensional scattering,” *Phys. Rev. B* **50**, 17415–17432.
- Notomi, M., K. Yamada, A. Shinya, J. Takahashi, C. Takahashi, and I. Yokohama, 2001, “Extremely Large Group-Velocity Dispersion of Line-Defect Waveguides in Photonic Crystal Slabs,” *Phys. Rev. Lett.* **87**, 253902.
- Nussenzweig, A., E. E. Eyler, T. Bergeman, and E. Pollack, 1990, “Line shapes of ionizing Stark resonances in helium,” *Phys. Rev. A* **41**, 4944–4957.
- Oliveira, L. N., and J. W. Wilkins, 1985, “Fano antiresonances in x-ray-absorption spectroscopy,” *Phys. Rev. B* **32**, 696–707.
- Opatrný, T., and D.-G. Welsch, 2001, “Coupled cavities for enhancing the cross-phase-modulation in electromagnetically induced transparency,” *Phys. Rev. A* **64**, 023805.
- Ott, H., J. Fortagh, G. Schlotterbeck, A. Grossmann, and C. Zimmermann, 2001, “Bose-Einstein Condensation in a Surface Microtrap,” *Phys. Rev. Lett.* **87**, 230401.
- Ozbay, E., 2006, “Plasmonics: Merging Photonics and Electronics at Nanoscale Dimensions,” *Science* **311**, 189–193.
- Pachos, J. K., and P. L. Knight, 2003, “Quantum Computation with a One-Dimensional Optical Lattice,” *Phys. Rev. Lett.* **91**, 107902.
- Palfy, A., Z. Harman, and W. Scheid, 2007, “Quantum interference between nuclear excitation by electron capture and radiative recombination,” *Phys. Rev. A* **75**, 012709.
- Pastawski, H. M., L. E. F. F. Torres, and E. Medina, 2002, “Electron-phonon interaction and electronic decoherence in molecular conductors,” *Chem. Phys.* **281**, 257–278.
- Patthey, F., M.-H. Schaffner, W.-D. Schneider, and B. Delley, 1999, “Observation of a Fano Resonance in Photoemission,” *Phys. Rev. Lett.* **82**, 2971–2974.
- Piao, G., R. A. Lewis, and P. Fisher, 1990, “Fano resonances in the absorption spectrum of singly ionised zinc in germanium,” *Solid State Commun.* **75**, 835–838.
- Pichl, L., H. Nakamura, and J. Horacek, 2000, “Complete reflection in two-state crossing and noncrossing potential systems,” *J. Chem. Phys.* **113**, 906–918.
- Qiang, Z., H. Yang, L. Chen, H. Pang, Z. Ma, and W. Zhou, 2008, “Fano filters based on transferred silicon nanomembranes on plastic substrates,” *Appl. Phys. Lett.* **93**, 061106.
- Ramaker, D. E., and D. M. Schrader, 1974, “Multichannel configuration-interaction theory: Application to some resonances in helium,” *Phys. Rev. A* **9**, 1980–1991.
- Raoult, M., and F. H. Mies, 2004, “Feshbach resonance in atomic binary collisions in the Wigner threshold law regime,” *Phys. Rev. A* **70**, 012710.

- Rau, A. R. P., 2004, “Perspectives on the Fano Resonance Formula,” *Phys. Scr.* **69**, C10–C13.
- Rayleigh, L., 1871a, “On the Light from the Sky, Its Polarization and Color,” *Phil. Mag.* **41**, 107.
- Rayleigh, L., 1871b, “On the Light from the Sky, Its Polarization and Color,” *Phil. Mag.* **41**, 274.
- Rayleigh, L., 1871c, “On the scattering of light by small particles,” *Phil. Mag.* **41**, 447.
- Rayleigh, L., 1907, “On the dynamical theory of gratings,” *Proc. R. Soc. London, Ser. A* **79**, 399.
- Redner, S., 2004, “Citation Statistics From More Than a Century of Physical Review,” arxiv:physics/0407137.
- Reimann, S. M., and M. Manninen, 2002, “Electronic structure of quantum dots,” *Rev. Mod. Phys.* **74**, 1283–1342.
- Rice, O. K., 1933, “Predissociation and the Crossing of Molecular Potential Energy Curves,” *J. Chem. Phys.* **1**, 375–389.
- Roney, P. L., 1994a, “Theory of spectral line shape. I. Formulation and line coupling,” *J. Chem. Phys.* **101**, 1037–1049.
- Roney, P. L., 1994b, “Theory of spectral line shape. II. Collision time theory and the line wing,” *J. Chem. Phys.* **101**, 1050–1060.
- Roney, P. L., 1995, “Theory of spectral line shape. III. The Fano operator from near to far wing,” *J. Chem. Phys.* **102**, 4757–4771.
- S. J. Xu, J. L., S.-J. Xiong, and H. Z. Zheng, 2006, “New type of Fano resonant tunneling via Anderson impurities in superlattice,” *Europhys. Lett.* **74**, 875–881.
- Saito, R., G. Dresselhaus, and M. S. Dresselhaus, 1998, *Physical Properties of Carbon Nanotubes* (Imperial College Press, London).
- Sanchez, D., and L. Serra, 2006, “Fano-Rashba effect in a quantum wire,” *Phys. Rev. B* **74**, 153313.
- Sanchez, I., and F. Martin, 1994, “Hidden Fano interferences in the resonant photoionization of He-like ions,” *Phys. Rev. A* **49**, 5116–5119.
- Sarrazin, M., J.-P. Vigneron, and J.-M. Vigoureux, 2003, “Role of Wood anomalies in optical properties of thin metallic films with a bidimensional array of subwavelength holes,” *Phys. Rev. B* **67**, 085415.
- Sasada, K., and N. Hatano, 2005, “Quantum interference effect of resonant transport in nano-scale systems,” *Physica E* **29**, 609 – 613.
- Sato, M., B. E. Hubbard, A. J. Sievers, B. Ilic, D. A. Czaplewski, and H. G. Craighead, 2003, “Observation of Locked Intrinsic Localized Vibrational Modes in a Micromechanical Oscillator Array,” *Phys. Rev. Lett.* **90**, 044102.
- Schmid, J., J. Weis, K. Eberl, and K. v. Klitzing, 1998, “A quantum dot in the limit of strong coupling to reservoirs,” *Physica B* **256-258**, 182 – 185.
- Schumm, T., S. Hofferberth, L. M. Andersson, S. Wildermuth, S. Groth, I. Bar-Joseph, J. Schmiedmayer, and P. Krüger, 2005, “Matter-wave interferometry in a double well on an atom chip,” *Nat. Phys.* **57–62**.
- Schwarz, U. T., L. Q. English, and A. J. Sievers, 1999, “Experimental Generation and Observation of Intrinsic Localized Spin Wave Modes in an Antiferromagnet,” *Phys. Rev. Lett.* **83**, 223–226.
- Seaton, M. J., 1966, “Quantum defect theory I. General formulation,” *Proc. Phys. Soc. London* **88**, 801–814.
- Serra, L., and D. Sánchez, 2007, “The Fano-Rashba effect,” *J. Phys.: Conf. Ser.* **61**, 1037.
- Shenstone, A. G., 1938, “Spectroscopy: I. atomic spectra,” *Rep. Prog. Phys.* **5**, 210–227.
- Siegner, U., M.-A. Mycek, S. Glutsch, and D. S. Chemla, 1995, “Quantum interference in the system of Lorentzian and Fano magnetoexciton resonances in GaAs,” *Phys. Rev. B* **51**, 4953–4961.
- Simonian, A. W., A. B. Sproul, Z. Shi, and E. Gauja, 1995, “Observation of Fano resonance in heavily doped p-type silicon at room temperature,” *Phys. Rev. B* **52**, 5672–5674.
- Simpson, J. A., and U. Fano, 1963, “Classification of Resonances in the Electron Scattering Cross Section of Ne and He,” *Phys. Rev. Lett.* **11**, 158–159.
- Smerzi, A., and A. Trombettoni, 2003, “Nonlinear tight-binding approximation for Bose-Einstein condensates in a lattice,” *Phys. Rev. A* **68**, 023613.
- Smirnov, B. M., 2003, *Physics of Atoms And Ions* (Springer, New York).
- Smith, D. D., H. Chang, K. A. Fuller, A. T. Rosenberger, and R. W. Boyd, 2004, “Coupled-resonator-induced transparency,” *Phys. Rev. A* **69**, 063804.
- Smith, K., D. E. Golden, S. Ormonde, B. W. Torres, and A. R. Davies, 1973, “Theoretical Model for Resonances in e-He Scattering near 60 eV,” *Phys. Rev. A* **8**, 3001–3011.
- Soljacic, M., and J. D. Joannopoulos, 2004, “Enhancement of nonlinear effects using photonic crystals,” *Nat. Mater.* **3**, 211–219.
- Soljačić, M., C. Luo, J. D. Joannopoulos, and S. Fan, 2003, “Nonlinear photonic crystal microdevices for optical integration,” *Opt. Lett.* **28**, 637–639.
- Spevak, I. S., A. Y. Nikitin, E. V. Bezuglyi, A. Levchenko, and A. V. Kats, 2009, “Resonantly suppressed transmission and anomalously enhanced light absorption in periodically modulated ultrathin metal films,” *Phys. Rev. B* **79**, 161406.
- Stefanski, P., 2003, “Quantum dots as scatterers in electronic transport: interference and correlations,” *Solid State Comm.* **128**, 29 – 34.
- Stefanski, P., A. Tagliacozzo, and B. R. Bulka, 2004, “Fano versus Kondo Resonances in a Multilevel ‘Semiopen’ Quantum Dot,” *Phys. Rev. Lett.* **93**, 186805.
- Stillinger, F. H., and D. R. Herrick, 1975, “Bound states in the continuum,” *Phys. Rev. A* **11**, 446–454.
- Sturm, K., W. Schulke, and J. R. Schmitz, 1992, “Plasmon-Fano resonance inside the particle-hole excitation spectrum of simple metals and semiconductors,” *Phys. Rev. Lett.* **68**, 228–231.
- Suh, W., Z. Wang, and S. Fan, 2004, “Temporal coupled-mode theory and the presence of non-orthogonal modes in lossless multi-mode cavities,” *IEEE J. Quant. Electron.* **40**, 1511.
- Swanson, B. I., J. A. Brozik, S. P. Love, G. F. Strouse, A. P. Shreve, A. R. Bishop, W.-Z. Wang, and M. I. Salkola, 1999, “Observation of Intrinsically Localized Modes in a Discrete Low-Dimensional Material,” *Phys. Rev. Lett.* **82**, 3288–3291.
- Syage, J. A., and J. E. Wessel, 1987, “Antiresonance in autoionizing Rydberg series of naphthalene,” *J. Chem. Phys.* **87**, 6207–6209.
- Taylor, D. P., and P. M. Johnson, 1993, “Resonance enhanced multiphoton ionization photoelectron spectra of CO[_{sub}2]. III. Autoionization dominates direct ionization,” *J. Chem. Phys.* **98**, 1810–1816.
- Teodoro, F. D., and E. F. McCormack, 1998, “Theoretical treatment of quasibound resonances in two-color resonant four-wave mixing spectroscopy,” *Phys. Rev. A* **57**, 162–173.
- Teodoro, F. D., and E. F. McCormack, 1999, “State-selective quantum beat spectroscopy via coherent control of

- Liouville-pathway interference in two-colour resonant four-wave mixing,” *J. Phys. B* **32**, 4389–4404.
- Terrones, M., H. Terrones, F. Banhart, J.-C. Charlier, and P. M. Ajayan, 2000, “Coalescence of Single-Walled Carbon Nanotubes,” *Science* **288**, 1226–1229.
- Tomita, M., K. Totsuka, R. Hanamura, and T. Matsumoto, 2009, “Tunable Fano interference effect in coupled-microsphere resonator-induced transparency,” *J. Opt. Soc. Am. B* **26**, 813–818.
- Tong, P., B. Li, and B. Hu, 1999, “Wave transmission, phonon localization, and heat conduction of a one-dimensional Frenkel-Kontorova chain,” *Phys. Rev. B* **59**, 8639–8645.
- Torio, M. E., K. Hallberg, S. F. A. E. Miroshnichenko, and M. Titov, 2004, “Spin filters with Fano dots,” *Eur. Phys. J. B* **37**, 399.
- Torres, L. E. F. F., H. M. Pastawski, and E. Medina, 2006, “Antiresonances as precursors of decoherence,” *EPL* **73**, 164–170.
- Trías, E., J. J. Mazo, and T. P. Orlando, 2000, “Discrete Breathers in Nonlinear Lattices: Experimental Detection in a Josephson Array,” *Phys. Rev. Lett.* **84**, 741–744.
- Tribelsky, M. I., S. Flach, A. E. Miroshnichenko, A. V. Gorbach, and Y. S. Kivshar, 2008, “Light Scattering by a Finite Obstacle and Fano Resonances,” *Phys. Rev. Lett.* **100**, 043903.
- Tribelsky, M. I., and B. S. Luk’yanchuk, 2006, “Anomalous Light Scattering by Small Particles,” *Phys. Rev. Lett.* **97**, 263902.
- Ueda, K., 1987, “Spectral line shapes of autoionizing Rydberg series,” *Phys. Rev. A* **35**, 2484–2492.
- Vicencio, R. A., J. Brand, and S. Flach, 2007, “Fano Blockade by a Bose-Einstein Condensate in an Optical Lattice,” *Phys. Rev. Lett.* **98**, 184102.
- Vittorini-Orgeas, A., and A. Bianconi, 2008, “From Majorana theory of atomic autoionization to Feshbach resonances in high temperature superconductors,” arXiv:0812.1551.
- Vlasov, Y. A., M. O’Boyle, H. F. Hamann, and S. J. McNab, 2005, “Active control of slow light on a chip with photonic crystal waveguides,” *Nature* **438**, 65.
- Waligorski, G., L. Zhou, and W. E. Cooke, 1997, “Technique for measuring the linewidth of autoionizing Rydberg states,” *Phys. Rev. A* **55**, 1544–1547.
- Ward, A. J., and J. B. Pendry, 1998, “Calculating photonic Green’s functions using a nonorthogonal finite-difference time-domain method,” *Phys. Rev. B* **58**, 7252–7259.
- Weidner, E., S. Combrié, A. de Rossi, N.-V.-Q. Tran, and S. Cassette, 2007, “Nonlinear and bistable behavior of an ultrahigh-Q GaAs photonic crystal nanocavity,” *Appl. Phys. Lett.* **90**, 101118.
- Wickenhauser, M., J. Burgdorfer, F. Krausz, and M. Drescher, 2005, “Time Resolved Fano Resonances,” *Phys. Rev. Lett.* **94**, 023002.
- Wiegmann, P. B., and A. M. Tselick, 1983, “Exact solution of the Anderson model: I,” *J. Phys. C* **16**, 2281–2319.
- Winstead, C., and P. W. Langhoff, 1991, “Feshbach–Fano formalism in Hilbert space: Application to shape resonances in molecular photoionization,” *J. Chem. Phys.* **95**, 3107–3118.
- Wood, R., 1902, “On the remarkable case of uneven distribution of light in a diffraction grating spectrum,” *Proc. R. Soc. London, Ser. A* **18**, 269.
- Wood, R. W., 1935, “Anomalous Diffraction Gratings,” *Phys. Rev.* **48**, 928–936.
- Wulf, U., and V. V. Skalozub, 2005, “Pulse propagation in resonant tunneling,” *Phys. Rev. B* **72**, 165331.
- Xu, Q., S. Sandhu, M. L. Povinelli, J. Shakya, S. Fan, and M. Lipson, 2006, “Experimental Realization of an On-Chip All-Optical Analogue to Electromagnetically Induced Transparency,” *Phys. Rev. Lett.* **96**, 123901.
- Xu, Y., Y. Li, R. K. Lee, and A. Yariv, 2000, “Scattering-theory analysis of waveguide-resonator coupling,” *Phys. Rev. E* **62**, 7389–7404.
- Yafet, Y., 1981, “Effect of shake-up transitions on the spectrum of Auger electrons in Fano resonances,” *Phys. Rev. B* **23**, 3558–3559.
- Yang, H., H. Pang, Z. Qiang, Z. Ma, and W. Zhou, 2008, “Surface-normal Fano filters based on transferred silicon nanomembranes on glass substrates,” *Electronics Letters* **44**, 858–860.
- Yang, X., C. Husko, C. W. Wong, M. Yu, and D.-L. Kwong, 2007, “Observation of femtojoule optical bistability involving Fano resonances in high-Q/ V_m silicon photonic crystal nanocavities,” *Appl. Phys. Lett.* **91**, 051113.
- Yanik, M. F., and S. Fan, 2004, “Stopping Light All Optically,” *Phys. Rev. Lett.* **92**, 083901.
- Yanik, M. F., S. Fan, and M. Soljačić, 2003a, “High-contrast all-optical bistable switching in photonic crystal microcavities,” *Appl. Phys. Lett.* **83**, 2739–2741.
- Yanik, M. F., S. Fan, M. Soljačić, and J. D. Joannopoulos, 2003b, “All-optical transistor action with bistable switching in a photonic crystal cross-waveguide geometry,” *Opt. Lett.* **28**, 2506–2508.
- Yanik, M. F., W. Suh, Z. Wang, and S. Fan, 2004, “Stopping Light in a Waveguide with an All-Optical Analog of Electromagnetically Induced Transparency,” *Phys. Rev. Lett.* **93**, 233903.
- Yi, W., L. Lu, H. Hu, Z. W. Pan, and S. S. Xie, 2003, “Tunneling into Multiwalled Carbon Nanotubes: Coulomb Blockade and the Fano Resonance,” *Phys. Rev. Lett.* **91**, 076801.
- Zhang, W., A. O. Govorov, and G. W. Bryant, 2006, “Semiconductor-Metal Nanoparticle Molecules: Hybrid Excitons and the Nonlinear Fano Effect,” *Phys. Rev. Lett.* **97**, 146804.
- Zhang, Z., and V. Chandrasekhar, 2006, “Signatures of phase coherence in the low-temperature transport properties of multiwall carbon nanotubes,” *Phys. Rev. B* **73**, 075421.
- Zhang, Z., D. A. Dikin, R. S. Ruoff, and V. Chandrasekhar, 2004, “Conduction in carbon nanotubes through metastable resonant states,” *Europhys. Lett.* **68**, 713–719.